White dwarfs in binaries and hierarchical triple systems as a test for mass transfer models and close binary formation mechanisms

Felipe Lagos Vilches

Instituto de Física y Astronomía
Facultad de Ciencias

Advisors: Mónica Zorotovic (UV) and Matthias Schreiber (USM)
Thesis defense commitee: Linda Schmidtobreick (ESO) and Maja Vuckovic (UV)

Universidad de Valparaíso
Doctorado en Astrofísica

Diciembre 2021
Valparaíso. Chile.

Dedicado con amor a mi Rayén, por ser la motivación más grande para continuar mejorando, y a la tía María, que de seguro bajará a darme ánimos el día de la defensa, al igual que en mi magíster.

This thesis is solely my own composition,
except where specifically indicated in the text.

Felipe Lagos Vilches
Diciembre 2021.
Valparaíso. Chile.

Agradecimientos

Este proyecto fue posible gracias al financiamiento otorgado por la Universidad de Valparaíso a través de la beca FIB UV durante el periodo 2018-2019, al Observatorio Europeo Austral (ESO) a través del ESO Studentship Programme durante el periodo 2020-2021 y a la Agencia Nacional de Investigación y Desarrollo (ANID) a través de la beca de doctorado nacional número 21211306 durante el año 2021.

Quisiera dar un agradecimiento especial a mis dos profesores guías, Matthias Schreiber Y Mónica Zorotovic. Matthias ha sido mi mentor desde mi magister hasta mi doctorado. Los conocimientos adquiridos, la forma de buscar soluciones a problemas en diversas investigaciones, los logros obtenidos durante estos años y básicamente mi carrera como científico han sido gracias a su constante guía, tiempo, paciencia y preocupación. Sin lugar a dudas sus enseñanzas y motivación seguirán conmigo. Mónica, también desde mi magister, ha jugado un rol importante en mi carrera como científico. Su gran conocimiento sobre binarias y su excelente disposición para explicar de manera muy simple conceptos que a veces son un tanto complejos han sido un enorme pilar en mi entendimiento del área. Más allá de lo experto y destacados que ambos son en astronomía, agradezco su calidad humana, lo cual ha hecho un agrado poder realizar este proyecto y continuar investigando.

También agradezco a mi mentora durante mi estadía en la ESO, Linda Schmidtobreick. Su excelente disposición para enseñar, explicar, empujarme a realizar nuevos proyectos, hacerme ver mis errores y aprender de ellos es algo de lo que siempre estaré agradecido. Sin lugar a dudas es otra de las personas que agradezco haberme topado durante mi doctorado.

Al Instituto de Física y Astronomía de la Universidad de Valparaíso, tanto profesores como compañeros, que no sólo tienen una calidad profesional del más alto nivel, sino también una gran calidad humana que genera un ambiente de trabajo muy grato.

A mi familia, la cual desde que supo que la astronomía era mi camino a seguir siempre me apoyó, incluso en esos momentos en que el camino se veía imposible, y a mi esposa Camila, quien sido un pilar fundamental a lo largo de estos años.

Abstract

Most stars with masses above $\approx 1M_{\odot}$ will end their lives as white dwarfs. Given that a non negligible fraction of such stars are in binary or multiple star systems, the characteristics of some of these white dwarfs will are affected by interactions between its progenitor and a close companion. These interactions can continue after the formation of the white dwarf producing a large variety of interesting objects and astrophysical phenomena like cataclysmic variables, double white dwarf binaries, super soft X-ray sources or type Ia supernovae. Formation of white dwarfs affected by binary interactions, or its subsequent interaction with a close companion, can be also enhanced due to perturbations exerted by a third companion. Under certain conditions, inner binaries in triple systems are prone to experience long term changes in their eccentricities, allowing otherwise non-interacting binaries to experience tidal migration, mass transfer, common envelope evolution or even mergers/collisions. In addition, although it is generally assumed that the interacting companion is another star, recent studies indicate that planets can interact with their host star, survive the metamorphosis of the latter into a white dwarf and later potentially pollute its atmosphere with heavy elements. Therefore, white dwarfs that reside in binary and triple configurations provide invaluable astrophysical laboratories to study stellar and binary evolution, orbital dynamics, and planet formation/evolution.

Despite remarkable progress made in the last forty years in modeling binary interactions and the secular dynamic evolution of triple systems, the physics behind several processes, in particular those involved in the former, is still not well understood. This is mainly due to the fact that most of the currently available modeling tools are based on analytical simplifications involving parameters that must be fitted through (extensive and detailed) observations. With the aim of reducing this gap in our knowledge, I present in this thesis three different cases in which binaries and hierarchical triple systems will allow to test and improve current models of binary interactions and to measure the impact of tertiary companions in the formation of tight binaries.

Contents

Chapter 1

Stellar evolution in binary stars and hierarchical triple systems

As a significant number of stars are members of binary and triple systems, and in many of these systems, some close members may interact, understanding stellar evolution is inherently linked to understanding binary star interactions. This is particularly important as close interacting binary stars are supposed to be responsible for some of the most luminous and most important explosions in the Universe, e.g. type Ia supernovae (SNe Ia) or kilo-nova events. In what follows, we outline the basic concepts of binary star interactions and triple dynamics to properly put into context the research results presented in this thesis.

1.1 The Roche-Lobe model

One of the most important concepts to understand binary star interactions is Roche geometry, which describes the effective gravitational potential exerted by the binary system on a massless test particle (the so called restricted three-body problem). This effective potential is defined in a co-rotating frame where the gravitational potential of both stars (with mass M_1 and M_2) and the centrifugal potential acting on the test particle are taken into account. Close to each star the equipotential surfaces are approximately concentric spheres, while at greater distances the equipotential surfaces

are distorted to tear drop-shapes, elongated parallel to the axis joining both stars. The Roche lobe of a star in a close binary system corresponds to the region in space where the test particle is gravitationally bound to one of the stars in the system.

The following assumptions are commonly used to describe the Roche model:

- The binary orbit is circular.
- The rotation of stars is synchronized with the orbital rotation.
- Stellar radii are small compared to the distance between them.
- The Coriolis force is neglected.

The Roche potential has five Lagrangian points where its gradient is zero (i.e., the forces that contribute to the potential cancel out each other). With respect to binary interactions, specifically mass transfer, the Lagrangian point L1 (or inner Lagrangian point), which is a saddle point of the effective potential (Fig.1.1), plays an important role: if a star fills its Roche lobe, then matter can flow through L1 to the other star. This mass transfer mechanism is called Roche-lobe overflow (RLOF).
Due to the complex geometry of the Roche lobe, approximations are used to model the distance between the star and L1. The effective Roche lobe radius for star '1' (the most massive) with mass M_1 is defined as the radius of a sphere with the same volume of the Roche lobe, and is often approximated using a prescription provided by Eggleton (1983):

$$R_{L,1} = \frac{0.49q^{-2/3}a}{0.6q^{-2/3} + ln(1 + q^{-1/3})} \tag{1.1}$$

which is better than $\approx 1\%$ in all cases. Here $q = M_2/M_1$ is the mas ratio and a the semi-major axis.

With respect to the Roche lobe geometry, we can distinguish three types of binaries:

- **Detached binaries**: both stars fill an equipotential surface that lies within their respective Roche-lobe. Interactions between stars are only carried out by means of tides and stellar winds. The evolution of each star is usually not significantly affected by its companion; therefore, both stars evolve approximately as single stars.

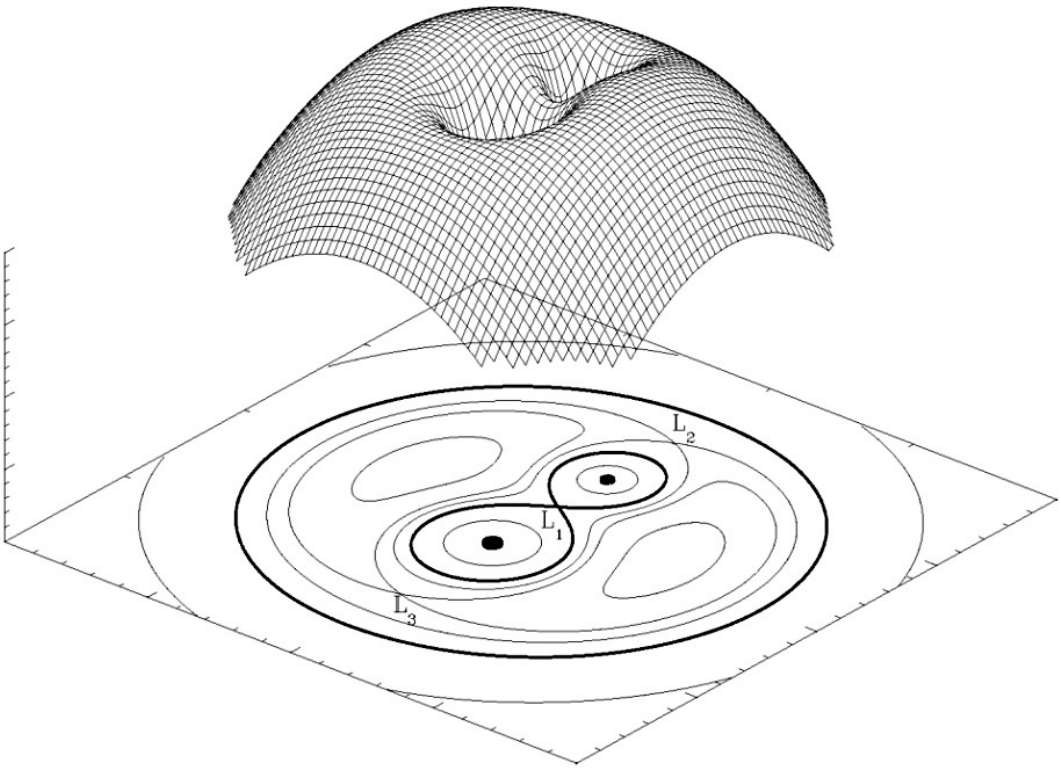

Figure 1.1: Roche lobe geometry for a binary star with a mass ratio of 2 in the co-rotating frame. The 3D surface plot (top) and a contour plot (bottom) show equipotential surfaces and the Lagrangian points L_1, L_2 and L_3. Figure taken from http://hemel.waarnemen.com/Informatie/Sterren/hoofdstuk6.html#h6.2

- **Semi-detached binaries**: one of the stars fills its Roche-lobe. Hydrostatic equilibrium is no longer possible near L1 and matter flows over from this point to the companion. Mass transfer affects considerably the evolution of both stars.
- **Contact binaries**: If both stars fill an equipotential surface just or beyond their Roche-lobes (i.e. beyond L1 but without reaching L2), they can exchange heat as well as mass. The stars are gravitationally distorted and wrapped in a common photosphere.

1.2 Mass transfer in binary systems

For the formation of close binary stars with at least one white dwarf component (which could evolve into SN Ia), mass transfer from one component to the other in

a semi-detached system, matters.
When one of the stars fills its Roche-lobe and mass transfer begins, the evolution of each component and the orbital properties of the system are affected. There are two possible ways to fill the Roche-lobe: the first is due to stellar evolution, in which the more massive star evolves off the main-sequence, and the second by orbital shrinking owing to angular momentum loss (AML). In the latter case, AML occurs due to tidal forces, gravitational waves or magnetic braking. Depending on the structure of the star that looses mass (the donor) and the response of both stars to mass loss/gain, mass transfer can be stable or unstable. In general, mass transfer stability depends mainly on two factors:

- The response of the donor's radius to the mass loss.
- The response of the Roche-lobe radius to the mass loss of the donor.

If the donor stars Roche-lobe overflow mass transfer, then mass transfer will be stable if the donor radius is able to keep its hydrostatic equilibrium by contracting faster than the Roche radius. If, on the other hand, the radius of the donor star becomes greater than the Roche radius (or the Roche radius becomes smaller than the radius of the donor star), mass transfer continues. This case corresponds to the general scenario of unstable mass transfer. The commonly used stability criterion comes from a simplified model of the binary system, where we compare the variation of both the stellar radius (R_d) and the Roche-lobe radius (R_L) of the donor star (with mass M_d) while loosing mass, assuming that the accretor star is an inert mass point (which is a very good assumption if it is a compact object). These variations in both radii are expressed by the so-called mass-radius exponents, defined as:

$$\zeta_d = \frac{d\log(R_d)}{d\log(M_d)} \tag{1.2}$$

$$\zeta_L = \frac{d\log(R_L)}{d\log(M_d)} \tag{1.3}$$

Then, if $\zeta_L \leq \zeta_d$, the system is stable against mass transfer.
Once the donor starts loosing (transferring) mass, both its hydrostatic and thermal equilibrium are disturbed. Since the hydrostatic readjustment occurs on a dynamic time-scale T_{dyn} (which is much shorter than the thermal time-scale T_{th}), the first response of the star can be assumed to be almost adiabatic. Thus, in this scenario mass

transfer will be stable if $\zeta_L \leq \zeta_{ad}$, where ζ_{ad} is the variation of the radius due to mass loss in the adiabatic regime. While mass transfer is stable during the adiabatic regime, the donor is able to recover hydrostatic equilibrium and thermal readjustment becomes relevant. In the thermal regime mass transfer will be stable if $\zeta_L \leq \zeta_{eq}$, where ζ_{eq} is the variation of the radius due to mass loss on the thermal time-scale.
In addition, if simultaneously $\zeta_L \leq \zeta_{eq}$ and $\zeta_L \leq \zeta_{ad}$, then mass transfer is *secularly stable* and it can be driven either by nuclear evolution of the donor star or orbital AML as long as $\zeta_{L,AML} \leq \zeta_{eq}$ and $\zeta_{L,AML} \leq \zeta_{ad}$, where $\zeta_{L,AML}$ is the variation of the Roche-lobe radius due to AML.

The response of the Roche-lobe radius to adiabatic mass loss depends mainly on the binary mass ratio q, while the response of the donor depends critically on the convective or radiative structure of its envelope. If the donor has a radiative envelope it shrinks in response to mass loss ($\zeta_{ad} \gg 0$), and for deeply convective envelopes the donor tends to expand or keep a nearly constant radius ($\zeta_{ad} \leq 0$).

1.2.1 Orbital evolution during mass transfer

Mass transfer also modifies the orbital properties of a given binary system. The total orbital angular momentum and its time derivative for $e = 0$ are:

$$J = \left(M_1 a_1^2 + M_2 a_2^2\right) \frac{G^{1/2}(M_1 + M_2)^{1/2}}{a^{3/2}} \tag{1.4}$$

$$\dot{J} = J\left(\frac{\dot{a}}{2a} - \frac{\dot{M}_{tot}}{2M_{tot}} + \frac{\dot{M}_1}{M_1} + \frac{\dot{M}_2}{M_2}\right), \tag{1.5}$$

where a_1 and a_2 represent the distance of each stellar component from the center of mass, $a = a_1 + a_2$ the semi-major axis and $M_{tot} = M_1 + M_2$ is the total mass of the system. In the simplest case, mass transfer is conservative, i.e., all the mass lost by the donor is accreted by its companion and the orbital angular momentum is conserved. In this scenario, mass transfer shifts the center of mass towards the accretor. The response of the orbital semi-major axis to mass loss can be described as follows:

$$\frac{\dot{a}}{a} = 2\left(\frac{M_d}{M_a} - 1\right)\frac{\dot{M}_d}{M_d}, \tag{1.6}$$

where M_a and M_d are the masses of the accretor and the donor respectively. Since $\dot{M}_d < 0$, the orbit shrinks as long as $M_d > M_a$, reaching a minimum when $M_d = M_a$. On the other hand, if $M_d < M_a$ the orbits expand.

Despite conservative mass transfer is a good first approach to understand the orbital evolution of the binary, a more realistic approach must include the effect of mass and angular momentum lost from the system. If we assume that a fraction β of the transferred mass is retained by the accretor ($\dot{M}_a = -\beta \dot{M}_d$) and that the mass lost by the binary take away a fraction γ of the orbital angular momentum ($\dot{J} = \gamma J \dot{M}_{tot} / M_{tot}$), then equation 1.5 can be written as

$$\frac{\dot{a}}{a} = -2\frac{\dot{M}_d}{M_d}\left(1 - \beta\frac{M_d}{M_a} - (1-\beta)(1/2+\gamma)\frac{M_d}{M_d + M_a}\right). \tag{1.7}$$

Compared to the conservative scenario, it is trivial to derive that in the fully non-conservative mass transfer scenario ($\beta = \gamma = 0$), the orbital semi-major axis always increases.

1.2.2 Common envelope evolution

We have in rather general terms described under which conditions mass transfer occurs and if it is stable or not. If mass transfer is dynamically unstable, it proceeds on the very short dynamical time scale of the donor star ($\approx$ 30 minutes for the Sun). As a consequence, the mass transfer timescale becomes much shorter than the thermal time scale of the accretor. Therefore, the transferred material accumulates in the Roche lobe of the accretor until it also fills its Roche-lobe and a gaseous envelope surrounding both stars is formed. This common envelope (CE) is not necessarily in hydrostatic equilibrium and it is generally assumed that it does not rotate at the same rate as the binary. This has two important consequences:

- The CE is not constrained by the equipotential surface passing through the L1-L2 Lagrangian point.
- Drag forces inside the CE remove orbital energy from the stars, heating up and expanding the envelope. This energy transfer causes the binary orbit to shrink as the two stars spiral-in towards their common center of mass until the CE is expelled. This either leads to the formation of a very close binary star or the coalescence of the two stars.

The general description given above is the most accepted scenario to describe the CE phase, in which the main uncertainty is how efficient orbital energy is used to eject the envelope. In this context, the most commonly used model is the so called $\alpha_{\rm CE}$-formalism, in which

$$\alpha_{\rm CE} = \frac{\Delta E_{gr}}{\Delta E_{orb}} \tag{1.8}$$

is defined as the fraction of the change in orbital energy $\Delta E_{orb} = E_{orb,i} - E_{orb,f}$ (subscripts i and f respresent the initial and final stages respectively) available to expand and eject the envelope, which experiments a change of gravitational energy $\Delta E_{gr} = E_{gr,i} - E_{gr,f}$ (complete ejection corresponds to $E_{gr,f} = 0$). Different prescriptions have been used to model the final and initial values of orbital and gravitational energy. According to the PRH (Podsiadlowski-Rappaport-Han) prescription (Zorotovic et al., 2010) the final orbital energy is calculated as the orbital energy between the core of the donor ($M_{d,c}$) and the accretor (M_a) at the final separation (a_f):

$$E_{orb,f} = \frac{1}{2}\frac{GM_{d,c}M_a}{a_f}, \tag{1.9}$$

while the initial orbital energy is calculated as the orbital energy between the donor and the accretor at the initial separation (a_i):

$$E_{orb,i} = \frac{1}{2}\frac{GM_dM_a}{a_i}. \tag{1.10}$$

The initial gravitational energy of the envelope is calculated as being between the envelope mass ($M_{d,e}$) and the mass of the donor (M_d):

$$E_{gr,i} = \frac{1}{\lambda}\frac{GM_dM_{d,e}}{R}, \tag{1.11}$$

where R is the donor star radius and λ depends on the internal structure of the donor star.

A second prescription called ILY (Iben-Livio-Yungelson, Zorotovic et al. 2010) takes the gravitational energy of the envelope as being between the envelope mass and the combined mass of the cores of the donor and accretor stars:

$$E_{gr,i} = \frac{G(M_{d,c} + M_a)M_{d,e}}{2a_i} \tag{1.12}$$

and the initial orbital energy as the orbital energy between the core of the donor and the accretor at the initial binary separation

$$E_{orb,i} = \frac{1}{2}\frac{GM_{d,c}M_a}{a_i}. \tag{1.13}$$

The main difference between the two prescription is the presence of λ, which can lead to high values of gravitational energy for PRH compared to IYL. Hydrodynamic simulations of common envelope evolution that follow the entire process are currently not available because of the complexity of the process. Therefore the common envelope efficiency is usually constrained by observations and, at least for systems with low-mass secondary stars, evidence is growing that $\alpha_{\rm CE}$ is relatively small (e.g. Zorotovic et al., 2010).

1.3 Supernova type Ia

In general terms, a supernova is the explosion of a star. This event is extremely energetic and their light curves can show peaks of luminosities of about $10^{43} ergs/s$ which decline on time-scales of weeks or months. There are two main types of supernova: (1) Core collapse supernovae correspond to the rapid collapse during the final stage in the evolutionary path of massive stars and (2) supernovae type Ia (hereafter SNe Ia), which are caused by the thermonuclear explosion of an accreting white dwarf approaching the Chandrasekhar mass limit of $\approx 1.44 M_\odot$.

SNe Ia have been very useful as standard distance candles to map out the extragalactic distance scale, providing evidence for the accelerating expansion of the Universe. The use of SNe Ia as standard candles relies on the facts that: (1) their light curves seem to result from the same physical process and (2) there is an empirical relation between the peak luminosity and the shape of the supernova light curve.

Despite their importance, the mechanisms and progenitors that trigger SNe Ia are still controversial. The general consensus is that SNe Ia are thermonuclear explosions of carbon-oxygen white dwarfs with masses near the Chandrasekhar mass limit at $\approx$

$1.44\,M_\odot$. This causes the ignition of carbon in the degenerated core, which completely destroys the white dwarf.

The two classical channels involving a white dwarf near the Chandrasekhar mass limit are the so called single-degenerated (SD) and double-degenerated (DD) channel. In the SD channel, the white dwarf accretes mass from a non-degenerate companion star until, close to the Chandrasekhar mass, the very high density results in the ignition of the carbon which triggers a thermonuclear runaway that destroys the white dwarf. The DD channel involves two carbon white dwarfs that merge due to loss of angular momentum by emission of gravitational waves. In order to reach the mass limit, the combined mass of both white dwarfs must be equal or greater to $1.44\,M_\odot$.
In the following we will summarize the most relevant *pros* and *cons* for both the SD and DD channels.

- SD *pros*
  - There are observed systems where the mass transfer rate is high enough to allow the material accreted by the white dwarf to be stably burned on its surface, thereby increasing the white dwarf mass. These systems are called *Supersoft X-ray Sources* (SSSs) and represent a direct path to produce SN Ia if the high mass transfer rate can be sustained until the white dwarf is dense enough to ignite carbon.
  - It can explain the presence of calcium, sodium, and other absorption lines possibly associated with a non-degenerate donor star (Patat et al., 2007; Simon et al., 2009; Sternberg et al., 2011; Dilday et al., 2012).
- SD *cons*
  - The accretion rate on the WD must be in a narrow range in order to avoid nova events (low accretion rate) and red-giant-like expansions (high accretion rate), which produce mass loss.
  - The predicted *delay time distribution* (SN Ia rate versus the time that would follow a brief burst of star formation; Maoz & Mannucci 2012), or DTD, drops drastically after a few Gyr. This can be understood as follows: as we move towards low mass WD progenitors, the mass transfer required to reach the Chandrasekhar mass must be greater. Low-mass donors do not meet the required quantities of mass and transfer rates, so only relatively massive short-lived stars can provide the necessary conditions.

- DD *pros*
  - The absence of hydrogen and helium in observed SN Ia spectra emerges as a natural consequence in a C-O WD merger.
  - It explains the presence of systems with short and long time delays, which come from the timescales required to form WDs and mergers (taking into account only gravitational radiation effects), respectively.
- DD *cons*
  - It is uncertain whether the WD merge can lead to a SN Ia or rather an accretion-induced collapse that ends with a neutron star (Nomoto & Kondo, 1991).
  - Despite the large amount of confirmed WD binaries (e.g Saffer et al., 1998), the discovery of a system with a total mass $> 1.4\,M_{\odot}$ has remained elusive.

1.4 Dynamical evolution of hierarchical triple systems

Detached binaries with orbital periods $P_{orb} \approx 100$ days can evolve into close binaries ($P_{orb} \lesssim 16$ days) mainly by means of tidal interactions. However, such a close configuration can also be achieved with a third companion perturbing the orbital properties of the binary (see e.g. Eggleton & Kisseleva-Eggleton, 2006; Naoz, 2016; Hamers & Portegies Zwart, 2016b). In what follows we present the effect of such perturbations, the so called Von Zeipel-Lidov-Kozai oscillations, introducing its physical formalism and variants.

1.4.1 The standard Von Zeipel-Lidov-Kozai Mechanism

Main-sequence triple systems usually have hierarchical configurations, which means that the orbital size of the inner binary is much smaller than that of the third star around the center of mass of the inner binary (i.e. the outer orbit). This configuration prevents the third companion from significantly perturbing the inner orbit on timescales of the order of the outer orbital period, keeping the orbits Keplerian. Even though the system is in a state of secular dynamic stability, the weak (but constant)

interaction between the third companion and the inner stars can produce long-term changes in both inner and outer orbits.

Historically, the secular-three body problem was independently studied in the early sixties by Lidov (1962), which studied the evolution of artificial satellites around the moon being perturbed by the Earth, and Kozai (1962) for the case of asteroids orbiting the Sun and being perturbed by Jupiter. In addition, Ito & Ohtsuka (2019) confirmed that already in the late nineteenth to early twentieth century there was a pioneering work by the Swedish astronomer Edvard Hugo von Zeipel on the secular-three body problem using a similar analysis as Lidov and Kozai.

Assuming a hierarchical configuration, the three-body Hamiltonian can be written as the sum of three main terms: (1) the Hamiltonian of an isolated ("inner") binary with point masses M_1 and M_2, (2) another isolated ("outer") binary with point masses $(M_1 + M_2)$ and M_3, and (3) a perturbative term representing the interaction between the inner and outer orbits (H_p):

$$H = \frac{G^2 M_1 M_2}{2a_{in}} + \frac{G^2 M_3 (M_1 + M_2)}{2a_{out}} + H_p\,, \tag{1.14}$$

where G is the gravitational constant, M_1, M_2 the masses of the objects in the inner binary and M_3 the mass of the outer companion. Since the triple system is hierarchical ($\alpha \equiv a_{in}/a_{out} \ll 0$) the perturbative term can be expanded in orders of α using Legendre polynomials as follows:

$$H_p = \sum_{n=2}^{\infty} \left(\frac{a_{in}}{a_{out}}\right)^n \left(\frac{r_{in}}{a_{out}}\right)^n \left(\frac{a_{out}}{r_{out}}\right)^{n+1} M_n P_n(cos\Phi). \tag{1.15}$$

In this expression P_n are the Legendre polynomials, r_{in} the relative position vector from M_1 to M_2, r_{out} the relative position vector of M_3 from the centre of mass of the inner binary, Φ the angle between r_{in} and r_{out} (Fig.1.2), and

$$M_n = M_1 M_2 M_3 \frac{M_1^{n-1} - (-M_2)^{n-1}}{(M_1 + M_2)^n}. \tag{1.16}$$

In general, a hierarchical triple system is well described by the lowest (n=2) order term in 1.15. This is called the quadrupolar expansion. However, still for a non-negligible fraction of triple systems, the octupolar expansion, i.e. when n=3, is required for an adequate description. High order terms, with n equal or greater than 4, are expected to be important only when the ratio between the inner and outer semi-major axis is larger. However, in this regime hierarchical triples are not expected to be dynamically stable (Hamers, 2012). Therefore, we can properly characterize the

orbital evolution of hierarchical triples if we consider the pertubative term up to the octupolar expansion.

The right panel of Figure 1.2 shows the coordinate system that is usually used to derive the secular expansion of the three-body Hamiltonian. In this referential frame, the total angular momentum G_{tot} lies in the vertical axis, and the plane perpendicular to the total angular momentum is known as the invariable plane. G_1, and G_2 are the inner and outer orbital angular momenta, and H_1 and H_2 are their vertical components. The total angular momentum is therefore equal to the sum of both vertical components. As a consequence of the quadrupolar expansion, the outer angular momentum G_2 is constant, which in turn implies that the outer eccentricity is also a conserved quantity. The conservation of G_2 means that the system is symmetric for the rotation of the outer orbit. For that reason, the quadrupolar approximation should be used only for an axisymmetric outer potential such as circular outer orbits. For triple systems with outer eccentric orbits, the octupolar approximation is more adequate.

The works of Lidov and Kozai explore the secular three body problem up to the quadrupolar expansion, and considered the case in which one of the objects in the inner binary has a negligible mass compared with the other two objects in the system. In this regime, called the test particle quadrupole (TPQ) approximation, the total angular momentum is much larger than the inner angular momentum, which in turn means that the vertical component of each orbit's angular momentum (H_j, $j = 1, 2$) is conserved. This implies the possibility of an exchange between inclination and eccentricity, as $H_j \propto \sqrt{1-e_j}\cos i_j$. These interactions are known as the Zeipel-Lidov-Kozai oscillations. For the particular case when the initial inner eccentricity and the argument of periapsis are zero, the maximum inner eccentricity is given by $e_{max} = \sqrt{1-(5/3)\,cos^2(i_{tot,0})}$, and solving for the cosine of the mutual inclination $i_{tot,0}$ between the inner and outer orbits it is found that the oscillations take place for angles between 39.2 and 140.77 degrees. These are known as the Kozai angles.

According to Li et al. (2015) the timescale of the eccentricity (inclination) oscillations is given by:

$$t_{SKM} = \frac{2\pi a_{out}^3 (1-e_{out}^2)^{3/2}\sqrt{(M_1+M_2)(1-e_{in}^2)}}{G^{1/2} a_{in}^{3/2} M_3}, \tag{1.17}$$

which in most hierarchical triples is at least ten times longer than the outer orbital period of the triple. For a triple system with $a_{in} = 5\,\mathrm{au}$, $a_{out} = 20\,\mathrm{au}$, $M_1 = 1\,M_\odot$, $M_2 = 0.5\,M_\odot$, $M_3 = 0.5\,M_\odot$ and $e_{out} = e_{in} = 0$ the value of t_{SKM} is about 30 times

longer than the outer period ($\approx 63\,\mathrm{yr}$).

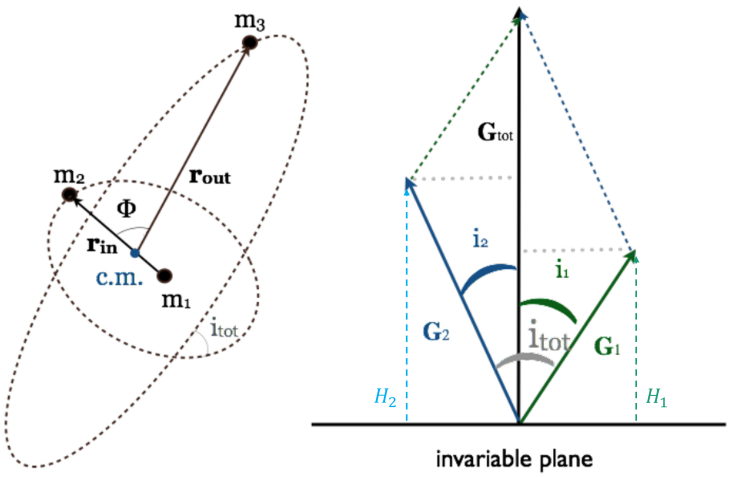

Figure 1.2: Left panel: Schematic description of the used coordinate system. The term "c.m." correspond to the center of mass between M_1 and M_2. **Right panel**: Schematic description of the invariable plane. Here G_{tot} corresponds to the total angular momentum vector, which is the sum of the angular momentum vector of the inner and outer orbits, i.e. G_1 (with angle i_1 respect to G_{tot}) and G_2 (with angle i_2 respect to G_{tot}) respectively, while H_1 and H_2 are their respective vertical components relative to the invariable plane. Figure adopted from Naoz (2016).

1.4.2 The eccentric Von Zeipel-Lidov-Kozai Mechanism

Although the quadrupolar approximation allows to describe new behaviours for the secular three-body problem, its limitation of being accurate only for circular outer orbits is insufficient to characterize the evolution of the whole population of triple systems, and may overlook other interesting effects. In fact, for nonzero outer eccentricities, the octupolar expansion can produce inner orbital flips relative to the total angular momentum (i_1 passing through 90 deg) and inner eccentricities close to 1 for initial mutual orbital inclinations outside the classic ZLK range between 39.2-140.77 deg derived in the TPQ approximation. Given that the outer orbit is eccentric, this evolutionary pathway is known as the eccentric Von Zeipel-Lidov-Kozai (eZLK) mechanism.

Without loss of generality, the octupolar expansion of the three-body Hamiltonian can be expressed as

$$F = F_q + \epsilon_{oct} F_{oct}, \tag{1.18}$$

where F_q represents the Hamiltonian up to the quadrupolar approximation, F_{oc} the new contribution to the Hamiltonian due to the octupolar approximation, and

$$\epsilon_{oct} = \left(\frac{M_1 - M_2}{M_1 + M_2}\right)\left(\frac{a_1}{a_2}\right)\frac{e_{out}}{1 - e_{out}^2} \tag{1.19}$$

measures the impact of the octupolar term on the orbital evolution of the system relative to the quadrupolar term. In general, it is assumed that the octupolar term plays a relevant role in the dynamics of the system when epsilon is $\gtrsim$0.001-0.01 (e.g. Naoz et al., 2011; Shappee & Thompson, 2013).

Figure 1.3 shows two configurations for a triple system with $\epsilon_{oct,1} = 0.03$ (left panels) and $\epsilon_{oct,2} = 0.06$ (right panels) illustrating that the TPQ approximation is not capable of capturing the flip and the extremely high values of eccentricity that even occur for an initial inclination of 1°. Another interesting effect in the octuple approximation is that beyond the Kozai angles the flips occur on a much shorter timescale. According to Li et al. (2015), the timescale for these extremely high inclinations and orbital flips is

$$t_{EKM} = \frac{t_{SKM}}{\epsilon_{oct}}. \tag{1.20}$$

Since hierarchical triples tend to have $\epsilon_{oct} << 1$, the eZLK timescale is longer than the standard ZLK timescale. Following the same triple systems used in the previous

section but using $e_{out} = 0.2$, the value of t_{EKM} is $\approx 1\,600$ times longer than the outer period.

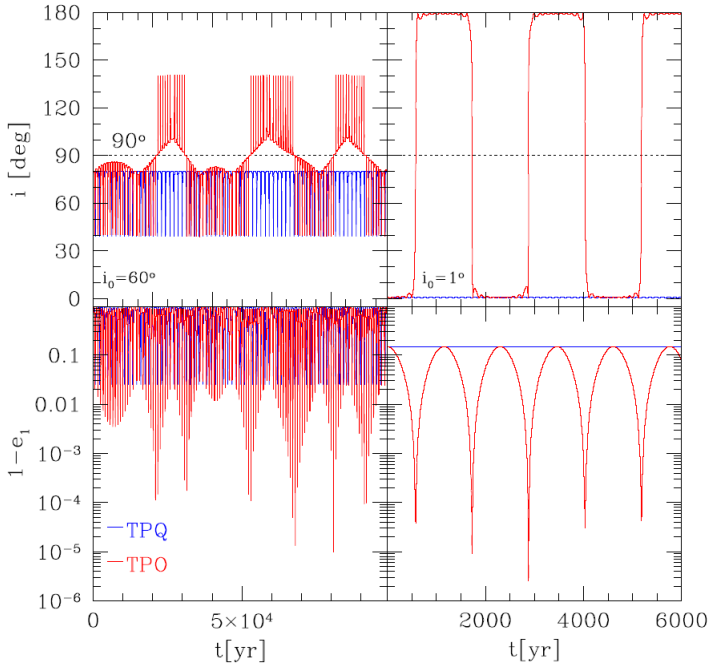

Figure 1.3: Comparison of the time evolution of inclination (top panels) and eccentricity (bottom panels) for the TPQ (blue line) and TPO (red line) approximations. The example considers a test particle at 135 AU around a $10^4 M_\odot$ black hole located 0.03 pc from a $10^6 M_\odot$ massive black hole. The initial configuration for the left panels is $e_{in} = 0.01$, $e_{out} = 0.7$, $i = 60°$, $\Omega_{in} = 60°$ and $\omega_{in} = 0°$. In the right panels the system is initially set with $e_{in} = 0.85$, $e_{out} = 0.85$, $i = 1°$, $\Omega_{in} = 180°$ and $\omega_{in} = 0°$. Figure taken from Naoz (2016).

1.4.3 ZLK Mechanism with tidal friction

When high eccentricities due to ZLK oscillations make the inner periapsis distance comparable to the stellar radii, tidal friction absorbs orbital energy and its period can be shortened by $\approx$1-2 orders of magnitude after formation. Harrington (1968) first suggested that Kozai cycles with tidal friction play an important role in the secular evolution of triple stars. Eggleton & Kisseleva-Eggleton (2006) explicitly suggested that this might produce many close or contact binaries. They also show that the effect of the apsidal motion due to either general relativity (GR) or the quadrupolar distortion of the components due to rotation may reduce the initial inclination and

the maximum eccentricity predicted in the TPQ approximation. Indeed, if the apsidal precession due to GR and/or tides occurs in the opposite direction than that of the ZLK mechanism, eccentricity oscillations can be suppressed, depending mainly on the different precession timescales involved. If the GR or tidal precession timescale is shorter than the precession timescale due to the ZLK mechanism, then high eccentricities and orbital flips can be suppressed, allowing the inner orbit to have enough time to shrink and being decoupled from the perturbation of the third companion, remaining on a small quasi-stable orbit. This scenario is depicted in the left panel of Fig. 1.4. If in contrast the eccentricity is excited on timescales much shorter than the GR or tidal precession, then the orbit can become almost radial and tides will not be faster enough to shrink the orbit, causing that the pericenter distance may be shorter than the Roche limit, producing mergers or collisions (e.g. see right panel of Fig. 1.4).

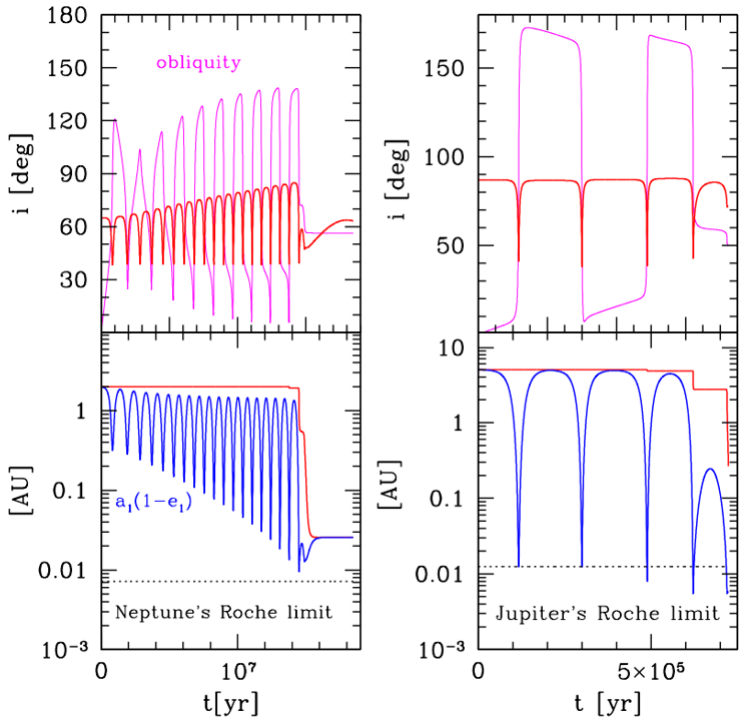

Figure 1.4: Left panel: Evolution of the obliquity (magenta line), mutual inclination (top red line), inner semi-major axis (bottom red line) and distance at pericenter (blue line) for a triple system composed of a Neptune-mass planet around a 0.32 $M_\odot$ star, with initial inner semi-major axis and eccentricity $a_1 = 2$ au and $e_1 = 0.01$ respectively. The tertiary companion is a brown dwarf with mass $m_3 = 10 M_j$ at 50 au, eccentricity $e_2 = 0.52$ and mutual inclination with respect to the inner binary $i = 65$ deg. At $\approx 1.4 \times 10^7$ yr tidal forces become strong enough to start shrinking the orbit until the ZLK oscillations timescale ($t_{ZLK} \propto a_2^3/a_1^{3/2}$) is sufficiently large to barely affect the dynamical evolution of the system. **Right panel**: Similar to left panel, but for an inner binary composed of a Jupiter-mass planet orbiting a solar-mass star at 5 au. The tertiary companion is another solar-mass star at 200 au with $e_1 = 0.001$, $e_2 = 0.75$ and $i = 87$ deg. In this configuration, the ZLK oscillation timescale is shorter than the GR/tidal precession timescale, preventing the tides from having enough time to shrink the inner orbit before the eccentricity reaches a value close to 1. This causes the distance at pericenter to be less than the Roche limit of the star, i.e. the brown dwarf is engulfed by its host star. Figure taken from Naoz (2016).

1.5 This thesis

Mass-transfer-related events, such as common envelope (CE) evolution, are fundamental to understand binary evolution. In particular, all channels expected to produce SNe Ia, grouped either in the single degenrate (SD) or double degenerate (DD) scenario, invoke CE evolution to produce a close binary composed of a white dwarf and main-sequence companion (WD+MS binaries) which will evolve through thermal-timescale mass transfer (SD scenario) or a second common envelope phase to form a close compact white dwarf binary (DD scenario). Therefore, a proper modeling of the CE phase (through the $\alpha_{\rm CE}$-formalism) is fundamental to constrain SNe Ia channels. This is, however, not an easy task, since the CE efficiency parameter α_{CE} (the most important parameter to model the CE phase together with λ) is not well characterized and depends on the assumed energy sources involved in the ejection of the envelope. To deal with this situation, observational efforts have been made during the last two decades to collect and characterize a large population of WD+MS binaries, managing to restrict the possible values of α_{CE} for white dwarfs with M-type companions. For white dwarfs with more massive companions, it is still uncertain whether they can be understood using a similar value or whether a different efficiency is required compared to WD+MS binaries with M-type stars. This poses a critical problem in the modeling of SNe Ia channels, since stars with masses $\gtrsim 1 M_\odot$ will allow the white dwarf to accrete enough mass to produce SNe Ia in the SD scenario or the formation of a second (and massive enough) CO white dwarf in the DD scenario.

In order to improve with this situation, an international group of (both theoretical and observational) experts in binary systems began a survey aimed to find post common envelope binaries consisting of a white dwarf and a main-sequence companion of spectral type A, F, G or K (WD+AFGK binaries) by combining optical/ultraviolet surveys with spectroscopic follow up. So far, six WD+AFGK binaries have been discovered, and along with them, four triple systems with the white dwarf being the third companion, or active stars rather than a white dwarf (i.e. non-WD+AFGK binaries). Continuing the work done during my master's thesis (and presented in Lagos et al. (2020)), the second chapter of this thesis presents the characterization of three of those triple systems, their expected fraction in the sample of WD+AFGK binaries and how their orbital properties suggest the possibility of an alternative channel to the CE phase for the formation of wide WD+AFGK binaries: stable-non-conservative mass transfer.

In chapter three, we test binary evolution models on the formation of EL CVn binaries, eclipsing binaries that contain an A- or F-type star and a very low mass helium white dwarf precursor, which are expected to form through stable-non-conservative mass transfer instead of CE evolution. This evolutionary channel implies a narrow and well-defined range of main-sequence progenitor systems with orbital periods less than 3 days in most of the cases. This remarkable feature implies that if binary models are correct, virtually all EL CVn binaries should have a tertiary companion, as it is well known that practically all main-sequence binaries with orbital periods less than three days are inner binaries of triple systems. With this idea in mind we look for additional companions around five EL CVn, finding in all of them detections consistent with tertiary stars. As in Chapter two, the research I performed shows the potential of triple systems as probes of binary evolution models.

Finally, in Chapter four we show how common envelope evolution is able to explain, under certain conditions, the short (≈ 1.4 days) orbital period of the first planet candidate orbiting a white dwarf. Furthermore, as the white dwarf is the outer third companion of a triple system, we also investigate the dynamical effect of the inner binary on the evolution of the planet candidate and how this may have helped to trigger a common envelope phase.

Chapter 2

The White Dwarf Binary Pathway Survey VII: Evidence for a bi-modal distribution of post mass transfer systems?

Binary systems consisting of a white dwarf and a main-sequence companion with orbital periods up to ≈ 100 d are often thought to be formed through common envelope evolution which is still poorly understood. To provide new observational constraints on the physical processes involved in the formation of these objects, we are conducting a large-scale survey of close binaries consisting of a white dwarf and an A to K-type companion. Here we present three systems with eccentric orbits and orbital periods between $\approx 10 - 42$ d discovered by our survey. Based on *HST* spectroscopy and high angular resolution images obtained with SPHERE-IRDIS, we find that two of these systems are most likely triple systems while the remaining one could be either a binary or a hierarchical triple but none of them is a post common envelope binary (PCEB). The discovery of these systems shows that our survey is capable to detect systems with orbital periods of the order of weeks, but all six PCEBs we have previously discovered have periods below 2.5 d. We suggest that the fact that all of the systems we identify

with periods of the order of weeks are not PCEBs indicates a transition between two different mechanisms responsible for the formation of very close ($\lesssim 10\,\mathrm{d}$) and somewhat wider WD+AFGK binaries: common envelope evolution and non-conservative stable mass transfer.

2.1 The White Dwarf Binary Pathways Survey and the discovery of triple systems

Observational and theoretical population studies of close binaries with white dwarf components are fundamental to progress with our understanding on their formation and evolution, with potentially deep implications for the predicted occurrence rates of systems as important as the progenitors of type Ia supernovae.

Close white dwarfs binaries are believed to form mainly through common envelope (CE) evolution (e.g. Webbink, 1984; Zorotovic et al., 2010; Ivanova et al., 2013) which occurs when the more massive ($\gtrsim 1\mathrm{M}_{\odot}$) star of an initial main-sequence binary becomes a giant that is filling its Roche lobe, which triggers dynamically unstable mass transfer. As the mass transfer time scale is shorter than the thermal time scale of the companion, a common envelope forms engulfing the core of the giant star and the companion. Drag forces between the companion and the envelope drive transfer of orbital energy and angular momentum from the orbit of the core of the giant and its companion to the envelope until the latter is fully ejected. The close binary emerging from CE evolution, i.e. the post common envelope binary (PCEB), consists of a white dwarf and a main-sequence companion star also known as the secondary star (e.g. Parsons et al., 2015).

Despite its importance for close compact binary formation theories, CE evolution is still not fully understood and its physical modelling is frequently simplified by using energy and angular momentum conservation equations involving free parameters that must be fitted through observations. Previous surveys have shown that close white dwarf binaries with M dwarf companions form through CE evolution and led to important constraints on the CE efficiency α_{CE}, which corresponds to the fraction of orbital energy that is used to unbind the envelope of the white dwarf progenitor. Evidence is accumulating that for PCEBs with M dwarf companions α_{CE} is rather small, i.e. between 0.2 and 0.3 (e.g. Nelemans et al., 2000; Zorotovic et al., 2010; Nebot Gómez-Morán et al., 2011a; Toonen & Nelemans, 2013). To progress with our under-

standing of CE evolution it is important to investigate the evolutionary history not only of PCEBs with M dwarfs but over a wide range of companion masses as this may either allow to derive constraints on a universal value for the CE efficiency or indicate the existence of processes that are not included in the simple energy equation.

To that end, we began a large scale survey of close white dwarfs with main sequence star companions of spectral type A, F, G, or K (WD+AFGK binaries). This survey is using the following strategy. As the white dwarf is outshone by the AFGK stars at optical wavelengths, we combined spectroscopic surveys with the Galaxy Evolution Explorer (*GALEX*) database (Bianchi et al., 2011, 2017) to identify AFGK stars with ultraviolet (UV) excess as indicative of a potential white dwarf companion (Parsons et al., 2016; Rebassa-Mansergas et al., 2017; Ren et al., 2020). We then use radial velocity measurements to identify close binary systems among our candidates. If radial velocity variations indicate the close binary nature of a given object, we then finally measure the orbital periods of those WD+AFGK candidate systems. We rely on *H*ST spectroscopy to confirm that the UV excess is indeed coming from a white dwarf and to measure the mass of the white dwarf.

Following this strategy, we have so far identified the first pre-supersoft X-ray binary system (Parsons et al., 2015), confirmed that our target selection is reliable and in virtually all cases the UV excess is indeed indicative of a white dwarf (Parsons et al., 2016), published the first results of our radial velocity campaign (Rebassa-Mansergas et al., 2017), estimated the limited contamination from triple systems motivated by the discovery of the first hierarchical triple system in the survey (Lagos et al., 2020), and identified and characterised 26 new close WD+AFGK systems (Ren et al., 2020) through radial velocity variations. Most importantly for this work, we measured the periods of six systems and found all of them to be PCEBs with periods below 2.5 days and circular orbits. We reconstructed their evolutionary history and found all of them to be consistent with a small common envelope efficiency (Parsons et al., 2015; Hernandez et al., 2021; Hernandez et al., 2022), in agreement with what was found for PCEBs with M dwarf companions (Zorotovic et al., 2010; Nebot Gómez-Morán et al., 2011a).

Here we show that our observing strategy does permit the identification of systems with longer orbital periods of the order of several weeks. We present the period determination of three systems, i.e. 2MASS J06281844-7621467, TYC 6996-449-1 and TYC 8097-337-1 (hereafter 2MASS J0628, TYC 6996 and TYC 8097 respectively), and find their orbital periods to be between 10 and 42 days and their orbits to be eccentric.

Using high resolution spectroscopy at optical wavelengths we constrain the stellar properties of the AFGK star, while with high-contrast imaging in the infrared we look for additional companions that could potentially cause eccentric orbits, for instance, through Von Zeipel-Lidov-Kozai oscillations (e.g. Naoz, 2016). We find that one systems (TYC 6996) is most likely a hierarchical triple system with the white dwarf being the distant tertiary. In the case of 2MASS J0628, HST spectroscopy does not detect a white dwarf and the UV excess is most likely caused by stellar activity of a lower mass main sequence star. For TYC 8097, given the current available data, we conclude that it could be a triple similar to TYC 6996, or a binary system with an M or K-type companion. In case of the latter, the UV excess comes either from stellar activity or an active background galaxy.

The fact that all systems from our survey where we measured a period of the order of weeks are not PCEBs, while all systems with periods of less than 2.5 days turned out to be PCEBs, provides crucial constraints on common envelope evolution with potentially deep implications for our understanding of SN Ia progenitor channels.

2.2 Observations

We performed high resolution spectroscopic and high contrast imaging observations of three targets that have been identified as WD+AFGK candidates by correlating optical surveys and *GALEX* data. In what follows we describe the details of our observational set-ups and the data reduction.

2.2.1 Du Pont echelle

We used the high resolution echelle spectrograph (1 arcsec slit, $R \simeq 40\,000$) on the 2.5-m Du Pont telescope located at Las Campanas Observatory, Chile to obtain spectra of our targets. Each science observation was bracketed by ThAr spectra to correct for instrumental drift. However, we place a lower limit on the velocity precision in a single spectrum of $0.5\,\mathrm{km\,s^{-1}}$ due to the unstable nature of the spectrograph. Standard data reductions were performed and the spectra optimally extracted and wavelength calibrated using the Collection of Elemental Routines for Echelle Spectra (CERES) package (Brahm et al., 2017).

2.2.2 FEROS

High resolution spectra were obtained with the FEROS echelle spectrograph ($R \simeq 48\,000$) on the 2.2-m Telescope at La Silla, Chile (Kaufer & Pasquini, 1998). FEROS covers the wavelength range from $\simeq$ 3 500 Å to $\simeq$ 9 200 Å. Observations were performed in Object-Calibration mode where one fibre is placed on the target while the other feeds light from a ThAr+Ne calibration lamp permitting velocity measurements to extremely high precision ($\simeq 10\,m/s$) and allowed us to correct for instrumental drift throughout the night. FEROS data were reduced using the CERES package.

2.2.3 CHIRON

Spectra were also obtained with the CHIRON echelle spectrometer (Tokovinin et al., 2013) on the 1.5-m SMARTS telescope at Cerro Tololo, Chile. We used 3×1 binning resulting in $R \simeq 40\,000$. CHIRON observations are automatically reduced by the CHIRON team using standard reduction methods. Like the Du Pont observations, we place a lower limit on the velocity precision in a single spectrum of $0.5\,\mathrm{km\,s^{-1}}$.

2.2.4 UVES

Additional spectra were obtained with UVES (Dekker et al., 2000), a high resolution echelle spectrograph mounted on the 8.2-m European Southern Observatory Very Large Telescope at Cerro Paranal, Chile. We used the dichroic 1 setup (390+564) with a 0.7 arcsec slit, resulting in $R \simeq 50\,000$. The data were reduced using the UVES data reduction pipeline (version 5.8.2). A $0.5\,\mathrm{km\,s^{-1}}$ lower limit was placed on the velocity precision in a single spectrum.

2.2.5 HST spectroscopy

We spectroscopically observed 2MASS 0628 with the Hubble Space Telescope (*HST*) in order to confirm that the UV excess is due to a white dwarf companion. We obtained four spectra with the Space Telescope Imaging Spectrograph (STIS) on 2021 April 23 under the program GO 16224 using the G140L grating ($R \sim 1\,000$), covering the wavelength range from $\simeq$ 1 150 Å to $\simeq$ 1 700 Å. 1D spectra were extracted with CALSTIS-6 – Version 3.4.2 from the bias-subtracted and flat-corrected FLT files, which were downloaded from the STScI archive. We forced the search to be performed around pixel 400 in the spatial axis, allowing a search of only 30 pixels. The location of the spectra

was found to be around the pixel 404. The spectrum was extracted from a box with a width of 11 pixels, while background regions were extracted from boxes above and below the spectrum with sizes of seven pixels. These regions were scaled to the size of the spectrum region.

2.2.6 High contrast imaging

The three eccentric systems were observed with the high contrast imager VLT/SPHERE (Beuzit et al., 2019) under the programme 100.D-0399. Acquisition of direct imaging with the N-ALC-YJH-S coronagraph was made in the IRDIFS observing mode, which includes IRDIS dual band imaging (Dohlen et al., 2008a; Vigan et al., 2010b) plus the integral field spectrograph working in Y-J mode (Claudi et al., 2008). For IRDIS dual-band filters $H2$ ($\lambda_{H2} = 1593$ nm) and $H3$ ($\lambda_{H3} = 1667$ nm) were used. Furthermore, the pupil tracking mode was implemented in order to perform angular differential imaging (ADI, Marois et al., 2006a).

The IRDIS data were first pre-processed (dark background subtraction, flat-fielding, bad-pixels correction) with the VLT/SPHERE python package[1] version 1.4.3 (Vigan, 2020). The frames were recentred based on star centre exposures using the four satellite spots. After pre-processing, and without any post-processing technique to remove speckle patterns produced by the coronograph, we detected one potential companion around 2MASS 0628 at 0.31 arcsec from the binary. We used the principal component analysis (PCA) algorithm available in the VORTEX IMAGE PROCESSING (VIP, Gomez Gonzalez et al., 2017; Amara & Quanz, 2012; Soummer et al., 2012) python package to look for fainter companions, finding one companion around TYC 6996, which is partially visible on the edge of the IRDIS field of view, and two extended sources in TYC 8097 (see Figure 2.1).

2.3 Stellar and binary parameters

From the observations, we derived basic binary and stellar parameters for all three systems. The orbital periods can be derived from our radial velocity measurements, the spectra also provide tight constraints on the nature of the secondary star in all three systems, and the SPHERE high-contrast imaging provides information on the potential triple nature of our targets.

[1] `https://github.com/avigan/SPHERE`

2.3.1 Orbital characterisation

Radial velocities were computed from all our echelle spectra using cross-correlation against a binary mask representative of a G2-type star (see Brahm et al. 2017 for more information). Barycentric correction was applied using ASTROPY (Astropy Collaboration et al., 2018). A full list of radial velocity measurements is given in Tables A.1, A.2 and A.3 for 2MASS J0628, TYC 8097, and TYC 6996 respectively in the Appendix.

In order to determine the orbital components of each system ($P_{\rm orb}$ - orbital period, e - eccentricity, K_2 - radial velocity semi-amplitude, γ - systemic velocity, T_P - time of periastron and ω - argument of periastron) we fitted the radial velocities using EXOFAST (Eastman et al., 2013). For all three targets a clear best fit was found. Uncertainties on the orbital components were determined using the Markov Chain Monte Carlo (MCMC) method (Press et al., 2007) implemented using the python package EMCEE (Foreman-Mackey et al., 2013), where the best fit parameters from EXOFAST were used as the starting values in the fit. The result of these fits and the radial velocity curves are shown in Table 2.1 and Figure 2.1 respectively, where from the latter it is clear that the shape of the three radial velocity curves correspond to eccentric orbits.

2.3.2 Characterisation of the AFGK stars

The CERES pipeline provides an initial estimate of the stellar parameters of the AFGK star, but only over a narrow parameter range relevant for main-sequence stars. In order to determine more accurate and precise stellar parameters for the AFGK stars in our systems we followed the method outlined in Hernandez et al. (2021), whereby the high-resolution echelle spectra were fitted using iSpec (Blanco-Cuaresma et al., 2014) to determine the effective temperatures $T_{\rm eff,AFGK}$, surface gravities ($\log g_{\rm AFGK}$) and metallicities [Fe/H] ($Z_{\rm AFGK}$), which were then used as priors when fitting the optical and infrared spectral energy distribution (SED) of the star in conjunction with the *Gaia* EDR3 parallaxes (Gaia Collaboration et al., 2020) to determine the radius ($R_{\rm AFGK}$). See Hernandez et al. (2021) for a more detailed description of this fitting process. Combining $R_{\rm AFGK}$ and $\log g_{\rm AFGK}$ then yielded the mass of the AFGK star ($M_{\rm AFGK}$). The best fit stellar parameters are listed in Table 2.1.

Parameter	TYC 6996	TYC 8097	2MASS J0628
$M_{\rm AFGK}$ [$M_\odot$]	1.12 ± 0.08	1.43 ± 0.16	0.99 ± 0.11
$R_{\rm AFGK}$ [$R_\odot$]	1.266 ± 0.020	1.715 ± 0.011	0.995 ± 0.009
$T_{\rm AFGK}$ [K]	6270 ± 35	5730 ± 40	5540 ± 50
$Z_{\rm AFGK}$ [[Fe/H]]	-0.31 ± 0.15	-0.07 ± 0.10	-0.07 ± 0.10
$P_{\rm orb}$ [d]	41.9950	20.9850	10.2121
	± 0.0017	± 0.0022	± 0.0013
e	0.497 ± 0.006	0.451 ± 0.003	0.266 ± 0.002
$K_{\rm AFGK}$ [km s^{-1}]	24.21 ± 0.21	31.05 ± 0.26	28.11 ± 0.10
γ [km s^{-1}]	2.54 ± 0.12	42.17 ± 0.09	-14.62 ± 0.02
$T_{\rm P}$ [BJD]	2 457 040.00	2 457 423.837	2 457 235.406
	± 0.02	± 0.001	± 0.001
ω [deg]	151.9 ± 0.8	329.0 ± 0.3	197.7 ± 0.4
Distance [pc]	$392.1^{+5.3}_{-5.4}$	$350.8^{+1.8}_{-1.5}$	$265.9^{+1.9}_{-1.4}$
triple system	most likely	inconclusive	most likely
UV excess source	White dwarf	White dwarf	Active stars
		Active galaxy	
		Active stars	

Table 2.1: Measured mass, radius, effective temperature and metallicity of the secondary star for each eccentric system. Orbital parameters are obtained from radial velocity measurements of the secondary star. Photogeometric distances from Bailer-Jones et al. (2021) are shown with errors based on the 16th and 84th percentiles of the distance posterior distribution. The last two rows represent whether they are triple systems and the most likely source of the UV excess.

2.3.3 Differential photometry of 2MASS 0628

Unlike TYC 6996 and TYC 8097, 2MASS 0628 is the only system which has a point source detection well located in the IRDIS field of view to perform photometry.

We use nine SPHERE/IRDIS flux calibration exposures (from the fits file SPHER.2017-12-30T03:54:37.371) to obtain the differential magnitudes $\Delta H2$, $\Delta H3$ of the companion relative to the instrumental photometry of the central binary. Given that a small fraction of the companion's Airy disk slightly overlaps the first Airy diffraction pattern of the central binary, we use an aperture radius of 4 pixels (i.e., the measured full width at half maximum of IRDIS in $H2$ and $H3$ filters) to avoid as much as possible flux-cross contamination. Sky substraction was performed by calculating the mean value of the pixels located inside an annulus centred at the same angular distance of the companion and width equal to the aperture diameter. The region of the annulus centred at the companion and with length equal to twice the diameter of the aperture was not considered in the calculation. The final differential magnitudes (i.e. the average of the nine exposures) for filters $H2$ and $H3$ are $\Delta H2 = 2.170 \pm 0.028$ and $\Delta H3 = 2.106 \pm 0.047$

2.4 The three eccentric systems

The three targets we present in this paper turned out to have eccentric orbits, which together with TYC 7218 (Lagos et al., 2020) brings the number of measured eccentric orbits with periods of the order of weeks to four. Given their eccentric nature, these systems are not probably formed though CE evolution (e.g. Ivanova et al., 2013). One possibility is that, like TYC 7218, they are triple systems. To elucidate their nature, we have performed detailed follow-up observations to characterise all three systems. In what follows we describe each system individually.

2.4.1 2MASS J06281844-7621467

Of all the PCEB candidates observed with *HST*, 2MASS J0628 has the faintest *GALEX* *FUV* magnitude ($m_{\rm FUV,GALEX} = 21.3691 \pm 0.3938$) . Based on the orbital properties derived from the radial velocity curve, the minimum mass for the companion to the G-type star is $\approx 0.3\,{\rm M}_{\odot}$.

The STIS spectra show no evidence for a white dwarf companion or any contribution from a spectral continuum. Averaging the two spectra (from files

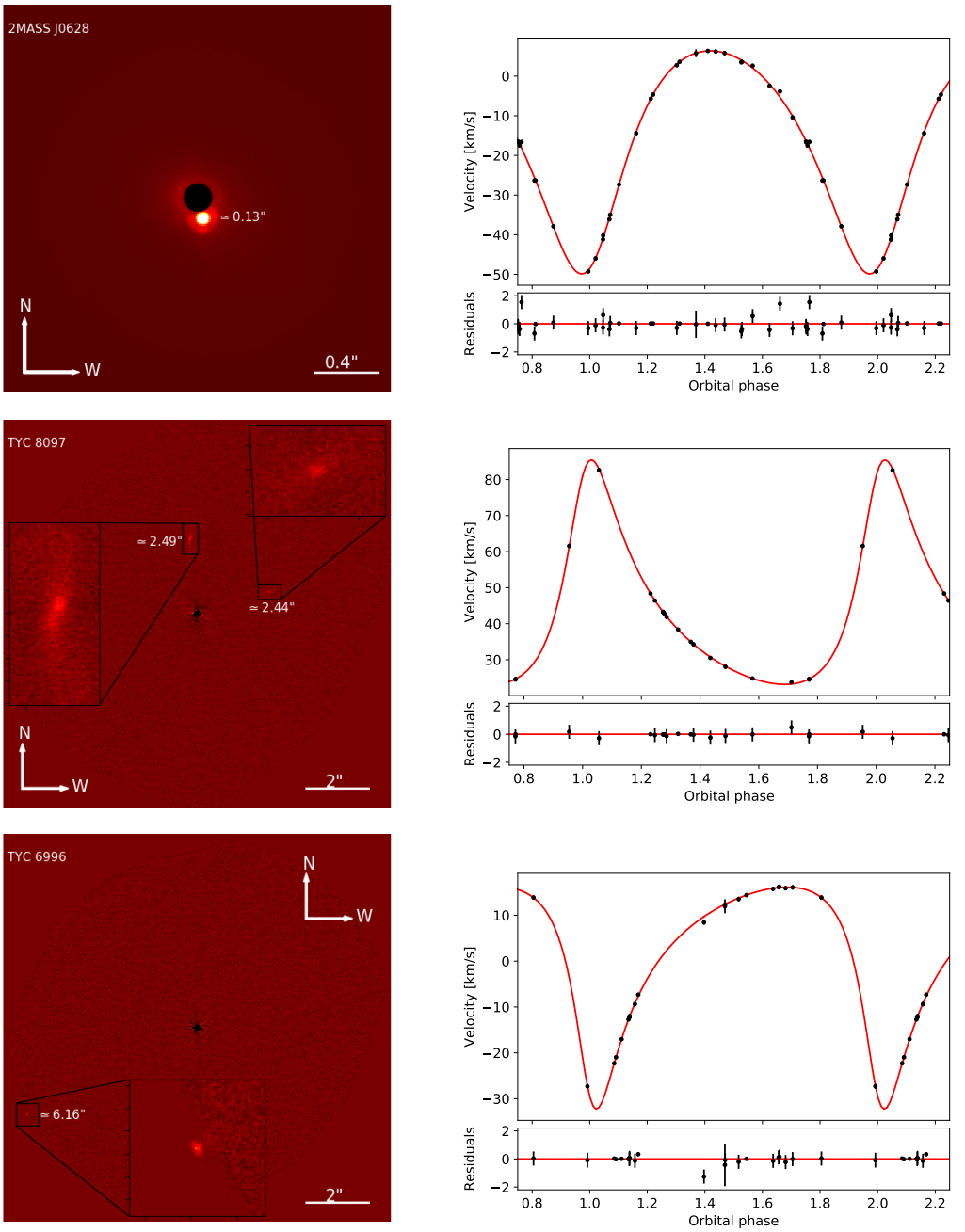

Figure 2.1: SPHERE/IRDIS *H*2 images (left panel) and radial velocity curves (right panel) for 2MASS 0628 (top), TYC 8097 (middle) and TYC 6996 (bottom). Black circles in each SPHERE image indicate the position of the coronagraph, while detections are accompanied by its projected separation in arcsec (white numbers). The star dominating at visible light is clearly part of an eccentric binary which excludes these systems to be post common envelope binaries. 2MASS J0628 is best explained as a triple systems with at least one active star while TYC 6996 is also a hierarchical triple with a white dwarf as a tertiary. In the case of TYC 8097 the origin of the UV excess remains mysterious. The three main candidates to the UV source(s) are the observed background galaxies (in case they are active), stellar activity from the M or K-type companion, or a white dwarf being the third companion in a hierarchical configuration.

oe9x08010_x1d.fits and oe9x08020_x1d.fits) with the best signal-to-noise ratio, we found two emission features corresponding to C II at 1335 Å and C IV at 1550 Å (Figure 2.2). Although the integrated flux of this spectrum through the *GALEX FUV* filter is insufficient to explain the observed UV excess, these lines are used as stellar activity tracers and can contribute to the enhanced UV flux produced during transient stages of high activity (e.g. Findeisen et al., 2011; Shkolnik & Barman, 2014; Loyd et al., 2018), suggesting that the UV excess may be caused by chromospheric and/or flare activity in at least one star in 2MASS J0628.

This idea is further supported by the following reasoning. The *NUV* flux from the stellar models of G stars do not include chromospheric emission. This explains why the models fail to explain the NUV flux of active stars (see the magenta circle in Figure 2.5 for 2MASS J0628). A similar discrepancy between the *GALEX* photometry, the *HST* data, and the stellar model for the AFGK star components has also been observed in one of the six confirmed WD+AFGK PCEBs in our survey: TYC 110-755-1 (Hernandez et al., 2022). The white dwarf model that fits best the *HST* spectrum is consistent with the *GALEX FUV* flux, but fails to reproduce the observed *GALEX NUV* flux (see their Figure 9). The authors conclude that chromospheric emission from the G star is the most likely explanation for the flux difference. Based on these two systems, it could be inferred that (1) if the *GALEX FUV*/*NUV* and *HST*/AFGK model fluxes disagree then variability due to stellar activity might occur in the binary, and (2) if the *GALEX FUV* and *HST* fluxes agree but the *GALEX NUV* flux is larger than the synthetic one, this indicates steady chromospheric emission from the AFGK star.

Furthermore, our SPHERE observations reveal the presence of a companion candidate at an angular separation of 0.13 arcsec, corresponding to a projected separation of $\approx$ 36 au using the photogeometric distance from Bailer-Jones et al. (2021). To calculate its apparent magnitude in the $H2$ and $H3$ filters we proceed as follows. First, we calculate the synthetic $H2$ and $H3$ magnitudes of 2MASS J0628 using the synthetic photometry tool available in the Spanish Virtual Observatory (SVO, Rodrigo et al., 2012; Rodrigo & Solano, 2020) and a BT-NextGen (Allard et al., 2012a) spectral template with effective temperature 5 500 K, surface gravity $\log g = 4.5$ and metallicity [Fe/H]=0, i.e., resembling the stellar properties shown in Table 2.1. Then, synthetic magnitudes were reddened using the 3D interstellar dust map from Lallement et al. (2019)[2]. The final synthetic magnitudes of the G star in the $H2$ and $H3$ filters are $H2_{\rm G} = 10.72$, $H3_{\rm G} = 10.58$, in good agreement with the archival magnitude in the

[2] https://astro.acri-st.fr/gaia_dev/#extinction

2MASS H filter of 10.44. With these values, and using the differential photometry, we derived synthetic magnitudes $H2_{\rm comp} = 12.75$ and $H3_{\rm comp} = 12.83$ for the companion candidate. Using this information, we estimate the likelihood of the companion to be a background source aligned by chance within an angular distance Θ following Brandner et al. (2000) as:

$$P(\Theta, m_{\rm lim}) = 1 - e^{-\pi\Theta^2\rho(m_{\rm lim})}, \tag{2.1}$$

where $\rho(m)$ is the cumulative surface density of background sources down to a limiting magnitude $m_{\rm lim}$ (i.e. the magnitude of the detection). In order to calculate $\rho(m_{\rm lim})$, we used the Besançon galaxy model[3] (Robin et al. 2004) to generate a synthetic 2MASS H photometric catalogue of point sources within 1 square degree, centred on the coordinates of 2MASS J0628. To avoid underestimating the value of $P(\Theta, m_{\rm lim})$ we set a limiting magnitude of 16 in the H band, i.e., three magnitudes fainter than the synthetic $H2$ and $H3$ magnitudes of the companion candidate. We found that the probability of the companion to be a background source is 0.001 per cent. It is worth mentioning that this result, based on a synthetic catalogue, is purely statistical and does not confirm the detected object being part of 2MASS J0628, but rather allows to strengthen the hypothesis about is triple nature, which needs to be ultimately confirmed via common proper motion through new high contrast observations, as the companion candidate is not resolved by *Gaia*.

With the evidence presented above, we conclude that 2MASS J0628 is most likely a main sequence triple system with at least one active component which produced the UV excess. This system represents the first of the 11 targets in our sample observed with HST that clearly does not contain a white dwarf. Furthermore, by placing 2MASS J0628 in the UV colour-temperature diagram of Parsons et al. (2016, their Figure 1), from which the *PCEB candidate* assignment is given, we might expect that some candidates with $GALEX\ FUV - NUV$ colour close or greater than the one of 2MASS J0628 ($FUV - NUV \approx 3.6$) contain UV sources different to white dwarfs, in particular, active stars.

2.4.2 TYC 6996-449-1

Previous *HST* observations of TYC 6996 using STIS were obtained by Parsons et al. (2016) under program GO 13704. They confirmed the UV excess is due to a white

[3] `https://model.obs-besancon.fr/`

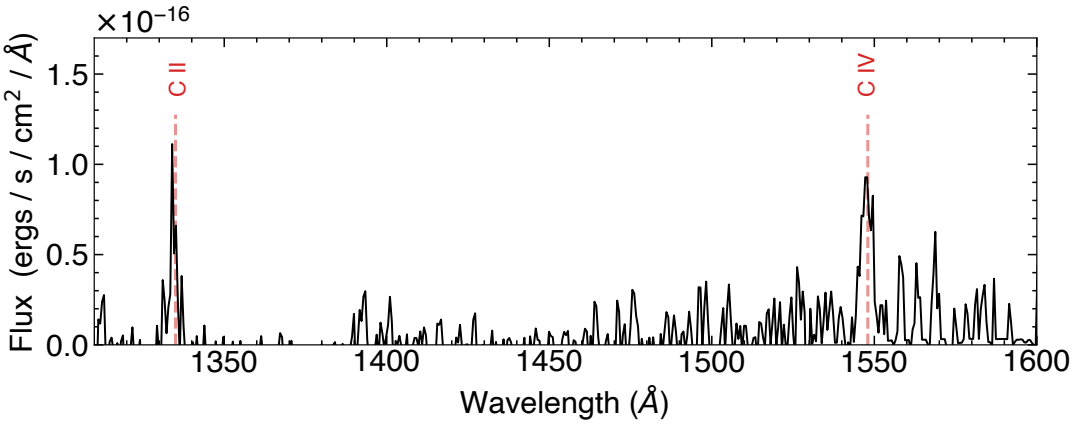

Figure 2.2: Average *HST*/STIS spectrum of 2MASS J0628. A detailed extraction (see text for details) shows clear emission of C II and C IV. These emission lines may suggest the presence of stellar activity.

dwarf. However, the flux of the *HST* spectrum for this object falls substantially below its measured *GALEX* magnitudes (see bottom panel of Figure 2.5), giving inconsistencies between the distance of the main-sequence star obtained from the RAdial Velocity Experiment (RAVE; Kordopatis et al., 2013) survey and the white dwarf distance they estimated. As initially suggested by Parsons et al. (2016), we show below that this flux difference is because TYC 6996 is most likely a spatially resolved hierarchical triple with the white dwarf as the tertiary companion. This caused the STIS slit to not be properly centred on the white dwarf losing a substantial part of its UV flux.

Using PCA in the IRDIS science data cube we detected the presence of a potential tertiary companion at $\approx$ 6.2 arcsec from TYC 6996, close to the edge of the IRDIS field of view (see the bottom left panel of Figure 2.1). This detection is consistent with a UV source detected by *GALEX* at the same coordinates, at $\approx$ 6.1 arcsec from TYC 6996 as shown in Fig. 2.3, confirming the idea that the white dwarf is either a resolved companion of TYC 6996 or a background source. According to the *Gaia* EDR3 parallax, the white dwarf is located somewhere between $\approx$ 330 $-$ 400 pc (Bailer-Jones et al., 2021), in agreement with the estimated distance of TYC 6996 ($\simeq$ 392 pc, see Table 2.1) which supports the triple hypothesis.

In their search of wide companions around stars hosting giant planets and brown dwarfs, Fontanive et al. (2019) found that relative differences of $\leq$ 20 per cent in the *Gaia* data release 2 parallaxes and in at most one of the proper motion coordinates between the wide companion candidates and the planet-host star may suggest that

they are likely part of a hierarchical system. Following this criterion, we calculate the relative differences in proper motion ($\Delta_{\alpha*}$ and $\Delta\delta$) and parallax ($\Delta\pi$) between the white dwarf and TYC 6996 using their *Gaia* EDR3 astrometric solutions, finding that $\Delta_{\alpha*} = 0.3 \pm 1.1$, $\Delta_{\delta} = 22.9 \pm 1$ and $\Delta\pi = 8 \pm 14$ per cent. The calculated relative differences meet the criterion that favour the triple nature of TYC 6996. However, the large error of the white dwarf parallax (ß $= 2.31 \pm 0.35$) translates into a large uncertainty of $\Delta\pi$, and therefore we cannot discard that its real value could be slightly above the threshold of 20 per cent. However, if the latter was true, and taking into account that the orbital separation of the white dwarf from the inner binary is at least $\approx$ 2431 au, the system may also be a triple system that was disrupted due to triple evolution, dynamical instability, galactic tides, encounters with passing field stars or interactions with giant molecular clouds (e.g. Weinberg et al., 1987; Correa-Otto & Gil-Hutton, 2017; Hamers et al., 2021; Toonen et al., 2021), in which case the white dwarf could still retain a fraction of the intrinsic proper motion of the former triple.

The presence of triple systems with white dwarfs in the survey has been previously discussed in Lagos et al. (2020), who found that the white dwarf detected in TYC 7218 is in fact a tertiary companion to a main sequence binary star. They derived an upper limit of 15 per cent for contaminants (i.e. non-PCEB systems) consisting of hierarchical triples with white dwarfs and M-dwarf companions, of which in 80 per cent of the cases the white dwarf is the third object. We therefore conclude that TYC 6996 is (or at least was) most likely a triple system, with the close companion to the F-type star being a low mass star with a minimum mass of $\approx 0.5\,M_{\odot}$ based on its orbital solution.

2.4.3 TYC 8097-337-1

Based on the orbital solution derived from the radial velocity curve, the minimum mass of the companion to the G-type star is $\approx 0.6 M_{\odot}$. Since this system was not observed with *HST*, we cannot confirm the presence of a white dwarf, and like 2MASS J0628, the companion to the G-type star could, in principle, be an active star producing the observed UV excess. Additionally, IRDIS images reveal the presence of two extended sources at ≈ 2.4 arcsec from the binary, which are most likely background galaxies that also might be the source of the UV excess. This is the first time in our survey that we have detected not one, but two potential non-stellar UV sources.

To quantify the FUV/NUV flux excess produced by the unknown UV source, we perform (as in section 2.4.1) synthetic FUV/NUV photometry using a BT-NextGen

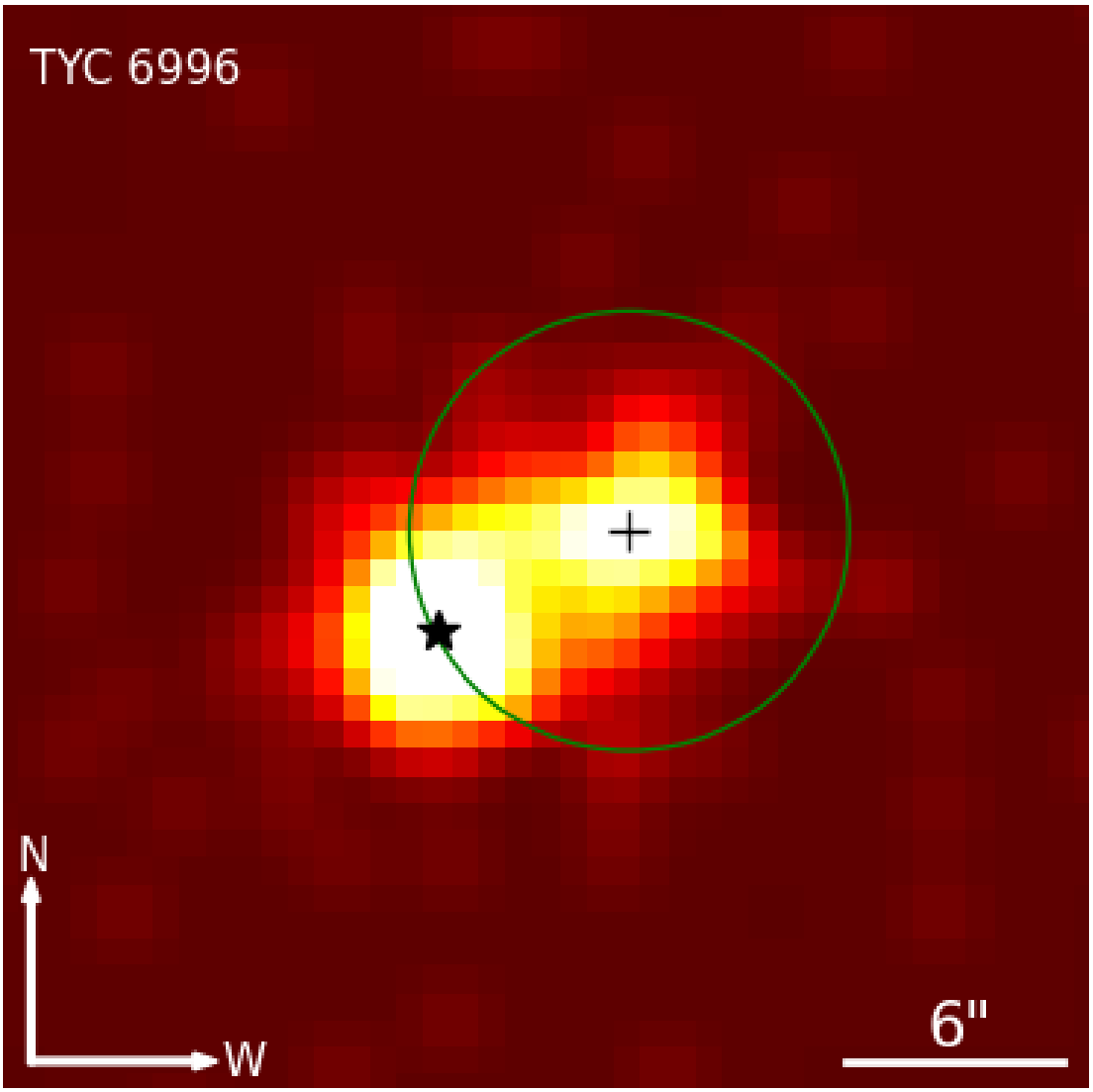

Figure 2.3: *GALEX* FUV image of TYC 6996 (black cross) and the white dwarf (black star). The SPHERE/IRDIS field of view centred in TYC 6996 is shown as a green circle. For display purposes the image has been smoothed with a Gaussian kernel.

spectral template with effective temperature $T_{\rm eff} = 5\,700$ K, surface gravity $\log g = 4$ and metallicity [Fe/H]=0, according to the stellar properties of the AFGK star given in Table 2.1. While in the *NUV* band the difference between observed and synthetic magnitudes ($m_{NUV,GALEX} = 17.06, m_{NUV,synt} = 17.22$) is ≈ 0.16 mag, the difference in the FUV band is ≈ 5.6 mag ($m_{FUV,GALEX} = 19.93, m_{FUV,synt} = 25.52$). This translates to UV magnitudes of the unknown UV excess source of $m_{NUV} \approx 19.5$ and $m_{FUV} \approx 19.9$.

To investigate if the presence of background galaxies can explain the UV excess, we used the *GALEX* ultraviolet atlas of nearby galaxies of Gil de Paz et al. (2007), which mostly contains regular (i.e. non active galactic nuclei, star-forming or ultraviolet-luminous) galaxies. Since the galaxies in this catalogue have a diameter larger than 1 arcsec, *FUV* and *NUV* magnitudes were scaled to such a distance that the projected angular area of the galaxy is roughly equal to that of the two galaxies found with SPHERE, i.e. $\approx 2.3 \times 10^{-5}$ arcmin^2 for a direct comparison with the catalogue. Given that the re-scaled *FUV* magnitude of the brightest galaxies in the catalogue is $\approx$ 26 mag, it seems very unlikely that two regular background galaxies are the unknown UV source. However, if one or both extended sources are active galactic nuclei galaxies, the UV excess can be perfectly explained as these type of galaxies can easily reach $m_{\rm FUV} \simeq 20$ mag (e.g. Welsh et al., 2011).

In an alternative scenario, the UV excess might be caused by stellar activity. We find that using a BT-Nextgen template with $T_{\rm eff} = 4000$ K, $\log g = 4.5$ and metallicity [Fe/H]=0 for a companion with 0.6 $M_\odot$, its estimated quiescent FUV magnitude is $\approx$39. This result may suggest that it is extremely unlikely that the observed FUV excess is due to stellar activity. However, the spectral template used does not include the chromospheric component, which may contribute $\gtrsim$ 99 per cent of the total emission in the *FUV* band and reach flux densities similar to the one observed in TYC 8097 (e.g. Stelzer et al., 2013). We therefore conclude that stellar activity cannot be excluded.

Finally, we test whether a white dwarf may be responsible for the UV excess as follows. Using the white dwarf cooling models[4] from Holberg & Bergeron (2006); Kowalski & Saumon (2006); Tremblay et al. (2011); Bédard et al. (2020) we made a chi-square minimisation to the archival *NUV*/*FUV GALEX* fluxes, leaving as a free parameter the distance of the white dwarf. To include in the minimisation the *FUV*/*NUV* flux contribution from the AFGK star we perform synthetic photometry using the same BT-NextGen spectral template described above. Synthetic magnitudes were reddened as explained in Section 2.4.1. We found that the best fit for the UV excess corresponds

[4] http://www.astro.umontreal.ca/~bergeron/CoolingModels/

to a white dwarf with $T_{\rm eff} = 14\,500$ K, $M = 0.926\,M_{\odot}$, $\log g = 8.5$ and $R_{\rm WD} = 0.97\,R_{\oplus}$, located 356 pc away, in agreement with the distance given in Table 2.1. In addition, we repeat the chi square minimisation, but this time leaving as a free parameter the white dwarf cooling models and keeping fixed the distance at 351 pc, finding that the best fit model corresponds to a white dwarf with $T_{\rm eff} = 17\,000$ K, $M = 1.2\,M_{\odot}$, $\log g = 9$ and $R_{\rm WD} = 0.63\,R_{\oplus}$, being consistent with the white dwarf model at 365 pc. Figure 2.4 shows that a white dwarf with similar characteristics to our best-fit models would have been detected in our SPHERE/IRDIS images, at least at an angular separation from the AFGK star greater than 0.27 arcsec (projected separation of $\approx$ 95 au). Given that the eccentricity of TYC 8097 excludes CE evolution as the formation channel of the binary, the white dwarf might be a tertiary with a close orbit completely hidden by the coronagraph, or we might just have been unlucky and the current location of a wide white dwarf tertiary is just behind the coronagraph. Although this interpretation is also in agreement with the expected fraction of triple systems in the survey with the white dwarf being the third companion, like TYC 7218 and most likely TYC 6996, the above scenario must be taken with caution as we only used two photometric points in the chi-square minimisation (Fig. 2.5) and only the *FUV* flux constrains the white dwarf model (making the fit highly degenerate).

We conclude that in the absence of *HST* observations, the UV source could be either an active galaxy, an active stars, or a white dwarf.

2.5 Discussion

In the white dwarf binary pathways survey we have so far discovered six short orbital period systems ($P_{\rm orb} \lesssim 2.5$ d) with circular orbits. These systems can easily be interpreted as PCEBs. At somewhat longer orbital periods (weeks), we have so far not yet identified a single PCEB but instead four systems, three in this work and one in Lagos et al. (2020), with eccentric orbits, which are most likely main sequence binaries or the inner binaries of hierarchical triple systems, either with no white dwarf at all or with the white dwarf being the distant tertiary companion candidate. In what follows we discuss the implications of this finding for our survey as well as for our understanding of white dwarf binary star formation.

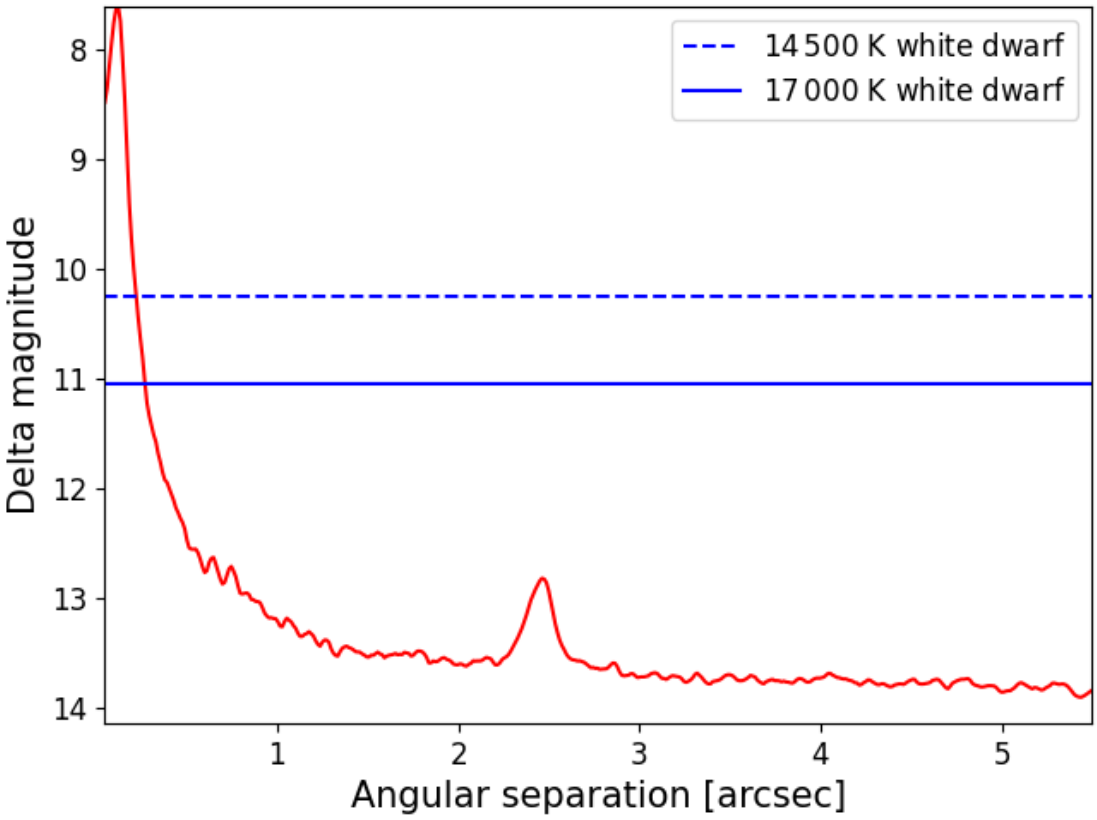

Figure 2.4: 5-sigma contrast curve in the *H*2 filter for a full-frame ADI-PCA using 10 principal components (red line) for TYC 8097. The solid and dashed blue lines represent the magnitude difference between the secondary star and the two best-fit models for a white dwarf companion as the source of the UV excess (see the text for more details). The intersection of each blue lines with the red line at ≈ 0.27 arcsec represent the limiting angular separation at which the white dwarf would be visible with SPHERE/IRDIS. The peak observed at $\approx$ 2.4 arcsec is due to the presence of the background galaxies. Curve generated with VIP.

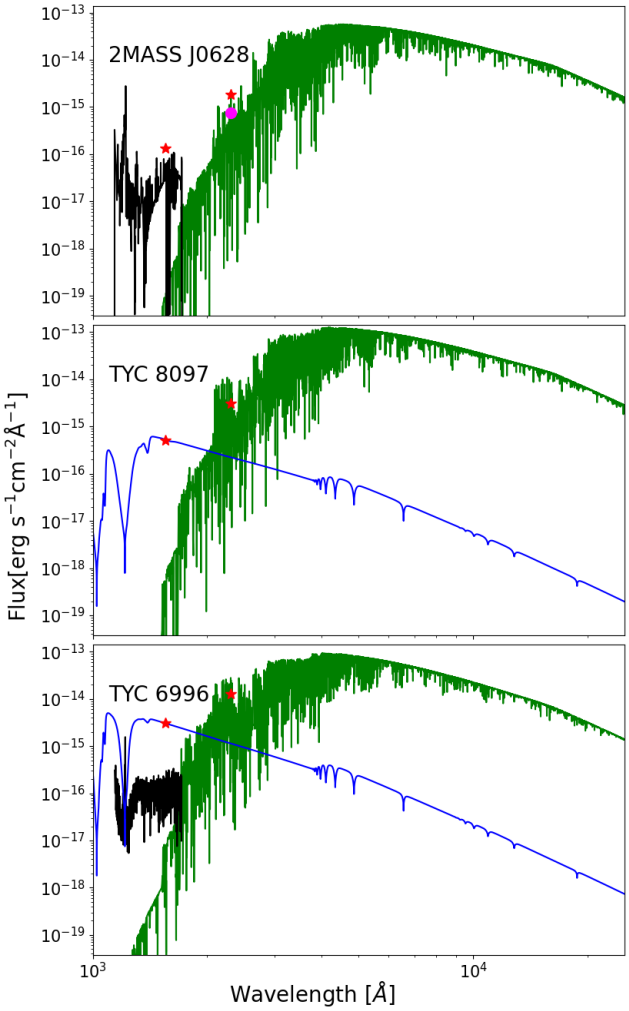

Figure 2.5: Best fit model spectrum of the AFGK star (green lines) and *GALEX* photometry (red stars) for all the three systems. The HST spectrum of 2MASS J0628 (black line) did not confirm the presence of a white dwarf and its flux integrated over the *GALEX FUV* filter is insufficient to explain the observed UV excess. Furthermore, the *NUV* flux obtained from the model of the G star (magenta circle) is $\approx$ 2.5 times less than the observed by *GALEX*. We conclude that transient events of stellar activity are responsible for the enhanced *GALEX* UV flux. For TYC 8097 we also plot the best white dwarf model fit ($T_{\rm eff}$ = 14 500 K, $\log g$ = 8.5, and M= 0.926 $M_{\odot}$, blue line) to the observed UV excess. While this is clearly just one possible solution, it illustrates that the UV excess can be explained by the presence of a white dwarf. For TYC 6996 we show the *HST* spectrum (black line) presented also in Parsons et al. 2016 from which the presence of the white dwarf was confirmed together with the best white dwarf model fit ($T_{\rm eff}$ = 16 500 K, $\log g$ = 8, and M= 0.616 $M_{\odot}$) to the *GALEX* photometry. Since the STIS slit was not properly centred on the white dwarf, the observed flux in the *HST* spectrum is smaller than the real one.

2.5.1 Expected contribution from different types of contaminants

Despite the effectiveness of the UV excess criterion used to identified white dwarfs with short orbital periods around AFGK-type stars (PCEB candidates), the sample is not free of contaminants, and even if the UV excess comes from a white dwarf, the system may not be formed through CE evolution. In this regard, the orbital characterisation of each candidate, and in particular its eccentricity has become an additional indicator of potential contaminants in the sample. The three eccentric PCEB candidates presented here reveal at least three main type of contaminants: (a) hierarchical triples with the AFGK star being orbited by a M-type star, with a white dwarf as the third object (AFGK/M+WD configuration), (b) binary (triple) systems with the AFGK star being orbited by one (two) M-type star(s) (AFGK/M configuration for binaries and AFGK/M+M for triples), of which one or both are the source of the UV excess due to chromospheric activity, and (c) Back(fore)ground UV sources like white dwarfs or non-stellar sources like galaxies.

The fraction of AFGK/M+WD triples in the survey was derived in Lagos et al. (2020), ranging from 1 up to 15 per cent of the sample of PCEB candidates. To roughly assess the fraction of type-(b) contaminants, we use an approach similar to that in section 5 of Lagos et al. (2020). For a population composed of 10^7 single, binary and triple systems, the number of PCEBs with AFGK secondaries is $\approx 2 \times 10^5$ (also including a small fraction formed in hierarchical triples). From the initial mass function of Kroupa et al. (1993), we estimate that ≈3.4 per cent of the population are AFGK stars (for the case of single stars) or have an AFGK star as the most massive component (for the case of binary and triple systems). By assuming that 8 per cent of those population of AFGK stars are triples with uniform mass ratio distributions for the inner and outer companions (Tokovinin, 2014), we found that ≈0.06 per cent of the population have triple systems with configuration AFGK/M+M (assuming that M-type stars are those with masses between 0.085 and 0.6 $M_\odot$). Compared with the number of PCEBs, the fraction of triples with configuration AFGK/M+M is ≈ 3 per cent. Taking into account the estimated activity lifetimes for M5-M0 and >M5-type dwarfs of up to 2 and 8 Gyr respectively (West et al., 2011), and a constant star formation rate, the final fraction of AFGK/M+M systems with at least one active star is reduced to ≈ 1 per cent. Using the same reasoning, but a binary fraction of 33 per cent (Tokovinin, 2014), we found that the fraction of AFGK/M systems with stellar activity relative to the number of

PCEBs is $\simeq 9$ per cent. Although the total fraction of type-(b) contaminants (≈ 10 per cent) is close to the upper limit estimated for AFGK/M+WD contaminants (≈ 15 per cent), we must recall that the obtained value represents an upper limit, as we assume that all AFGK/M and AFGK/M+M contaminants bypass the UV excess criterion.
The probability for spurious alignments with back(fore)ground UV sources is very difficult to measure as the fraction of this type of contaminants depends on the type of UV source taken into account and on how crowded the region of the sky around the candidate is. However, since most of the PCEB candidates have galactic latitude and longitude in the range $|b| \gtrsim 30\,\mathrm{deg}$ and $200 \lesssim l \lesssim 360\,\mathrm{deg}$, i.e. avoiding the crowded regions of the galaxy, we expect their contribution to be negligible compared with type-(a) and (b) contaminants.

2.5.2 Possible transition between systems evolved via common envelope evolution and stable non-conservative mass transfer?

On the one hand, our survey has successfully identified six PCEBs, all of them with orbital periods less than 2.5 days. On the other hand, the four contaminants identified so far have orbital periods in the range $10 \lesssim \mathrm{P_{orb}} \lesssim 42\,\mathrm{d}$. This shows that our survey is capable to detect wider WD+AFGK binaries thanks to the high precision of our radial velocity measurements. Therefore, if PCEBs with periods longer than 2.5 days would exist in significant numbers, we should have detected them with our observing strategy.

In order to find possible explanations for this lack of wider WD+AFGK PCEBs, it is illustrative to look at the secondary mass-period relation of confirmed WD+AFGK binary stars. In Figure 2.6 (similar to the Figure 6 of Hernandez et al. 2021), we show WD+MS binaries collected from the literature and those discovered in our survey. Apart from the six PCEBs identified by our survey, two more WD+AFGK systems have similar short orbital periods, V471 Tau ($P_{\mathrm{orb}} \approx 0.52\,\mathrm{d}$; O'Brien et al., 2001) and GPX-TF16E-48 ($P_{\mathrm{orb}} \approx 0.3\,\mathrm{d}$; Krushinsky et al., 2020). In the period range where we found four systems that are clearly not PCEBs, only one WD+AFGK binary is known, IK Peg ($P_{\mathrm{orb}} \approx 21.7\,\mathrm{d}$, $e \approx 0.03$; Wonnacott et al., 1993). At orbital periods longer than $\simeq 80\,\mathrm{d}$, a population of WD+AFGK binaries has been discovered through the self lensing effect (Kawahara et al., 2018; Masuda et al., 2019). We note that a number of white dwarf + A star binaries with similarly long orbital periods are suspected to be

present in the Kepler sample statistically analysed by Murphy et al. (2018).

Figure 2.6 indicates a paucity of WD+AFGK binaries in the period range between a few days and more than two months. The only system in this period range is IK Peg. Given that four contaminating systems but not a single PCEB in this period range have been discovered by our survey, this paucity is clearly not caused by the fact that longer orbital periods are more difficult to measure by our radial velocity survey.

Another striking feature illustrated in Figure 2.6 is the large difference between the results obtained in previous surveys on WD+M binaries (Nebot Gómez-Morán et al., 2011a) and the results of our current survey of WD+AFGK. In case of the first, long orbital period (between 80 and 1000 d) systems do not seem to exist, i.e. only PCEBs with periods shorter than a few days and resolved systems with separations exceeding 100 au are known (Ashley et al., 2019; Farihi et al., 2010). Our survey of WD+AFGK binaries finds PCEBs with similar characteristics, but there seems to exist a population of systems with orbital periods of several months which is not seen in the M dwarf sample. In what follows we discuss possible implications of these findings.

Binary evolution simulations of PCEBs carried out by Zorotovic et al. (2014) showed that, for systems with $P_{orb} \lesssim 10$ days, the observed relation between the orbital period and the mass of the secondary is well reproduced for a wide range common envelope and recombination energy efficiencies ($0.25 \leq \alpha_{CE} \leq 1.0$ and $0 \leq \alpha_{rec} \leq 0.25$ respectively, see their figure 5). However, WD+AFGK binaries with $P_{orb} \gtrsim 100$ days (such as SBL1, SBL2, SBL3 and KIC 8145411) are only reproduced for models with significant contributions from recombination energy (i.e. $\alpha_{rec} = 0.25$). Such strong contributions from recombination energy would lead to the prediction of a relatively large number of WD+M PCEBs with periods between 10 days and several months which is clearly not observed. If all the systems (except of the contaminants of course) shown in Figure 2.6 were indeed PCEBs, one would need to explain why nature switches from inefficient envelope extraction for WD+M PCEBs to very efficient envelope extraction including contributions from recombination energy for a fraction of WD+AFGK binaries (i.e from the panels of the left hand side in Fig. 5 of Zorotovic et al. (2014) to the right hand panels of the same figure). Given that the amount of recombination energy that is used to unbind the envelope is neither theoretically nor observationally well constrained, (see e.g. Ivanova, 2018; Soker et al., 2018), we cannot exclude such a dependence of the common envelope efficiencies on the secondary mass. However, we propose an alternative scenario which we think can naturally explain the observations illustrated in Figure 2.6.

We suggest that a different mechanism than CE evolution is responsible for the formation of wide WD+AFKG binaries (with periods of months), and that the period range between 10 and 100 days, populated so far only by our contaminants and two WD+AFGK binaries (IK Peg and KOI-3278), might indeed contain very few post mass transfer white dwarf binaries. Assuming a universal and low value for the CE efficiency, like the one obtained for PCEBs with M-type secondaries ($\alpha_{\rm CE} \approx 0.2 - 0.3$ Zorotovic et al. 2010), PCEBs mostly populate the period domain up to 10 days, predicting only a tail of very few systems with longer periods up to periods of $P_{\rm orb} \approx 100$ days (see figure 2 of Zorotovic et al. 2014). CE evolution can explain all the WD+M systems as well as the short orbital period WD+AFGK binaries and probably even IK Peg and KOI-3278 as two of the rare longer period PCEBs if a very small fraction of the available recombination energy contributed (Zorotovic et al., 2014). Under these assumptions, however, CE evolution does not predict WD+AFGK with periods of several months as observed and we therefore propose that these systems are not PCEBs. Instead, dynamically stable non-conservative mass transfer (e.g. Kawahara et al., 2018) represents a reasonable candidate to be the mechanism responsible for the formation of these wider WD+AFGK binaries.

The condition for stable mass transfer, under the assumption of adiabatic response of the donor, is generally met when the initial mass ratio $q_i = M_a/M_d$ between the accretor and the white dwarf progenitor is above a critical mass ratio $q_{\rm crit}$. For the particular case of conservative mass transfer and donors in the range $1 \lesssim M_d[M_\odot] \lesssim 6$, $q_{\rm crit} \approx 1 - 0.7$ at the termination of the red giant branch (Ge et al., 2020), meaning that stars that are able to evolve off the main sequence within the Hubble time and develop cores (white dwarfs) with masses $\approx 0.5 M_\odot$ (as those observed in SBL1, SBL2 and SBL3) can undergo stable mass transfer when the accretor is an AFKG-type star. If a fraction of the mass lost by the donor escapes from the binary (non-conservative case), then the value of $q_{\rm crit}$ may be somewhat lower compared to the conservative mass transfer case.

Indeed, for KIC 8145411, one of the long orbital period post mass transfer WD+AFGK systems, Masuda et al. (2019) suggests a formation channel involving stable (and most likely non-conservative) mass transfer. Furthermore, non-conservative stable mass transfer, unlike CE evolution, can also explain the long orbital periods of SBL1, SBL2 and SBL3 and KIC 8145411. As shown in Woods et al. (2012), the final semi-major axis is positively correlated with mass loss rate and initial mass ratio (note that they used $q_i = M_d/M_a$ instead), being able to increase the orbital period by a

factor of five for a binary with $q_i \approx 1$, $M_d \approx 1.1 M_\odot$, and initial orbital period of ≈ 100 days. Finally, if the longer period WD+AFGK stars are descendants from stable mass transfer an obvious explanation for the absence of WD+M binaries in this period range is available: for these systems the mass ratio of the progenitor must have been below 0.5, i.e. the mass of the accretor (the M dwarf) was always too small for stable mass transfer and CE evolution was unavoidable.

While the outlined scenario is entirely consistent with the currently available observations, as a note of caution, we stress that radial velocity surveys of WD+M binaries have not been sensitive to periods exceeding 10 d (Nebot Gómez-Morán et al., 2011a) and that the discovery of self-lensing white dwarf binaries is biased towards systems with larger and brighter companions. A dedicated search of longer period WD+M binaries with a negative result would further confirm our hypothesis.

In addition, given that only ten systems in our survey are well characterised so far (including both PCEBs and contaminants), we admit that despite being plausible, the above outlined interpretation of the observational result remains uncertain. By increasing the number of well characterised post mass transfer WD+AFGK binary stars, we can further test our hypothesis and provide crucial constraints on the two formation channels. This is particularly relevant in the context of SNe Ia progenitors, as WD+AFGK binaries evolving through stable non-conservative mass transfer might experience a subsequent phase of non-stable mass transfer and CE evolution (Woods et al., 2012), leaving as end product a double white dwarf binary that may contribute to the SNe Ia rate via the double degenerate scenario.

2.6 Conclusion

We report the discovery of three WD+AFGK close binary star candidates whose radial velocity curves revealed unexpected eccentric orbits, suggesting that these systems cannot have formed through common envelope evolution. By combining high resolution imaging and spectroscopy techniques we confirm the latter, and conclude that two of them are most likely hierarchical triple systems. 2MASS J06281844–7621467 has a main-sequence inner binary consisting of G-type primary star and a M or K type companion, which is in turn orbited by another M or K-type star. Since the HST spectrum only shows C II and C IV emission lines, the source of the UV excess in this systems is most likely due to one or more active stars. TYC 6996-449-1 has a main-sequence inner binary, consisting of a F-type primary star and a K or M-type compan-

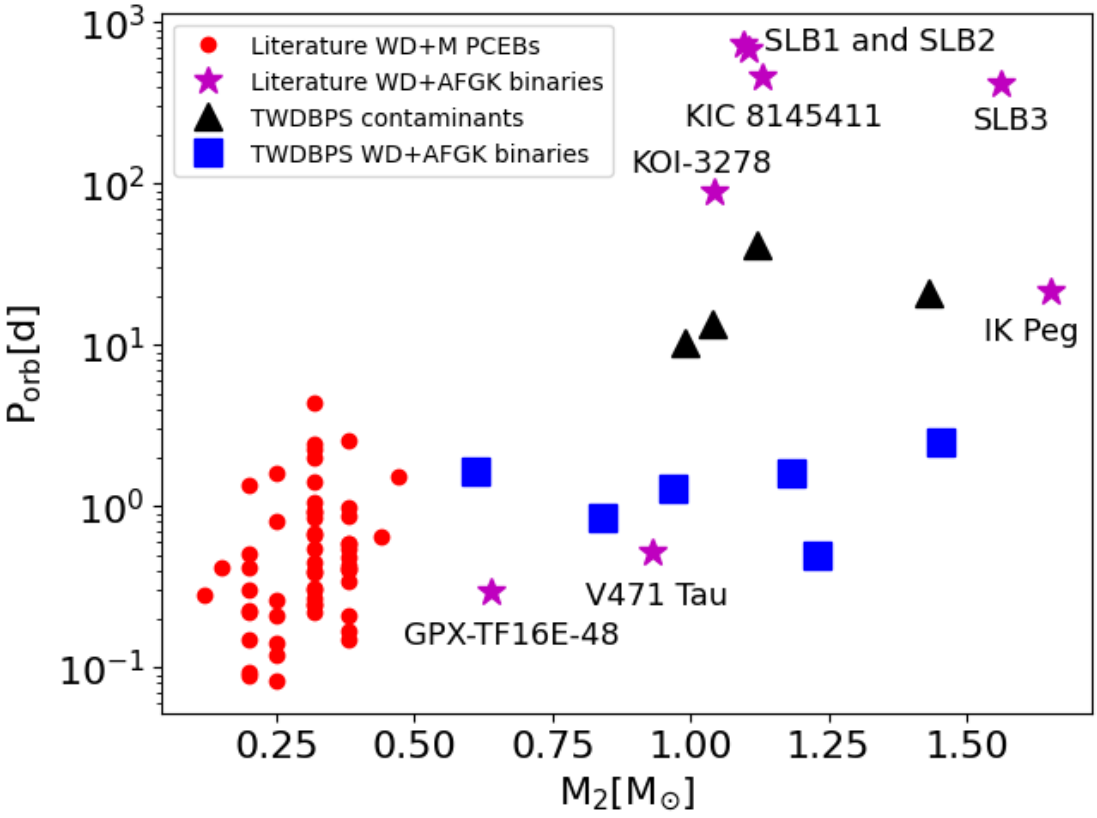

Figure 2.6: Observed relation between orbital period and secondary mass for WD+MS binaries. Red dots are PCEBs with M-type secondaries from Nebot Gómez-Morán et al. (2011a), magenta stars are WD+AFGK binaries from Wonnacott et al. (1993); O'Brien et al. (2001); Kruse & Agol (2014); Kawahara et al. (2018); Masuda et al. (2019); Krushinsky et al. (2020), blue squares are PCEBs with AFGK secondaries from The White Dwarf Binary Pathways Survey (TWDBPS, Parsons et al., 2015; Hernandez et al., 2021; Hernandez et al., 2022), black triangles are the contaminants found in our survey presented in this work and in Lagos et al. (2020).

ion, being orbited by an outer white dwarf. The remaining system, TYC 8097-337-1, could be either a binary consisting of a slightly evolved primary G-type star orbited by a K or M-type lower mass companion, or a triple system with a white dwarf as the third companion.

The fact that only contaminants have been found in the orbital period range between 10 and 40 days, may suggests two different mechanisms to form close WD+AFGK binaries: common envelope evolution for orbital periods less than ≈ 10 days, and stable non-conservative mass transfer for orbital periods above ≈ 100 days. Since binaries evolving through the latter mechanism are expected to end as double white dwarfs after a phase of unstable mass transfer and common envelope evolution, they could play an important role in the formation of supernovae type Ia through the double degenerate scenario. Given the still low number of known WD+AFGK binaries, further characterisation of additional candidates is required to test this hypothesis.

CHAPTER 3

Most EL CVn systems are inner binaries of hierarchical triples

In spite of their importance for modern astronomy, we do not fully understand how close binary stars containing at least one white dwarf form from main sequence binary stars. The discovery of EL CVn binaries, close low mass pre-white dwarfs with A/F main sequence star companions, offers now the unique possibility to test models of close compact binary star formation. Binary evolution theories predict that these EL CVn stars descend from very close main sequence binaries with orbital periods shorter than 3 days. If this is correct, nearly all EL CVn stars should be inner binaries of hierarchical triples because more than 95 per cent of very close main sequence binaries (the alleged progenitor systems) are found to be hierarchical triples (Tokovinin et al., 2006). In this chapter we present SPHERE/IRDIS observations of five EL CVn binaries, finding in all of them tertiary objects, as predicted. We conclude that EL CVn systems are inner binaries of hierarchical triples and indeed descend from very close main sequence binaries that experience stable mass transfer.

3.1 Triple systems as probes of binary evolution models

A large variety of close white dwarf binaries exist, including objects as interesting as super soft X-ray sources, catalcysmic variables (CVs) and their detached progenitors (e.g. Schreiber & Gänsicke, 2003) or double white dwarf binaries (Han, 1998). For all these close white dwarf binaries, theories for their formation and evolution, in most cases involving common envelope evolution (Webbink, 1984; Zorotovic et al., 2010), have been developed.

However, as our prescriptions for mass transfer interactions and angular momentum loss are relatively simple conservation equations containing a number of neither theoretically nor observationally well constrained parameters, binary population simulations are unable to reliably predict detailed characteristics of most white dwarf binary populations. In fact, in several cases, the predictions of theoretical binary population models strongly disagree with the observations. To provide just three examples, current models are unable to produce double degenerate systems via a combination of two common envelope phases (Nelemans & Tout, 2005) and require either stable mass transfer or additional energy sources contributing during common envelope evolution (Webbink, 2008a). No model for supernovae Ia, the thermonuclear explosion of a white dwarf growing in mass through binary star interactions, is able to reproduce the observed delay time distribution (e.g. Yungelson & Kuranov, 2017). Even worse, in CVs several predictions of the standard model for their evolution drastically disagree with the observations (e.g. Zorotovic et al., 2011). While some of these problems are solved in a recently suggested revision of the model (Schreiber et al., 2016), others remain (Pala et al., 2017; Belloni et al., 2020).

To test and eventually calibrate theoretical models of close white dwarf binary formation it would be ideal to have reliable and concrete information about the main sequence binary progenitors for a given type of white dwarf binary. In general, this is illusory. However, here we present, to the best of our knowledge, the first case where such information is indeed available: EL CVn binaries.

EL CVn-type binaries are eclipsing binaries that contain an A- or F-type star and a very low mass (typically 0.2 solar masses) helium white dwarf precursor (pre-Helium WD). The orbital periods of EL CVn stars are typically very short, i.e. 1-3. days. A number of these compact binary stars have been discovered in the Wide Angle Search for Planets, Kepler photometric surveys, or with the Palomar Transient Factory

(Maxted et al., 2014a; van Roestel et al., 2018), and have been found to show different types of pulsations (e.g. Maxted et al., 2014b).

What makes EL CVn binaries special for close white dwarf binary evolution theories is the following. While most white dwarfs and pre-white dwarfs in close binaries are assumed to have formed through common envelope evolution, according to current theories, EL CVn stars must form from dynamically stable mass transfer when the more massive star of the initial main sequence binary was at the end of its main sequence lifetime or just entered the sub-giant branch (Chen et al., 2017). This condition is required as otherwise the core of the more massive star will grow to masses exceeding measurements of pre-white dwarfs in EL CVn binaries. Such an early start of mass transfer implies that the orbital period of the progenitor binary star system must have been shorter than ~ 3 days, as the radius of the primary star was still close to that of a main sequence star when mass transfer began. For longer orbital periods, the sub-giant star is simply too small to fill its Roche-lobe.

The prediction of very short orbital periods for the progenitor main sequence binary stars has fascinating consequences. Virtually all close main sequence stars with orbital periods below $\sim$ 3 days are known to be the inner binaries of hierarchical triple systems (Tokovinin et al., 2006). Even if the mass transfer of the inner binary was not conservative and a certain amount of mass was expelled from the inner binary (thereby increasing the orbit of the tertiary), the third companions should still be there after the mass transfer phase. This implies that, if current theories for the formation of EL CVn stars are correct, virtually all EL CVn stars must be the inner binaries of hierarchical triples.

We here present SPHERE (Beuzit et al., 2019) observations of five EL CVn binaries and indeed find strong candidates for tertiary objects in all of them. We conclude that EL CVn binaries form from the inner and very close binaries of hierarchical triple systems in perfect agreement with the formation channels described in Chen et al. (2017).

3.2 SPHERE Observations and data reduction

The separations of the potential tertiary companions to the inner (EL CVn) binary are expected to be in the rage from 10 to 10000 au (Tokovinin et al., 2006). With the spatial resolution of roughly 100 mas and the field of view of SPHERE/IRDIS (11 x 11 arcsec^2, Dohlen et al. 2008b), our targets must be at distances between $\approx$200$-$1800 pc in order

Target	Distance [pc]	H_{2MASS}	P_{orb}	q	Proper Mot.
	$\pm$	$\pm$	[d]	$\pm$	[mas/yr]
TYC 5204-1575-1	745.37	11.308	1.29	0.130	12.8
	46	0.022		0.026	
TYC 9337-2511-1	1572.55	11.874	1.162	0.148	9.5
	66	0.023		0.026	
TYC 6736-69-1	424	9.924	2.173	0.136	13.7
	85	0.021		0.041	
TYC 6631-538-1	540.07	10.432	0.901	0.143	8.9
	13	0.027		0.027	
TYC 5450-1192-1	447.37	9.748	0.793	0.176	12.8
	8.5	0.022		0.012	

Table 3.1: Distances, 2MASS H photometry, orbital period, mass ratios and proper motion of all EL CVn stars studied in this work. Orbital periods and mass ratios are obtained from Maxted et al. (2014a). Distances are obtained from Bailer-Jones et al. (2018), except for TYC 6736, whose distance has been obtained from data release 5 of the RAVE survey (Kunder et al., 2017).

to cover a large range of the predicted separations for all our targets. We selected five EL CVn binaries from the sample of Maxted et al. (2014a) with distances between $420-1600$ pc and magnitudes in the 2MASS H band between 9.7 and 11.9. We used *Gaia* distances except for TYC 6736. For the latter, the *Gaia* measurement implies an unrealistically large distance (2080 pc). In fact, the poorly constrained paralax (0.46 ± 0.23 mas) derived by *Gaia* may already indicate the presence of a companion. Instead of the *Gaia* value, we used the distance from RAVE data release 5 (Kunder et al., 2017) for TYC 6736. Table 3.1 summarizes the parameters of our targets. Thanks to the extreme contrast of $8-14$ mags that can be reached with SPHERE our observations are even sensitive to low-mass ($\approx 0.1 M_{\odot}$) stellar companions to our most distant objects.

The five objects that we selected were observed with the high contrast imager SPHERE between 2019 April 9 and August 13. Acquisition of direct imaging was made with IRDIS in the dual band imaging mode (Vigan et al., 2010a) using the broad band H filter ($\lambda_{\rm H} = 1625 \pm 290$ μm). Furthermore, the pupil tracking mode was implemented in order to perform angular differential imaging (ADI, Marois et al., 2006b). We used the N-ALC-YJH-S coronagraph.

At the beginning and end of each observing sequence, we obtained *flux* (with

the neutral density filter ND 1 to avoid saturation) and *star centre* calibration images, adding one more exposure for the latter in the middle of the sequence. A total of 112 science images were taken with an exposure time of 32 s for each target except TYC 6736 for which only 66 science images were taken due to bad weather. The IRDIS data were first pre-processed (sky background subtraction, flat-fielding, bad-pixels correction) with the VLT/SPHERE python package[1]. The frames were recentred based on star centre exposures using the four satellite spots. After pre-processing, and without any post-processing technique to remove speckle patterns produced by the coronograph, we detected at least one potential companion in all five EL CVn binaries. We used the principal component analysis (PCA) algorithm available in the VORTEX IMAGE PROCESSING (VIP, Gonzalez et al., 2017) python package to look for fainter companions, only finding one extra candidate in TYC 5450 (TYC 5450 d, see Fig. 3.1).

Making use of the strong signal of our detections, we derotated and median-collapsed the science images to perform aperture photometry and obtained their relative magnitudes $\Delta H_{\rm mag}$ with respect to the central binary. Since the object detected in TYC 6736 surpassed the IRDIS saturation threshold, flux calibration images were used to obtain $\Delta H_{\rm mag}$. As a complementary approach we also used the negative fake companion technique coupled with a Markov chain Monte Carlo algorithm available in VIP to calculate $\Delta H_{\rm mag}$, without finding any discrepancy between both methods.

3.3 The tertiaries to EL CVn stars

In all five cases, our SPHERE observations revealed potential tertiary companions (Fig. 3.1). In what follows we show that the probability for these detections to be background objects is very small and estimate the possible nature of the companions.

3.3.1 Excluding background contamination

We calculated the probability P(Θ, m) for each detection to be a chance alignment with a background source within an angular distance Θ following Brandner et al. (2000) as

$$P(\Theta, m_{\rm lim}) = 1 - e^{-\pi\Theta^2\rho(m_{\rm lim})}, \tag{3.1}$$

[1] `https://github.com/avigan/SPHERE`

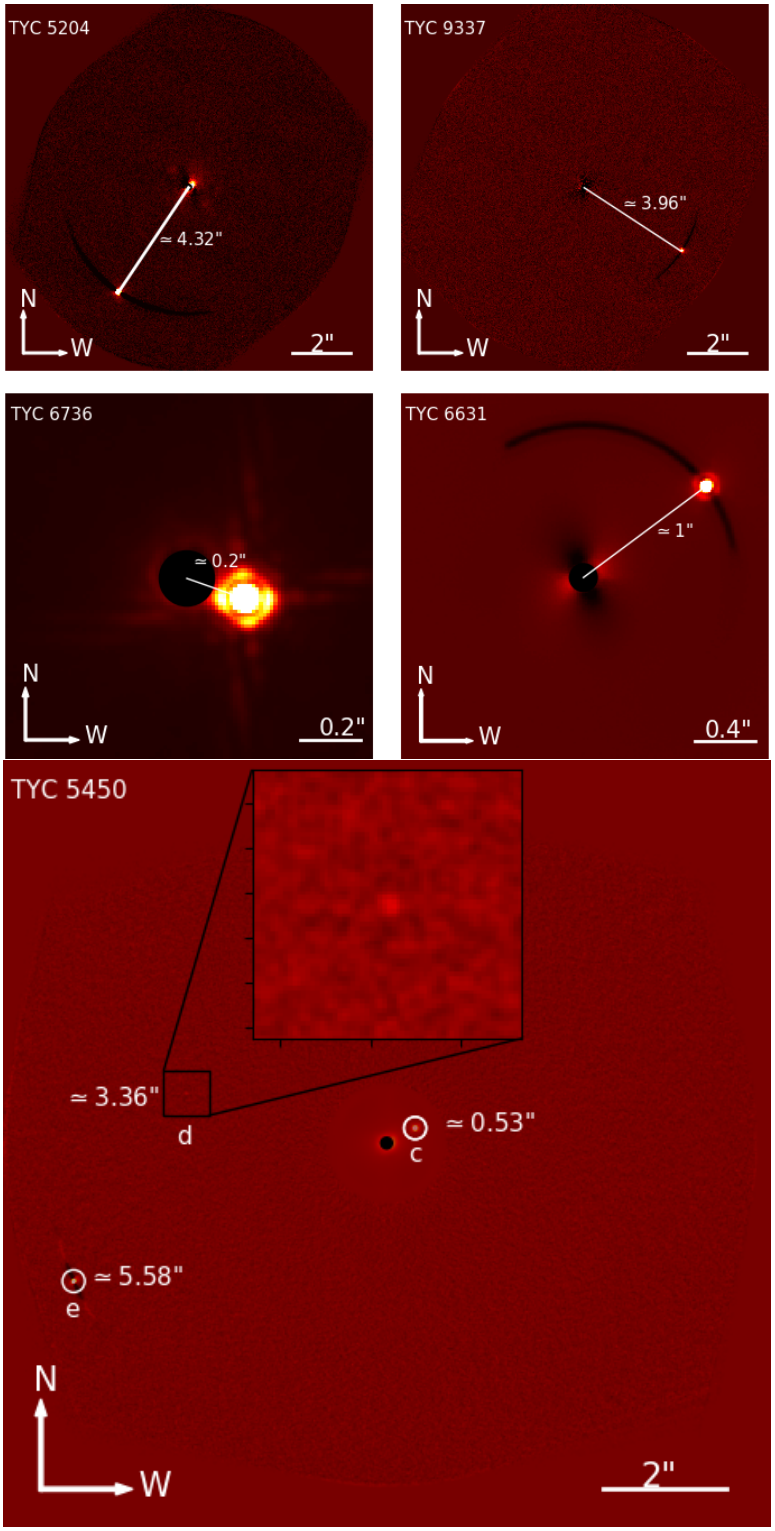

Figure 3.1: SPHERE/IRDIS images of the five EL CVn stars that we observed. In all cases we find at least one potential tertiary. The magnitude difference obtained for the possible companions extend from 1.3 to 14 mags. The probabilities for being background objects are small in all cases with values in the range of $0.0002 - 3\%$ (except for TYC 5450 d and e).

where $\rho(m)$ is the cumulative surface density of background sources down to a limiting magnitude m_{lim} (i.e. the magnitude of the detections). In order to calculate $\rho(m_{lim})$, we used the Besançon galaxy model (Czekaj, M. A. et al. 2014) to generate a synthetic 2MASS H photometric catalogue of point sources within 1 square degree, centred on the coordinates of each target. To calculate m_{lim}, we assumed that both SPHERE and 2MASS H filters are identical, so that the relation between the SPHERE ΔH_{mag} of our candidates and their apparent 2MASS H magnitudes (H_{2MASS}) is given by

$$H_{2MASS} = H_{arch,2MASS} + 2.5\log(1+\alpha), \tag{3.2}$$

where $H_{arch,2MASS}$ is the 2MASS archival magnitude of the EL CVn and $\alpha = 10^{0.4\Delta H_{mag}}$ the value of ΔH_{mag} expressed in terms of the counts ratio between the EL CVn and the candidate. To avoid underestimating the value of $P(\Theta, m_{lim})$, we added 0.5 magnitudes to m_{lim}. We note that discrepancies between 2MASS and SPHERE H bands are clearly irrelevant. We used VOSA's (Bayo et al., 2008) synthetic photometry tool coupled with the BT-NextGen spectral library (Allard et al., 2012b), finding differences of 0.06 magnitudes at most. Table 3.2 lists the final apparent magnitudes and probabilities for being a background object for each candidate.

Combining the obtained probabilities we derive a probability for all five EL CVn binaries to be triple systems or higher multiples of 0.95, i.e. with 2σ significance we measured that five out of five EL CVn stars are triples or higher multiples.

For any assumed true triple fraction of EL CVn stars we can now calculate the significance for rejecting this hypothesis. Given an assumed triple fraction p, the probability of measuring five out of five is simply p^5. This implies that we can say with one (two) sigma significance that the true fraction of EL CVn stars exceeds 80 (55) per cent.

In Fig. 3.2 we compare our result with the triple fraction of sun-like stars as a function of orbital period. Apparently, the measured high fraction of tertiaries in EL CVn binaries corresponds to those of close binary stars with periods below 3 days, in perfect agreement with theoretical predictions.

In general one could further strengthen this result by confirming common proper motions of the candidates with respect to the central EL CVn binary. According to the proper motions listed in Table 3.1 and the IRDIS pixel scale (12.25 mas), the time between observations would need to be at least 3 yr. However, such second epoch observations would only slightly improve an already highly significant result given that for two objects independent evidence for the companion nature of our candidates is already provided by *Gaia*. As mentioned previously, the large uncertainty and

Object	Θ	$\Delta H_{\rm mag}$	Proj. Sep. [au]	$P(\Theta, m_{\rm lim})$	Mass [$M_\odot$]
	[arcsec]	$H_{\rm 2MASS}$	$\pm$		$T_{\rm eff}$ [K]
TYC 5204 c	4.32	$4.988 \pm .018$	3193	0.023	0.3-0.4
		$16.29 \pm .08$	198		3400-3500
TYC 9337 c	3.96	$6.946 \pm .016$	6227	0.031	0.2-0.3
		$18.82 \pm .08$	261		3200-3400
TYC 6736 c	0.2	$1.330 \pm .030$	88	$2 \cdot 10^{-6}$	≈ 0.9
		$11.53 \pm .09$	18		5300-5500
TYC 6631 c	1.0	$3.595 \pm .008$	544	$4 \cdot 10^{-4}$	≈ 0.6
		$14.03 \pm .07$	13		3700-4000
TYC 5450 c	0.53	$4.701 \pm .014$	235	$1.6 \cdot 10^{-4}$	≈ 0.5
		$14.45 \pm .07$	5		≈ 3700
TYC 5450 d	3.36	$13.86 \pm .15$	1503	0.089	< 0.07
		$23.6 \pm .2$	28		< 1600
TYC 5450 e	5.58	$10.402 \pm .120$	2497	0.15	< 0.07
		$20.15 \pm .18$	47		< 1600

Table 3.2: Measured separations, magnitude differences, apparent magnitudes, projected separations, probabilities for chance alignment with a background source, mass and effective temperature for the seven detections.

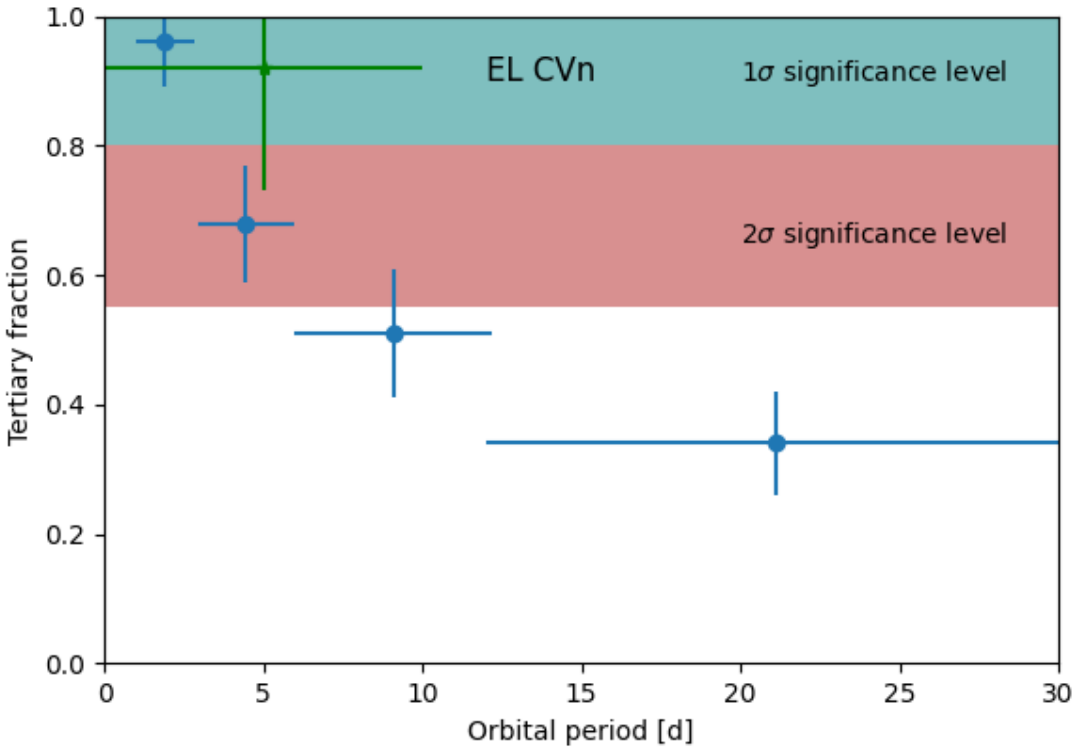

Figure 3.2: Triple fraction for stellar binaries (blue) and hot Jupiter/Brown dwarfs (green) from Tokovinin et al. (2006) and Fontanive et al. (2019). In both cases the fraction of systems with tertiary companions is very large, suggesting that close binaries (including those with massive Jupiter or brown dwarf companion) form through disc fragmentation (see also Moe & Kratter, 2019). The teal and red shaded regions represent the 1σ and 2σ significance level for rejecting the hypothesis that the tertiary fraction of EL CVn stars is less than 80 and 55 per cent respectively. The large triple fraction clearly implies that EL CVn stars descend mostly from close inner binaries of hierarchical triples.

unrealistic value of the *Gaia* paralax of TYC 6736 is consistent with the presence of a companion. In the case of TYC 5204, *Gaia* even detected the companion and, despite relatively large uncertainties, the *Gaia* astrometric solution is consistent with common proper motion. Given this independent evidence, and the very low background probabilities, our result would remain nearly unchanged even if the Galaxy model we used was significantly underestimating the background object probability.

3.4 Potential nature of the companions

The optical and IR emission of EL CVn binaries is dominated by their A (or F) star. If our detections are physically bound to the EL CVn binary, we would expect they were later G, K or M type dwarfs. Although a full characterization of the potential companions is impossible given the limited data currently available, we can derive a rough estimate of their masses and temperatures by using isochrones for main sequence low-mass stars (Baraffe et al., 2015).

Chen et al. (2017) showed that EL CVn binaries with orbital periods shorter than 2.2 days descend from main sequence binaries where the most likely mass for the pre-Helium white dwarf progenitor is in the range $1.15 - 1.2 M_{\odot}$. As the mass transfer that led to the formation of the EL CVn system started after/at the end of main sequence evolution, the age of our systems should be at least $\approx 5 - 7$ Gyr. By comparing the derived distance-modulus corrected H_{2MASS} magnitude with those values in the isochrones between 5 and 10 Gyr, the companions for TYC 5204, TYC 9337, TYC 5450 and TYC 6631 are consistent with with M and K type stars, while for TYC 6736 the closest companion is likely a G type star (Table 3.2).

3.5 Discussion

Binary evolution theory predicts that EL CVn stars descend from very close main sequence binary stars. Multiplicity surveys show that practically all such close main sequence binaries host a distant tertiary, i.e. they are the inner binaries of triple systems. Our observations with SPHERE/IRDIS of five EL CVn confirm this prediction: we find strong companion candidates in all five systems. In what follows we discuss the implications of our finding on the evolutionary history and the future of EL CVn stars.

3.5.1 The evolutionary history of EL CVn triples

EL CVn binaries descend from hierarchical main sequence triple star systems where the inner binary has a very short orbital period of $\lesssim 3$ days. The formation of such close binaries has been a mystery for decades as they cannot form directly via fragmentation of molecular clouds or protostellar discs. Fabrycky & Tremaine (2007) and Naoz & Fabrycky (2014) proposed that Kozai-Lidov oscillations coupled with tidal friction could be responsible for the formation of these close binaries. However, Moe & Kratter (2018) showed that the close binary fractions of very young stars is consistent with those of field stars and that Kozai-Lidov oscillations are too slow to reproduce the observations. Instead, they suggest that energy dissipation due to interactions with the primordial disc during the pre-main sequence is the main mechanism driving the formation of inner binaries with periods less than 10 days.

Key information concerning the origin of very close binary stars may come from combining statistics of stellar multiples with those of the most massive planets and brown dwarfs. Recently, Fontanive et al. (2019) showed that the fraction of tertiaries in systems with close substellar companions is even higher than in the case of stellar binaries. We compare the triple fraction of EL CVn stars with both samples as a function of orbital period in Fig.3.2. As also noted by Moe & Kratter (2019), the similar large fractions of systems with a distant tertiary indicate a similar formation mechanism which is most likely disc fragmentation followed by disc migration. Why this disc fragmentation and subsequent migration occurs nearly only in hierarchical triples is not entirely clear. Either the total initial mass required for this to work is large enough that it is virtually always accompanied by core fragmentation, or a close companion formed through core fragmentation is triggering disc fragmentation at an early stage. In any case, we conclude that according to current theories of close binary formation, EL CVn systems are triple systems with a close inner binary formed through disk fragmentation and subsequent migration. After the main sequence triple has formed, it is assumed to evolve quietly until the more massive star of the inner binary moves off the main sequence and crosses the Hertzsprung gap. This star then fills its Roche-lobe before entering the first giant branch and thermal time scale mass transfer starts. It depends then on the thermal time scales and on the masses of both stars that to what degree this dynamically stable mass transfer remains conservative and how much the orbital period is increased during the mass transfer phase. Mass transfer stops when the envelope of the initially more massive star has been fully stripped off. The result

is an inner binary consisting of the exposed low-mass core and a secondary that is more massive than it initially was (Chen et al., 2017). The tertiary is affected little by the evolution of the inner binary. In most cases it simply spirals out depending on the total mass lost by the inner binary: an EL CVn triple system, as the ones we observed, is born.

3.5.2 The future of EL CVn triples

The evolutionary phase in which the triple system appears as an EL CVn binary with a distant tertiary is probably relatively short. Given the short periods of the EL CVn binaries and in particular of the sample observed by us (see Table 3.1), a second phase of mass transfer is unavoidable. For shorter periods the main sequence star either fills its Roche-lobe while still on the main sequence or in the Hertzsprung gap. In both cases it will not have a deep convective envelope and mass transfer will be stable for mass ratios as large as 3-5 (see Ge et al., 2015, their Fig. 8 and 9). Nevertheless, the mass ratios of the EL CVn stars we observed exceed this limit (table 3.1, using $1/q$ for a proper comparison) and it is therefore likely that the second phase of mass transfer will be dynamically unstable and lead to common envelope evolution. As the orbital energy that is available will not be sufficient to expel the entire envelope of the main sequence star, both stars will merge, hydrogen burning will start around the core until the envelope will be expelled. In other words, the triple systems we currently observe will evolve into wide binary systems with one component being a post-merger white dwarf. If a significant part of the secondary is expelled during this merger process, the white dwarf may not significantly grow in mass and remain in the low-mass white dwarf regime. Interestingly, such a system has recently been observed (Vos et al., 2018) and the authors concluded that it most likely descended from a triple, in perfect agreement with our prediction for the future of close EL CVn binaries.

EL CVn stars with slightly smaller mass ratios than the systems we observed will start thermal time scale mass transfer and evolve into double degenerate stars consisting of two low-mass white dwarfs. These EL CVn stars might therefore be the progenitors of observed double white dwarfs (Bours et al., 2014; Parsons et al., 2020). EL CVn stars with significantly longer periods have not been observed but predicted to exist (though in small numbers). These objects will start mass transfer when the main sequence star evolves into a giant star which will lead to common envelope evolution. Due to the larger initial orbital period, these systems may survive the common enve-

lope phase and form very close double degenerates. For both scenarios, the amount of mass lost during mass transfer or common envelope evolution would be, in most cases, not enough to unbound the third object, even in an *impulsive mass-loss* regime (Veras et al., 2011), i.e. the distant tertiary will move to a larger separation but remain bound to the system. As EL CVn systems are likely to evolve into systems containing extremely low-mass (ELM) white dwarfs, the sample established by the ELM survey (e.g. Brown et al., 2010) might contain a significant number of triple systems. The outlined future evolution of EL CVn stars and the origin of ELM white dwarfs can be tested by searching for these tertiaries.

3.6 Conclusions

The characteristic configuration of EL CVn binaries, close A-F type dwarfs with a very low-mass pre-white dwarf evolving towards higher effective temperatures at nearly constant luminosity, offers a unique way to test the latest white dwarf binary formation theories. The narrow parameter space predicted for the progenitor systems, i.e. orbital periods below $\sim$ 3 days and white dwarf progenitors with masses $\simeq 1.15 - 1.20 M_{\odot}$, implies that (if theories are correct) nearly all EL CVn binaries must be the inner binary stars of hierarchical triples because virtually all main sequence binary stars with periods shorter than 3 days are known to be the inner binaries of such triples.

We performed SPHERE/IRDIS observations of five EL CVn stars and indeed found very strong companion candidates in all five systems. Our results represent a unique and independent confirmation of the predictions of formation theories for EL CVn stars. Discussing the future of EL CVn binaries we found that EL CVn stars and their tertiaries either evolve into wide binaries with a low-mass white dwarf component or into triples with inner binaries consisting of at least one extremely low-mass (ELM) white dwarf. EL CVn triples therefore represent a link between hierarchical main sequence triples with very close inner binary stars and a sub-population of systems containing ELM white dwarfs.

Chapter 4

WD 1856 b: a close giant planet around a white dwarf that could have survived a common-envelope phase

The discovery of a giant planet candidate orbiting the white dwarf WD 1856+534 with an orbital period of 1.4 d poses the questions of how the planet reached its current position. In this final chapter we reconstruct the evolutionary history of the system assuming common envelope evolution as the main mechanism that brought the planet to its current position. We find that common envelope evolution can explain the present configuration if it was initiated when the host star was on the AGB, the separation of the planet at the onset of mass transfer was in the range 1.69–2.35 au, and if in addition to the orbital energy of the surviving planet either recombination energy stored in the envelope or another source of additional energy contributed to expelling the envelope. We also discuss the evolution of the planet prior to and following common envelope evolution. Finally, we find that if the system formed through common envelope evolution, its total age is in agreement with its membership to the Galactic thin disc. We therefore conclude that common envelope evolution is at least

as likely as alternative formation scenarios previously suggested such as planet-planet scattering or Zeipel-Lidov-Kozai (ZLK) oscillations.

4.1 Evidence of planets surviving the evolution of its host star

The vast majority of the stars in the Galaxy, including our Sun and virtually all known planet hosts will end their lives as white dwarfs. It is now well established that planets can survive the transformation of their host star into a white dwarf (Villaver & Livio, 2007; Mustill & Villaver, 2012; Rao et al., 2018; Ronco et al., 2020). Indirect observational evidence for the existence of planets around white dwarfs comes from the detection of photospheric metal absorption lines found in $20-30$ per cent of all white dwarfs (Zuckerman et al., 2010; Koester et al., 2014; Hollands et al., 2017), the discovery of dusty (Zuckerman & Becklin, 1987; Farihi et al., 2009; Rocchetto et al., 2015; Wilson et al., 2019) and gaseous discs (Gänsicke et al., 2006, 2007; Dennihy et al., 2020; Melis et al., 2020) around a small sub-sample of these white dwarfs, the detection of a transiting planetesimal (Vanderburg et al., 2015) in the process of disintegration (Gänsicke et al., 2016), orbital motion in the gaseous disc around the white dwarf SDSS J1228+1040 which potentially indicates the presence of a planetary remnant (Manser et al., 2019), and finally an evaporating giant planet in close orbit around the young and hot white dwarf WD J0914+1914 (Gänsicke et al., 2019). In all the above cases, the planetary material in close orbit around the white dwarf is usually assumed to have been scattered inward by gravitational interactions with a larger body, most likely a massive gas giant planet (Nordhaus & Spiegel, 2013; Mustill et al., 2018), or by the eccentric ZKL mechanism if the white dwarf is a member of a wide binary (Stephan et al., 2017).

Very recently, Vanderburg et al. (2020) reported the discovery of a giant planet candidate, WD 1856 b, orbiting the cool and old white dwarf WD 1856+534 (hereafter WD 1856) with a short orbital period ($\simeq 1.4$ d). The authors discussed several evolutionary scenarios that could in principle explain the close orbit of the massive planet ($\leq 14 M_{jup}$), including common envelope (CE) evolution, dynamical instability in a multiplanet system through the ZLK mechanism (the white dwarf belongs to a visual triple star system) or planet-planet scattering events, both followed by tidal circularization, as well as other less likely scenarios such as instabilities due to galactic

tides, close stellar encounters, close encounter scattering events between two planets near the periastron, tidal dissipation during the stellar giant phase, and partial tidal disruption. In line with the generally accepted interpretation for planetesimals and even Neptune-mass planets found in the proximity of white dwarfs, Vanderburg et al. (2020) concluded that dynamical instabilities through close encounters with an additional object in the system, which excited large orbital eccentricities and subsequent tidal circularization, is the most reasonable explanation for the close orbit of WD 1856 b.

Here we take a closer look at one scenario that has been considered unlikely by Vanderburg et al. (2020), i.e. CE evolution. We reconstruct the CE phase following the evolution of the progenitor of the white dwarf and find that CE evolution is in fact a plausible scenario to explain the current orbital configuration of the system. As in several close binary systems that most likely formed through CE evolution, only a small fraction of recombination energy is required to contribute to the envelope ejection process.

4.2 Reviewing the arguments against common envelope evolution

Vanderburg et al. (2020) concluded that a CE evolution was highly unlikely to be the origin of the planet's current proximity to the white dwarf based on two arguments. The authors highlighted that the known white dwarf (and subdwarf) plus brown dwarf binaries collated by Nelson et al. (2018) differ from WD 1856 as all have short ($\lesssim$4 h) orbital periods and large ($\gtrsim$50 M_{jup}) masses, i.e. rather different from the much longer period and lower mass of the planet candidate in WD 1856, providing an empirical argument that it might not have survived CE evolution. However, the sample listed by Nelson et al. (2018) is small, and likely subject to significant selection effects. The majority of these systems were identified via the detection of either eclipses (Geier et al., 2011) or emission lines from the irradiated companion (Maxted et al., 2006). Companions with longer orbital periods have a rapidly dropping probability of eclipsing the white dwarf, and their surfaces intercept less flux from the white dwarf resulting in weaker or absent emission lines. The latter is of course also true for companions orbiting cooler white dwarfs. We note here that GD 1400 is a nearby ($\simeq$ 46 pc) white dwarf with a long-period ($\simeq$ 10 h, Burleigh et al. 2011) brown dwarf

companion identified initially as a weak infrared excess (Farihi & Christopher, 2004).

The much larger sample of post CE binary stars with low-mass stellar companions spans a wider range of orbital periods and both the CE efficiency as well as the contributions from additional energy sources required to reconstruct their evolutionary paths can vary (Nebot Gómez-Morán et al., 2011b; Zorotovic et al., 2014). The longer period of WD 1856 b might therefore, on its own, not represent a strong argument against CE evolution.

Vanderburg et al. (2020) also performed a simple reconstruction of CE evolution based on an analytic study of the parameterized equation that relates the binding energy of the envelope and the change in orbital energy:

$$\frac{GM_1M_\mathrm{e}}{\lambda R_\mathrm{L}} = \alpha_\mathrm{CE}\left[\frac{GM_\mathrm{c}M_2}{2a_\mathrm{f}} - \frac{GM_1M_2}{2a_\mathrm{i}}\right] \tag{4.1}$$

where M_1, M_e, M_c and M_2 are the masses of the primary star (the white dwarf progenitor), its envelope, its core (the future white dwarf) and the companion (the planet candidate), respectively, at the onset of CE evolution. R_L is the equivalent volume radius of the Roche-lobe (defined by $V = 4/3\pi R_\mathrm{L}^3$ with V being the Roche-volume), usually calculated with the Eggleton formula (Eggleton, 1983). At the onset of CE evolution this radius is identical to the radius of the primary star. a_i and a_f correspond to the orbital separation at the onset of the CE phase and immediately after the CE is ejected. The CE efficiency, α_CE, corresponds to the fraction of orbital energy lost during the CE phase that is used to unbind the envelope of the white dwarf progenitor, while λ is a binding energy parameter that depends on the mass and evolutionary stage of the giant star. Vanderburg et al. (2020) neglected the second term in the right-hand side of Eq. 4.1 and used an analytical expression for the maximum radius of the star that only depends on its core mass (Eq. 8 in their article). Using those assumptions, they derived the orbital period at the onset of the CE phase which combined with Eq. 4.1 translates into an expression for the minimum $\alpha_\mathrm{CE}\lambda$ needed to unbind the envelope (avoiding a merger) that only depends on the measured parameters (white dwarf mass, companion mass and orbital period) and on the mass of the white dwarf progenitor. Vanderburg et al. (2020) found that the values of $\alpha_\mathrm{CE}\lambda$ they derived were larger than the tabulated results of Xu & Li (2010), which were computed for different progenitor masses and for a range of typical radii, even when including recombination energy, and concluded that CE evolution is a highly unlikely scenario. However, a caveat to that conclusion is that the resolution in stellar mass of the tables from Xu & Li (2010) is very coarse ($1\mathrm{M}_\odot$), and that these authors did not consider mass loss

prior to the envelope ejection. It is evident from Xu & Li (2010, their Fig. 1) that the λ parameter has a completely different behavior when changing from one to two solar masses, even reversing the slope of its dependence on the radius. A finer grid, especially in the range of $1 - 2\,M_\odot$, which brackets the likely initial mass of the white dwarf progenitor of WD 1856, is essential to derive a firmer conclusion.

Here we therefore perform a more detailed reconstruction of the CE phase, considering mass loss prior to this phase, the possible contribution of recombination energy to the process of ejection of the envelope, and proper calculations for λ depending on the mass and the evolutionary state of the primary star.

4.3 Reconstructing common envelope evolution

Based on its kinematics, Vanderburg et al. (2020) found that WD 1856 most likely belongs to the thin disc of the Galaxy, which puts an upper limit of $\simeq 10\,\mathrm{Gyr}$ on the age of the system. As already noted by Vanderburg et al. (2020), if the white dwarf formed from single star evolution, this age limit is in conflict with the best-fit white dwarf mass ($0.518 \pm 0.055\,M_\odot$), i.e. the sum of the white dwarf cooling age and the main-sequence life time of its progenitor exceed the age of the thin disc.

We revisit this problem by calculating the total age of WD 1856 using the single star evolution (SSE) code (Hurley et al., 2000) for the main sequence and post main sequence evolution and the white dwarf models of Bédard et al. (2020) to determine the cooling age of the white dwarf. Given the atmosphere of WD 1856 is most likely a mixture of hydrogen and helium (Vanderburg et al., 2020), we computed the age for the two limiting cases, where, for a given mass, the pure hydrogen and pure helium case represent an upper and lower limit on the cooling age of the white dwarf. The total age of WD 1856, if formed through single star evolution, is illustrated by the blue dashed line in Fig. 4.1, clearly indicating that the white dwarf mass has to be $\gtrsim 0.57\,M_\odot$ for its age to be below 10 Gyr, with the exact value depending on the (uncertain) atmosphere composition. If the white dwarf mass is as small as measured by Vanderburg et al. (2020), every evolutionary scenario for WD 1856 and its close-in planet that assumes the white dwarf has formed through single star evolution, implies an age of the white dwarf in conflict with its membership to the thin disk of the Galaxy. CE evolution can truncate the core-growth of a giant star and therefore more massive stars, with a shorter main sequence lifetime, can be the progenitors of low-mass white dwarfs, which reduces the total age of the system.

To evaluate the possibility of CE evolution for WD 1856 we here use an algorithm that we previously applied to reconstruct CE evolution of white dwarfs with close low-mass star companions (Zorotovic et al., 2010, 2014). In brief, the algorithms works as follows. We calculated a grid of stellar evolution tracks using SSE with initial masses up to eight solar masses (with a step size of $0.01 M_{\odot}$). As CE evolution truncates the core growth of the giant star, the core mass of the giant star at the onset of CE evolution must have been equal to the white dwarf mass in the post-CE system. We therefore first search our grid for giant stars with a core mass equal to the measured white dwarf mass. As we know the radius and the mass of each of the identified potential white dwarf progenitor stars, we can for all of them determine the orbital period at the onset of CE evolution using the mass of the companion and Roche-geometry. In other words, we can determine the period and stellar masses for every possible progenitor system. Knowing the stellar masses and the period at the onset of CE evolution and comparing it with those of the post-CE system, provides the change in orbital energy during CE evolution for each of these potential progenitor binary star systems. As we also know the amount of recombination energy stored in the envelope of the giant at the onset of CE evolution, computed as in Claeys et al. (2014) and Hurley et al. (2002), we can test whether sufficient energy is available to unbind the envelope of the giant. If this is the case, we consider this particular system a possible progenitor configuration. Searching our finely space gird, we can therefore find virtually all possible progenitors for a given white dwarf mass, post-CE orbital period, and companion mass. If the effective temperature of the white dwarf is known as well, we can also calculate the total age of each potential progenitor system by summing the cooling age of the white dwarf (obtained from the tracks of Bédard et al. 2020) as well as the main sequence and post main sequence lifetime of the progenitor star (obtained from SSE). Our reconstruction algorithm does not consider the evolution of the system prior to mass transfer. We will discuss possible evolutionary scenarios that lead to the onset of CE evolution in the next section.

We searched for CE progenitor configurations for WD 1856 over a range of white dwarf masses covering twice the uncertainty in mass provided by Vanderburg et al. (2020), i.e. $0.408 - 0.628\,M_{\odot}$. We used the measured current orbital period of 1.41 d, and adopted the largest possible mass of $14\,M_{\rm jup}$ for the planet, which corresponds to the upper end of the mass range derived by Vanderburg et al. (2020), and again the two limiting cases for the composition of the atmosphere (pure hydrogen and pure helium). The shaded regions in Fig. 4.1 show the possible progenitor systems that

we identified as a function of total age and white dwarf mass. We distinguish three cases for the contribution of recombination energy to unbind the CE: no recombination energy used (i.e. $\alpha_{\rm rec} = 0$, black area), less than 10 per cent of contribution (i.e. $0 < \alpha_{\rm rec} \leq 0.1$, solid gray area), and up to 100 per cent of contribution (i.e. $0 < \alpha_{\rm rec} \leq 1$, shaded gray area). The vertical line shows the best-fit white dwarf mass of Vanderburg et al. (2020), and the two lower and upper horizontal red lines give the estimated age for the thin disc of the Galaxy and the Hubble time, respectively.

To what degree recombination energy can contribute to CE ejection is intensively discussed. While Ivanova et al. (2015) suggest that recombination energy can play a fundamental role, others (e.g. Soker & Harpaz, 2003) argue that the opacity of the envelope is too small for recombination energy to provide an important contribution. Based on the latter argument and on the fact that the evolutionary history of two post-CE binary star systems with long orbital periods (IK Peg and KOI-3278) can be understood by assuming a small fraction (1 and 2 per cent) of recombination energy to contribute (Zorotovic et al., 2010, 2014), we here consider as realistic those cases in which the efficiency of recombination energy remains below 10 per cent. Table 4.3 lists the orbital parameters, initial and at the onset of CE evolution, for the possible solutions, taking into account the restriction in age (total age below 10 Gyr) and keeping the fraction of recombination energy below 10 per cent (dark grey and black regions in Fig. 4.1). The values provided for λ include contributions from recombination energy. Therefore λ can become significantly larger than one (see also e.g. Dewi & Tauris, 2000) and the left-hand side of Eq. 4.1 corresponds to the binding energy reduced by a fraction of recombination energy contributing to unbinding the envelope.

All possible progenitors that filled their Roche-lobes on the first giant branch ($M_{\rm WD} < 0.5 {\rm M}_{\odot}$ in Fig. 4.1) exceed the age limit significantly, reaching total ages even larger than the Hubble time for smaller white dwarf masses. This includes post-CE binaries in which the white dwarf evolves first into a Helium burning horizontal branch star and the envelope is fully expelled. In all the reconstructed cases that fulfill the age (below 10 Gyr) and recombination energy constraint (not more than 10 per cent), the progenitor had to be on the thermally pulsating asymptotic giant branch (TPAGB) phase when it filled its Roche lobe. During this phase the binding energy parameter λ can take values well above unity when recombination energy is considered (see Fig. 5 in Camacho et al., 2014), which implies that the envelope can be very loosely bound. Therefore, even considering only a small fraction of the available recombination energy to contribute to the ejection process allows us to reconcile the current

Parameter	Pure-H model	Pure-He model
Initial mass of the progenitor ($M_\odot$)	$1.51 - 2.31$	$1.41 - 2.31$
Mass of the progenitor at CE onset ($M_\odot$)	$1.20 - 2.07$	$1.09 - 2.07$
Age of the progenitor at CE onset (Gyr)	$1.00 - 3.03$	$1.00 - 3.78$
Orbital separation at CE onset (au)	$1.69 - 2.35$	$1.69 - 2.35$
Radius of the progenitor at CE onset (au)	$1.23 - 1.73$	$1.23 - 1.73$
Post-CE white dwarf mass ($M_\odot$)	$0.561 - 0.628$	$0.551 - 0.628$
$\alpha_{\rm CE}$	$0.36 - 1.00$	$0.36 - 1.00$
$\alpha_{\rm rec}$	$0.04 - 0.10$	$0.04 - 0.10$
λ	$3.72 - 10.95$	$3.08 - 10.95$

Table 4.1: Range of reconstructed parameters for the white dwarf progenitor + planet candidate binary assuming a CE evolution, restricting $\alpha_{\rm rec} \leq 0.1$ and the total age of the system to be less than 10 Gyr.

configuration of the white dwarf and the surrounding planet candidate with CE evolution. Also, according to our reconstruction code, the progenitor of the white dwarf must have already lost $\simeq 20$ per cent of its initial mass when the CE phase occurred, which facilitates the ejection.

The large number of possible solutions we find with our reconstruction algorithm clearly illustrates that CE evolution represents a plausible scenario for the formation of WD 1856 and its close planetary companion. In particular, CE evolution allows for a larger range of masses and younger ages for the white dwarf than formation scenarios that assume the white dwarf formed through single star evolution.

However, it is important to keep in mind that so far we assumed a planetary mass corresponding to the upper limit provided by Vanderburg et al. (2020), i.e. 14 $M_{\rm jup}$. If the mass of the planet is smaller than this upper limit, which cannot be excluded, the number of possible solutions found by our reconstruction algorithm decreases. We ran our algorithm for smaller planet masses and for values below five $M_{\rm jup}$ we did not find solutions with ten per cent or less of the available recombination energy contributing to expelling the envelope. If the planet mass can be measured in the future and turns out to be below five $M_{\rm jup}$, CE evolution should therefore be considered a rather unlikely scenario. For larger planet masses, CE evolution represents a convincing explanation for the existence of the system.

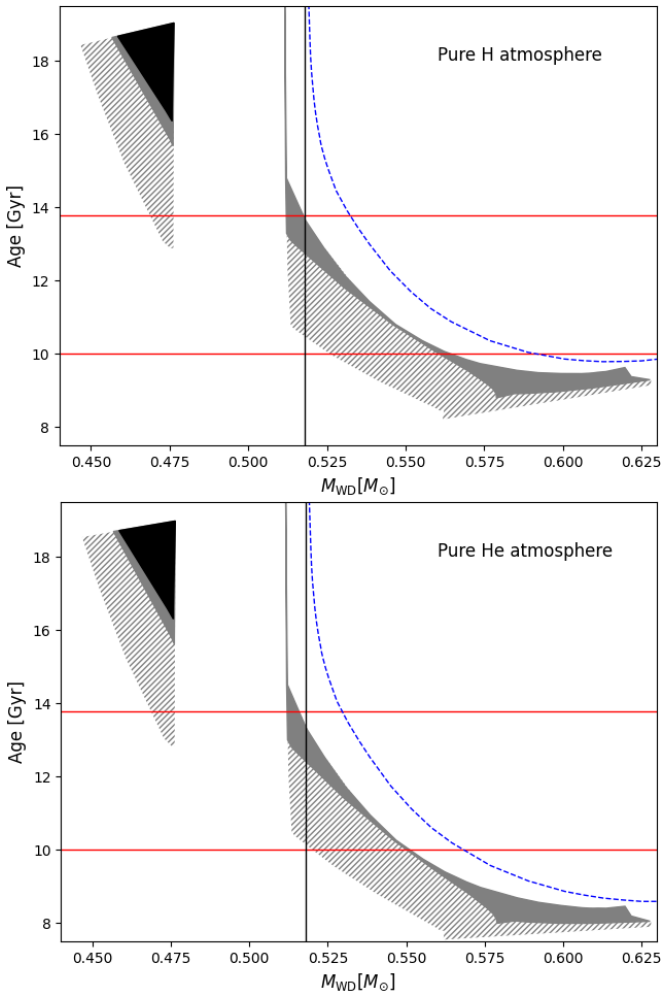

Figure 4.1: Total system age of WD 1856 as a function of the white dwarf mass derived from our reconstruction for CE evolution and adopting cooling ages for pure-hydrogen (left panel) and pure-helium (right panel) atmospheres. We assumed that recombination energy contributed not at all to the ejection of the CE (solid black area), less than 10 per cent (solid gray area), or up to 100 per cent (shaded gray area). For comparison, the blue dashed line corresponds to the estimated age of the white dwarf assuming single star evolution (i.e. no CE phase). We searched for possible CE progenitor systems across a range of white dwarf masses in the range $0.408 - 0.628$, i.e. bracketing the best-fit measurement ($0.518\,M_\odot$, vertical black line, Vanderburg et al. 2020) by twice the uncertainty of the measurement ($\pm 0.055\,M_\odot$). The upper and lower horizontal red lines correspond to the age of the Universe (13.8 Gyr) and the estimated age of the oldest stars within the thin disc of the Galaxy (10 Gyr), respectively. CE solutions exist for white dwarf masses in the considered white dwarf mass range and with total ages below the age of the thin disk while single star evolutionary models require a slightly large white dwarf mass.

4.4 Prior to common envelope evolution

In order to trigger CE evolution, the planet WD 1856 b must have been located at $1.69 - 2.35$ au at the end of the main sequence evolution of its host star. This separation can be achieved early during the pre-main sequence due to angular momentum exchange between the planet and the protoplanetary disc. The classical core accretion formation scenario (Mizuno, 1980; Bodenheimer & Pollack, 1986; Pollack et al., 1996), along with type I and II disc migration (Ward, 1997; Tanaka et al., 2002; Lin & Papaloizou, 1986; Armitage, 2007), can naturally lead to formation of planets like WD 1856 b at locations in the range of $\sim 1 - 10$ au (see Mordasini, 2018, for details). Furthermore, even planets formed through gravitational instability can be subject to disc migration (Boss, 2005; Cha & Nayakshin, 2011). In particular, with 2D hydrodynamical simulations Baruteau et al. (2011) showed that these planets can migrate inward due to their interactions with the disc on the fast type I migration-like timescales.

If the planet around WD 1856 migrated inward to separations of a few au while the protoplanetary disk was still present, it must later have survived the first giant branch evolution of the host star and triggered mass transfer and a subsequent CE phase. We tested how realistic this scenario is using the code by Ronco et al. (2020) but applying the eddy turnover time scale given in Villaver & Livio (2009) in the description of tidal forces. We found that for an initial stellar mass of $1.5 M_\odot$ and considering stellar tides, the initial semi-major axis for a $10 M_{\rm jup}$ planet to survive the RGB and to possibly generate CE evolution during the AGB is beyond 2.20 au. For larger stellar masses (e.g $2 M_\odot$), smaller separations are possible as the tip of the first giant branch is very short and therefore tides during the first giant branch have less impact on the planet separation. It is therefore entirely possible that the planet migrated inward to a separation exceeding a few au, survived the first giant branch evolution, was brought further in due to tides when the star was on the AGB, and finally triggered mass transfer when reaching a separation in the range of $1.69 - 2.35$ au as predicted by our reconstruction of CE evolution.

Given that WD 1856 and its planetary companion are members of a multiple star system, with a distant M-dwarf binary, an alternative evolution of the system prior to CE evolution are ZLK oscillations (Kozai, 1962; Lidov, 1962). In order to evaluate this possibility, we used the SECULARMULTIPLE code (Hamers & Portegies Zwart, 2016a; Hamers, 2018, 2020), which allows to calculate the secular orbit-averaged evolution

of the planet during the main sequence evolution of the host star, including the effect of tidal bulges, tidal friction and general relativity. We also implement the single-star-evolution (SSE) code (Hurley et al., 2000) to model radial expansion, contraction, structure changes, and mass loss due to stellar evolution of the white dwarf progenitor. We found that for the case of 1.41 and 2.31 $M_\odot$ white dwarf progenitor masses and initial semi-major axis exceeding 4 au, the star can experience Roche lobe overflow during the asymptotic giant branch as required to trigger CE evolution. While the exact outcome of the quadruple dynamics is very sensitive on the initial values of the argument of periapsis, longitude of ascending nodes, and eccentricity of the outer binary, and in particular the mutual inclination, this shows that quadruple dynamics offer an alternative mechanism that might have brought WD 1856 b close enough to generate a CE phase. Figure 4.2 shows one of the simulations in which Roche-lobe overflow and therefore CE evolution is triggered (black line). This simulation also illustrates that the assumption for initially circular planetary orbits in our reconstruction algorithm is reasonable as tidal forces circularize the orbit before dynamically unstable mass transfer leads to CE evolution.

4.5 Evaporation during and after the common envelope phase

While stellar companions clearly survive orbiting within a CE (as long as they do not merge with the core of the giant star), this is not necessarily true for planetary mass companions. In fact, Nelemans & Tauris (1998) considered evaporating or merging planetary mass companions as a possible explanation for observed single low-mass white dwarfs without a stellar companion. In order to evaluate whether the planet candidate around WD 1856 would have survived inside the envelope, we here follow their approach.

As the planet will move inside the envelope during CE evolution, it can be completely evaporated. Soker (1998) suggested that this occurs if the local sound speed (c_s) in the envelope reaches the escape velocity (v_{esc}) of the planet, i.e.

$$c_s^2 \approx v_{esc}^2 \iff \gamma \frac{k_B T}{\mu m_u} \approx \frac{2 G M_p}{R_p}, \tag{4.2}$$

where R_P and M_P are the radius and the mass of the planet, and T is the temperature of the envelope at the distance from the core (r). Using this criterion and assuming the

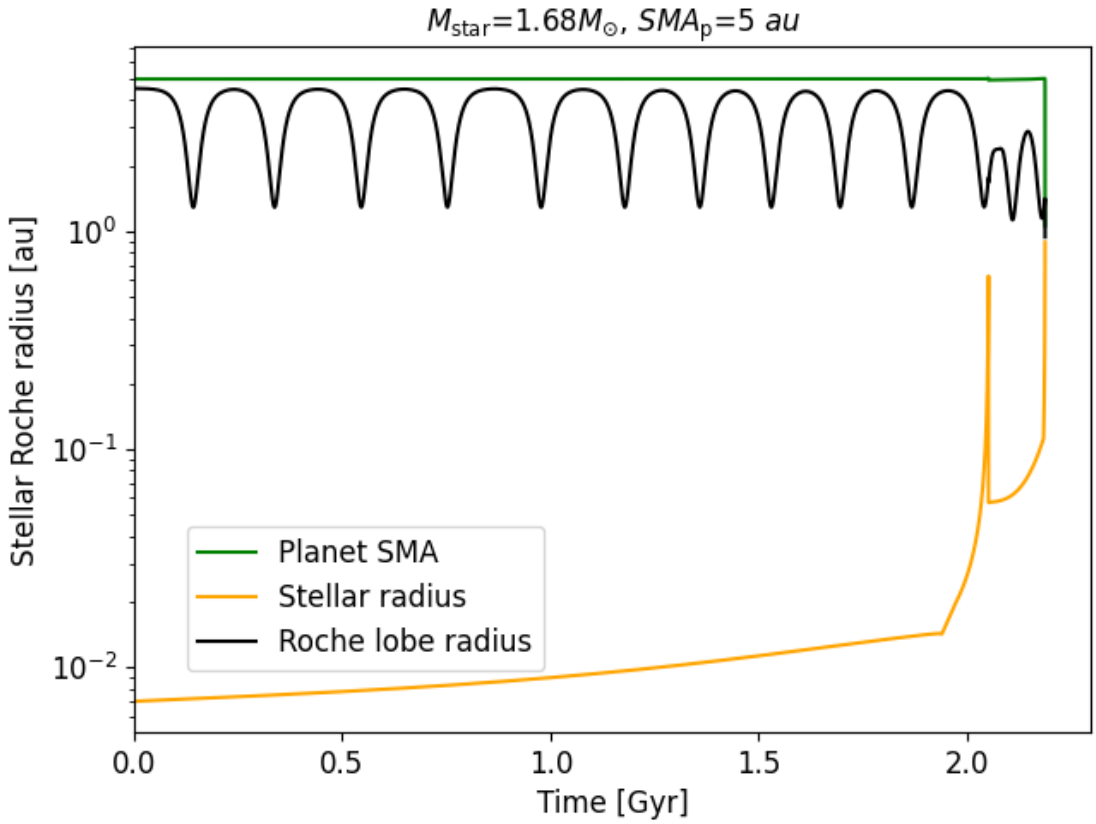

Figure 4.2: Secular evolution of the stellar Roche lobe radius for a 1.68 $M_\odot$ white progenitor being orbited by a 14 M_{jup} planet with a semi-major axis of 5 au. The gravitational perturbation exerted by the M-dwarf binary located at 1000 au trigger KL oscillations on the planet, which combined with tidal forces during the red and asymptotic giant branch approaches the planet to the star until the latter fills its Roche lobe during the asymptotic giant branch. The initial eccentricities for the planet, M-dwarf binary and outer orbit are 0.001, 0.3 and 0.3 respectively. Both the argument of periapsis (ω) and longitude of the ascending node (Ω) are set to 0 for the outer and M-dwarf binary orbits. For the planet's orbit we set $\omega_p = 60°$ and $\Omega_p = 80°$.

same temperature structure of the envelope as Nelemans & Tauris (1998), i.e.

$$T \simeq 1.78 \times 10^6 \times (r/\mathrm{R}_\odot)^{-0.85}\mathrm{K}, \tag{4.3}$$

we can estimate at which separation form the core (the future white dwarf) a planet with a given mass and radius would be fully evaporated inside the giant stars envelope. For the measured parameters of WD 1856 we find that for separations exceeding $0.71\mathrm{R}_\odot$ the planet should survive inside the giants envelope which is well below the current separation of the planet.

As has been shown by Bear & Soker (2011b), evaporation may remain an issue for planets that survived CE evolution. Indeed, immediately after the envelope has been expelled, the strong EUV radiation by the hot white dwarf generates hydrodynamic escape in hydrogen dominated atmospheres up to orbital distances of several astronomical units and may even generate detectable accretion onto the hot white dwarf (Schreiber et al., 2019). To estimate whether WD 1856 b could have survived this phase of strong EUV evaporation at its current position, we use simple scaling laws for hydrodynamic escape.

For large EUV fluxes, mass loss due to hydrodynamic escape can be in the energy limited or the recombination limited regime. In the first case mass loss is proportional to the EUV irradiation while it scales with the square root of the EUV irradiation in the latter. For a Jupiter-mass planet, the transition between both regimes is usually assumed to occur at $10\,000\,\mathrm{erg\,cm^{-2}s^{-1}}$. For the mass loss rate in the energy limited regime of irradiated giant planets we used (Murray-Clay et al., 2009):

$$\dot{M} = \frac{\epsilon \pi F_{\mathrm{EUV}} R_{\mathrm{P}}^3}{G M_{\mathrm{P}} K(\xi)} \tag{4.4}$$

where F_{EUV} is the incident EUV flux, and ϵ the efficiency of using the incident energy, which we set to $\epsilon = 0.3$ (Murray-Clay et al., 2009; Owen & Alvarez, 2016). As WD 1856 b is quite close to the white dwarf, where the Roche-lobe ($R_{\mathrm{L_P}}$) and planet radius become somewhat comparable, mass loss is slightly enhanced. This is accounted for by the correction term $K(\xi = R_{\mathrm{L_P}}/R_{\mathrm{P}})$ for which we used equation 17 from Erkaev et al. (2007). We calculated the EUV fluxes from the same model spectra used in Schreiber et al. (2019); Gänsicke et al. (2019) and used the above equations to estimate the mass loss rate. Figure 4.3 shows the resulting mass loss rate as a function of effective temperature (and cooling age). The total mass loss is clearly negligible and we therefore conclude that neither during nor after CE evolution the planet was significantly affected by evaporation.

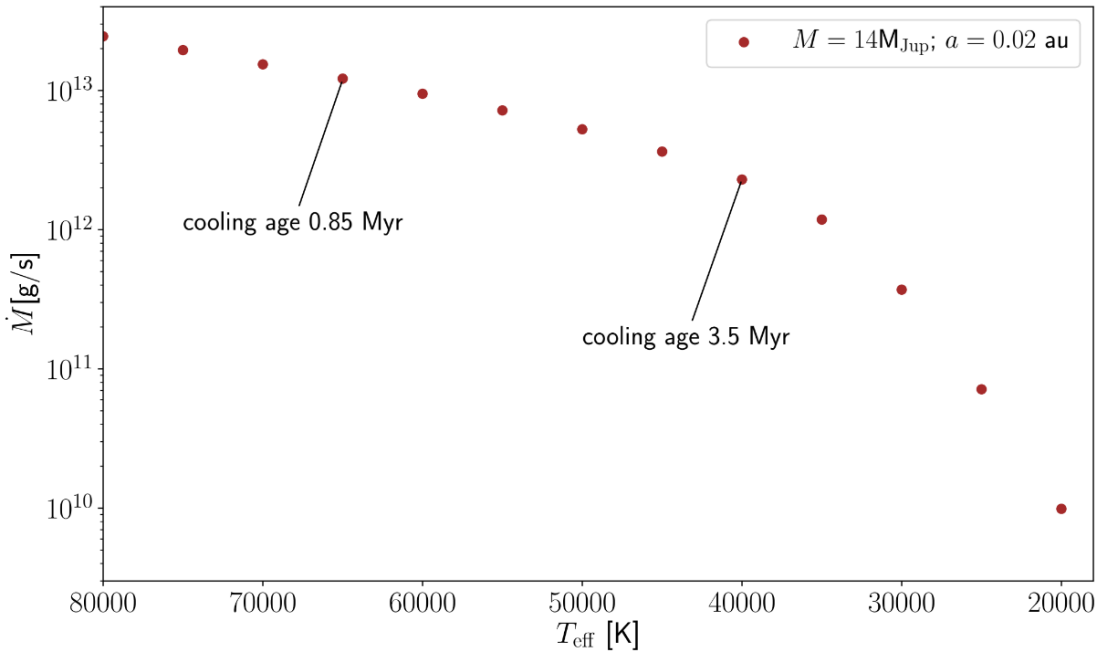

Figure 4.3: Mass loss rate of the planet due to the strong EUV irradiation by the hot white dwarf following CE evolution as a function of effective temperature. While the mass loss rate must have led to detectable accretion for several million years, the total mass loss is far below one per cent of the planets mass and is clearly negligible.

4.6 Concluding discussion

We have re-evaluated CE evolution as a possible mechanism to explain the existence of the gas giant planet candidate in a close 1.4 day orbit around the white dwarf WD 1856. Reconstructing the CE evolution we found that it offers a reasonable evolutionary scenario for this system. There exist plenty of mechanisms, including triple dynamics, that could have brought the planet to the location required to trigger CE evolution (separations of $1.69 - 2.35$ au). The planet would also not have suffered important mass loss due to evaporation, neither during nor after CE evolution. Most importantly, we find that during CE evolution enough energy is available to unbind the envelope. If only $4 - 10$ per cent of the available recombination energy contributed to expelling the envelope and the mass of the planet is between five M_{jup} and the upper limit of $14\,M_{jup}$ derived by Vanderburg et al. (2020), the evolution of WD 1856 can be fully understood in the context of CE evolution, similar to the cases of the post-CE binary stars IK Peg and KOI-3278 (Zorotovic et al., 2014).

Our results clearly show that if energy in addition to the orbital energy provided by the spiral-in of the planet contributed to expelling the envelope, CE evolution can explain the current configuration of WD 1856. In our simulations we assumed this additional energy to be recombination energy. However, in theoretical considerations of CE evolution the opinions on whether recombination energy can indeed significantly contribute to the envelope ejection process differ drastically. While Webbink (2008b) as well as more recently Ivanova et al. (2015) and Ivanova (2018) found that recombination energy can play an important role, others argue that most of the recombination energy is radiated away and that it therefore has a limited impact on the envelope ejection process (e.g. Sabach et al., 2017; Grichener et al., 2018; Soker et al., 2018). If recombination energy turns out to be indeed largely inefficient, other energy sources might have helped the planet to unbind the envelope of the giant. Examples for possible energy sources that have been discussed, but are usually considered less likely to provide important contributions, include accretion energy, nuclear energy, enthalpy (see Ivanova et al., 2013, for more details), or jets (Sabach et al., 2017). Recently, Wilson & Nordhaus (2019) added that the ejection efficiency is sensitive to the properties of the surface-contact convective region and that including convection may aid ejection without the need for additional energy sources. Potentially most interesting in the case of WD 1856, however, is the possibility that orbital energy of an additional giant planet played a role. This hypothetical additional planet could have initially been lo-

cated somewhat closer to the star than WD 1856 b and therefore did not survive the metamorphosis of the host star, but a fraction of its orbital energy could have helped WD 1856 b in its effort to expel the giant envelope. A scenario involving inner planets that are engulfed has been suggested earlier by Bear & Soker (2011a) to explain the existence of the later refuted planet around the horizontal branch star HIP 13044. As this alleged planet had a long orbital period (16.2 days) for a post CE system, the theoretical scenarios that were developed towards explaining its existence are worth to be considered for WD 1856 b. Apart from the multi-planet suggestion, the incomplete envelope ejection scenario proposed by Bear et al. (2011) could apply to WD 1856 b. According to this model, the planet was engulfed for a short period of time at the end of the first giant branch evolution of the host star and only a fraction of the common envelope was ejected (see also Passy et al., 2012).

Given the large variety of evolutionary scenarios involving a CE, given that WD 1856 is not alone with its need for additional energy, and given the fact that several realistic mechanisms that might have provided this extra energy are in principal available, CE evolution clearly represents a reasonable scenario for the evolutionary history of WD 1856 and its close planetary companion.

Alternative scenarios that have been suggested for the formation of WD 1856 and its close planetary companion are planet-planet scattering (Vanderburg et al., 2020) and triple dynamics (O'Connor et al., 2020; Muñoz & Petrovich, 2020; Stephan et al., 2020). An important observational constraint on possible evolutionary scenarios would be provided by a mass measurement of the planet. The currently available observations allow for planet masses between $14\,M_{jup}$ and $0.1\,M_{jup}$. The eccentric ZLK mechanism works only for planet masses as small as $1-3\,M_{jup}$ (Muñoz & Petrovich, 2020) and also planet-planet scattering is more likely to bring lower mass planets to close orbits around the white dwarf (Maldonado et al., 2020). In contrast, CE evolution predicts the planet mass to most likely exceed five M_{jup}.

However, for all alternative scenarios to CE evolution, the likely membership of WD 1856 to the Galactic thin disc, limiting its age to $\simeq 10\,$Gyr, poses an additional problem if the white dwarf mass is as small as measured by Vanderburg et al. (2020). This conclusion does not depend on the assumed metallicity of the white dwarf progenitor or the initial to final mass ratio. Table 4.2 lists the white dwarf progenitor masses for a sample of initial to final mass ratios and the corresponding main sequence lifetime derived using SSE, assuming a white dwarf mass of $0.52M_{\odot}$. The time since the end of the main sequence until the progenitor becomes a white dwarf is around

$M_{ms}(M_\odot)$	τ_{ms}(Gyr)	IFMR reference
1.154	6.45	Weidemann (2000)
1.403	3.35	Williams et al. (2009)
0.948	13.53	Catalán et al. (2008)
1.363	3.66	Casewell et al. (2009)
1.156	6.65	Kalirai et al. (2008)
0.885	14.51	SSE (z = 0.01)
1.020	10.20	SSE (z = 0.02)
1.170	6.83	SSE (z = 0.03)

Table 4.2: Main-sequence mass and lifetime for a 0.52 $M_\odot$ white dwarf progenitor. The progenitor masses were derived using five different initial to final mass relations from the literature (first five rows) and the evolutionary code SSE (Hurley et al., 2000) with three different metallicities (last three rows). The main-sequence lifetimes were all derived using SSE, assuming solar metallicity for the first five rows.

1-1.7 Gyr, depending on the assumed metallicity. The cooling age, calculated from the Bédard et al. (2020) cooling sequences, lies between 5.77 and 6.11 Gry depending on the composition of the white dwarf atmosphere. Adding the post main sequence lifetime and the cooling age to the main sequence lifetimes listed in Table 4.2, we find that all of the listed initial to final mass ratios lead to total ages exceeding the age of the Galactic thin disc (10 Gyr), even assuming the shortest times derived for the post main sequence evolution and the white dwarf cooling. We therefore conclude that CE evolution is the most likely scenario for the history of WD 1856 if the white dwarf mass is $\simeq 0.52 \pm 0.05 M_\odot$ as measured by Vanderburg et al. (2020). If the white dwarf mass is somewhat larger, i.e. $\simeq 0.6 M_\odot$, CE evolution remains one possibility together with alternative models such as close encounters with other planets in the system or ZLK oscillations triggered by the distant companions. As CE evolution is the only scenario currently available consistently solving the age issue, we predict the planet mass to be above five M_{jup}.

CHAPTER 5

Summary and future prospects

In thesis I present three different science cases in which binaries and hierarchical triple systems with white dwarf remnants provide crucial information concerning mass transfer mechanisms and the role of the tertiary star in the dynamical evolution of triple systems.

We have shown that the orbital periods and primary masses of eccentric main-sequence binaries (most of them most likely part of hierarchical triples) discovered in a sample of post common envelope binaries (PCEBs) with A, F, G or K -type secondaries suggest that, together with common envelope evolution, stable non-conservative mass transfer might have an important role in the formation of close white dwarf + AFGK main-sequence binaries and double white dwarf, i.e. supernovae type Ia progenitor. Despite our hypothesis is subject to some observational biases and a small sample of well-characterised white dwarf + AFGK PCEBs, it presents a consistent scenario with the current observations. The white dwarf binary pathways survey team is actively working to increase the number of confirmed white dwarf + AFGK PCEBs, and we are currently working on a new eccentric binary which turned out to be part of a triple system. Given its particular configuration with an extremely low mass (ELM) white dwarf and an inner period of ≈ 52 d, this systems supports the stable non-conservative mass transfer scenario. These results will be published in an upcoming paper.

We also have used triple systems to test current models on the formation of EL CVn binaries, composed of an ELM pre-Helium white dwarf and an A or F-type compan-

ion. According to the $\alpha_{\rm CE}$-formalism for common envelope evolution, these binaries could not have formed through this mechanism, being the most likely formation scenario non-conservative mass transfer. A consequence of the latter is that most EL CVn progenitors must have orbital periods $\lesssim 3$ d, which in turn, based on current surveys of multiple star systems, implies that EL CVn progenitors, and most likely current EL CVns binaries are inner binaries of hierarchical triples. Our discovery of tertiary companion candidates in all five systems we observed present a clear confirmation of the non-conservative mass transfer scenario, and together with our survey of PCEBs, confirms the relevance of this mechanism on the formation of close binaries with white dwarfs. In fact, we believe that the triple system with the ELM white dwarf found in our PCEB survey is descended from an EL CVn binary. Both studies will be connected in the already mentioned upcoming paper.

Finally, we have shown that the small semi-major axis (≈ 0.02 au) of a planet candidate discovered around a white dwarf could be explained through common envelope evolution. In our models (based on the $\alpha_{\rm CE}$-formalism) we found that common envelope evolution is possible if less than 10 per cent of recombination energy is used to eject the envelope. This fraction of recombination energy is consistent with the amount required to explain the orbital period on the order of weeks-months of two previously discovered white dwarf + AFGK binaries believed to have formed through this mechanism. We also probe that the planet candidate is not affected by evaporation during and after this phase, and since the white dwarf is part of a hierarchical triple, Zeipel-Lidov-Kozai oscillations induced by the distant M-dwarf binary could contribute to the planet to reach the required separation to trigger a common envelope phase. Although in this study we use recombination energy to unbind the envelope, it remains an open question how efficient it is at ejecting the envelope, and the contribution of other energy sources is not ruled out. In the near future (during my first postdoc position) I will work on the same topic but focus on the spectral characterisation of white dwarfs with heavy elements, which will reveal more clues about the fate of planets once its host star evolves off the main-sequence.

APPENDIX A

Appendix

A.1 Chi-square minimisation

In order to fit the *GALEX* archival photometry of TYC 8097-337-1 to a model where the total flux in each filter comes from the secondary star and a white dwarf companion, we look for white dwarf models and distances that minimise the following quantity

$$\chi^2 = \sum_{\mathrm{i}=1}^{\mathrm{N}} \left(\frac{F_{\mathrm{obs,i}} - F_{\mathrm{synth,i}}}{\sigma_{\mathrm{obs,i}}} \right)^2, \tag{A.1}$$

i.e., the *chi-square* statistic. The sum is over all photometric filters i taken into account in the fit, with $F_{\mathrm{obs,i}}$, $\sigma_{\mathrm{obs,i}}$, being the archival photometry with its associated error. The synthetic photometry in filter i is given by:

$$F_{\mathrm{synth,i}} = \mathrm{D}^{-2} \mathrm{A_i} \sum_{\mathrm{j}=1}^{\mathrm{M}} \mathrm{R_j^2 F_{j,i}}, \tag{A.2}$$

where $\mathrm{A_i}$ is the galactic extinction for filter i, D the distance in pc, $\mathrm{R_j}$ the stellar radius of star j and $\mathrm{F_{j,i}}$ the flux in filter i for star j. The sum is over all M stars in the system that contributes to the flux in filter i. For the particular case of TYC 8097-337-1 we are only dealing with the secondary star and the hypothetical white dwarf companion, therefore equation A.2 can be written as

$$F_{\mathrm{synth,i}} = \mathrm{D}^{-2} \mathrm{A_i} \left(\mathrm{R_2^2 F_{2,i}} + \mathrm{R_{WD}^2 F_{WD,i}} \right), \tag{A.3}$$

with R_2, R_{WD} and F_2, F_{WD} being the radius and fluxes if the secondary and the white dwarf respectively. After calculating the partial derivative of equation A.1 and imposing $\left(\partial\chi^2/\partial D\right) = 0$ for each one of the HKBT white dwarf models (see section 2.4.3) we arrive to the best distance-fit:

$$D = \left(\frac{\sum_{i=1}^{N} \frac{F_{synth,i}^2}{\sigma_{obs,i}^2}}{\sum_{i=1}^{N} \frac{F_{obs,i}.F_{synth,i}}{\sigma_{obs,i}^2}} \right)^{1/2} \tag{A.4}$$

A.2 Radial velocity measurements

Table A.1: Secondary star radial velocity measurements for 2MASS J06281844-7621467

BJD (mid-exposure)	RV ($km\,s^{-1}$)	Err ($km\,s^{-1}$)	Instrument
2457002.698	-5.709	0.010	FEROS
2457003.719	3.619	0.010	FEROS
2457004.723	6.349	0.010	FEROS
2457025.740	5.803	0.500	Du Pont echelle
2457026.735	2.613	0.500	Du Pont echelle
2457027.704	-3.866	0.500	Du Pont echelle
2457028.749	-16.597	0.500	Du Pont echelle
2457269.813	5.767	0.976	CHIRON
2457277.905	-14.416	0.500	CHIRON
2457291.845	3.494	0.500	CHIRON
2457292.847	-2.470	0.500	CHIRON
2457299.769	2.753	0.500	CHIRON
2457303.876	-10.430	0.500	CHIRON
2457317.805	-36.106	0.500	CHIRON
2457332.714	3.576	0.500	CHIRON
2457365.629	-16.683	0.500	CHIRON
2457378.850	-41.177	0.500	UVES
2457386.668	-26.322	0.010	FEROS
2457389.630	-27.349	0.010	FEROS
2457439.599	-49.261	0.500	UVES
2457472.531	-4.665	0.010	FEROS
2457674.735	-45.979	0.500	UVES
2457712.834	-16.520	0.500	UVES
2457723.627	-26.336	0.500	UVES
2457744.722	-37.877	0.500	UVES
2457753.736	-17.528	0.500	UVES
2457760.689	6.203	0.500	UVES
2457787.586	-34.963	0.500	UVES
2457797.547	-40.193	0.500	UVES

Table A.2: Secondary star radial velocity measurements for TYC 8097-337-1

BJD (mid-exposure)	RV ($km\,s^{-1}$)	Err ($km\,s^{-1}$)	Instrument
2457386.724	48.370	0.010	FEROS
2457387.640	43.159	0.010	FEROS
2457387.718	42.778	0.010	FEROS
2457388.695	38.390	0.018	FEROS
2457389.603	34.955	0.010	FEROS
2457471.552	43.303	0.011	FEROS
2457586.921	24.652	0.010	FEROS
2457643.893	28.042	0.500	UVES
2457645.824	24.803	0.500	UVES
2457655.836	82.594	0.500	UVES
2457674.689	61.560	0.500	UVES
2457680.816	46.421	0.500	UVES
2457684.782	30.497	0.500	UVES
2457711.565	23.734	0.500	UVES
2457712.817	24.490	0.500	UVES
2457723.621	41.890	0.500	UVES
2457725.542	34.282	0.500	UVES

Table A.3: Secondary star radial velocity measurements for TYC 6996-449-1

BJD (mid-exposure)	RV ($km\,s^{-1}$)	Err ($km\,s^{-1}$)	Instrument
2456833.851	-20.966	0.022	FEROS
2456835.781	-12.243	0.025	FEROS
2457001.563	-22.285	0.024	FEROS
2457002.645	-17.019	0.026	FEROS
2457003.648	-12.729	0.021	FEROS
2457025.548	16.137	0.500	Du Pont echelle
2457026.569	15.903	0.500	Du Pont echelle
2457027.586	16.080	0.500	Du Pont echelle
2457188.839	14.403	0.027	FEROS
2457255.781	-12.018	0.500	CHIRON
2457266.632	8.456	0.500	CHIRON
2457269.684	11.963	1.515	CHIRON
2457276.712	15.748	0.500	CHIRON
2457283.761	13.860	0.500	CHIRON
2457297.742	-12.244	0.500	CHIRON
2457311.706	12.334	0.500	CHIRON
2457313.682	13.547	0.500	CHIRON
2457319.630	16.206	0.500	CHIRON
2457333.623	-27.295	0.527	CHIRON
2457340.552	-9.372	0.500	UVES
2458600.893	-7.305	0.055	FEROS

Bibliography

Allard F., Homeier D., Freytag B., 2012a, Philosophical Transactions of the Royal Society of London Series A, 370, 2765

Allard F., Homeier D., Freytag B., 2012b, Philosophical Transactions of the Royal Society of London Series A, 370, 2765

Amara A., Quanz S. P., 2012, MNRAS, 427, 948

Armitage P. J., 2007, ApJ, 665, 1381

Ashley R. P., Farihi J., Marsh T. R., Wilson D. J., Gänsicke B. T., 2019, MNRAS, 484, 5362

Astropy Collaboration et al., 2018, AJ, 156, 123

Bailer-Jones C. A. L., Rybizki J., Fouesneau M., Demleitner M., Andrae R., 2021, AJ, 161, 147

Bailer-Jones C. A. L., Rybizki J., Fouesneau M., Mantelet G., Andrae R., 2018, AJ, 156, 58

Baraffe I., Homeier D., Allard F., Chabrier G., 2015, A&A, 577, A42

Baruteau C., Meru F., Paardekooper S.-J., 2011, MNRAS, 416, 1971

Bayo A., Rodrigo C., Barrado Y Navascués D., Solano E., Gutiérrez R., Morales-Calderón M., Allard F., 2008, A&A, 492, 277

Bear E., Soker N., 2011a, MNRAS, 411, 1792

Bear E., Soker N., 2011b, MNRAS, 414, 1788

Bear E., Soker N., Harpaz A., 2011, ApJ, 733, L44

Bédard A., Bergeron P., Brassard P., Fontaine G., 2020, The Astrophysical Journal, 901, 93

Bédard A., Bergeron P., Brassard P., Fontaine G., 2020, ApJ, 901, 93

Belloni D., Schreiber M. R., Pala A. F., Gänsicke B. T., Zorotovic M., Rodrigues C. V., 2020, MNRAS, 491, 5717

Beuzit J.-L. et al., 2019, Astronomy & Astrophysics, 631, A155

Bianchi L., Herald J., Efremova B., Girardi L., Zabot A., Marigo P., Conti A., Shiao B., 2011, Ap&SS, 335, 161

Bianchi L., Shiao B., Thilker D., 2017, ApJS, 230, 24

Blanco-Cuaresma S., Soubiran C., Heiter U., Jofré P., 2014, A&A, 569, A111

Bodenheimer P., Pollack J. B., 1986, Icarus, 67, 391

Boss A. P., 2005, ApJ, 629, 535

Bours M. C. P. et al., 2014, MNRAS, 438, 3399

Brahm R., Jordán A., Espinoza N., 2017, PASP, 129, 034002

Brandner W. et al., 2000, AJ, 120, 950

Brown W. R., Kilic M., Prieto C. A., Kenyon S. J., 2010, The Astrophysical Journal, 723, 1072–1081

Burleigh M. R. et al., 2011, in American Institute of Physics Conference Series, Vol. 1331, Schuh S., Drechsel H., Heber U., eds, American Institute of Physics Conference Series, p. 262

Camacho J., Torres S., García-Berro E., Zorotovic M., Schreiber M. R., Rebassa-Mansergas A., Nebot Gómez-Morán A., Gänsicke B. T., 2014, A&A, 566, A86

Casewell S. L., Dobbie P. D., Napiwotzki R., Burleigh M. R., Barstow M. A., Jameson R. F., 2009, MNRAS, 395, 1795

Catalán S., Isern J., García-Berro E., Ribas I., 2008, MNRAS, 387, 1693

Cha S.-H., Nayakshin S., 2011, MNRAS, 415, 3319

Chen X., Maxted P. F. L., Li J., Han Z., 2017, MNRAS, 467, 1874

Claeys J. S. W., Pols O. R., Izzard R. G., Vink J., Verbunt F. W. M., 2014, A&A, 563, A83

Claudi R. U. et al., 2008, in Society of Photo-Optical Instrumentation Engineers (SPIE) Conference Series, Vol. 7014, McLean I. S., Casali M. M., eds, Ground-based and Airborne Instrumentation for Astronomy II, p. 70143E

Correa-Otto J. A., Gil-Hutton R. A., 2017, A&A, 608, A116

Czekaj, M. A. , Robin, A. C. , Figueras, F. , Luri, X. , Haywood, M. , 2014, A&A, 564, A102

Dekker H., D'Odorico S., Kaufer A., Delabre B., Kotzlowski H., 2000, in Society of Photo-Optical Instrumentation Engineers (SPIE) Conference Series, Vol. 4008, Iye M., Moorwood A. F., eds, Optical and IR Telescope Instrumentation and Detectors, p. 534

Dennihy E. et al., 2020, arXiv e-prints, arXiv:2010.03693

Dewi J. D. M., Tauris T. M., 2000, A&A, 360, 1043

Dilday B. et al., 2012, Science, 337, 942

Dohlen K. et al., 2008a, Society of Photo-Optical Instrumentation Engineers (SPIE) Conference Series, Vol. 7014, The infra-red dual imaging and spectrograph for SPHERE: design and performance. p. 70143L

Dohlen K. et al., 2008b, Society of Photo-Optical Instrumentation Engineers (SPIE) Conference Series, Vol. 7014, The infra-red dual imaging and spectrograph for SPHERE: design and performance. p. 70143L

Eastman J., Gaudi B. S., Agol E., 2013, PASP, 125, 83

Eggleton P. P., 1983, ApJ, 268, 368

Eggleton P. P., Kisseleva-Eggleton L., 2006, Ap&SS, 304, 75

Erkaev N. V., Kulikov Y. N., Lammer H., Selsis F., Langmayr D., Jaritz G. F., Biernat H. K., 2007, A&A, 472, 329

Fabrycky D., Tremaine S., 2007, ApJ, 669, 1298

Farihi J., Christopher M., 2004, AJ, 128, 1868

Farihi J., Hoard D. W., Wachter S., 2010, ApJS, 190, 275

Farihi J., Jura M., Zuckerman B., 2009, ApJ, 694, 805

Findeisen K., Hillenbrand L., Soderblom D., 2011, AJ, 142, 23

Fontanive C., Rice K., Bonavita M., Lopez E., Mužić , K., Biller B., 2019, MNRAS, 485, 4967

Foreman-Mackey D., Hogg D. W., Lang D., Goodman J., 2013, PASP, 125, 306

Gaia Collaboration , Brown A. G. A., Vallenari A., Prusti T., de Bruijne J. H. J., Babusiaux C., Biermann M., 2020, arXiv e-prints, arXiv:2012.01533

Gänsicke B. T. et al., 2016, ApJ, 818, L7

Gänsicke B. T., Marsh T. R., Southworth J., 2007, MNRAS, 380, L35

Gänsicke B. T., Marsh T. R., Southworth J., Rebassa-Mansergas A., 2006, Science, 314, 1908

Gänsicke B. T., Schreiber M. R., Toloza O., Fusillo N. P. G., Koester D., Manser C. J., 2019, Nature, 576, 61

Ge H., Webbink R. F., Chen X., Han Z., 2015, ApJ, 812, 40

Ge H., Webbink R. F., Chen X., Han Z., 2020, ApJ, 899, 132

Geier S. et al., 2011, ApJ, 731, L22

Gil de Paz A. et al., 2007, ApJS, 173, 185

Gomez Gonzalez C. A. et al., 2017, AJ, 154, 7

Gonzalez C. A. G. et al., 2017, The Astronomical Journal, 154, 7

Grichener A., Sabach E., Soker N., 2018, MNRAS, 478, 1818

Hamers A. S., 2012

Hamers A. S., 2018, MNRAS, 476, 4139

Hamers A. S., 2020, MNRAS, 494, 5492

Hamers A. S., Perets H. B., Thompson T. A., Neunteufel P., 2021, arXiv e-prints, arXiv:2107.13620

Hamers A. S., Portegies Zwart S. F., 2016a, MNRAS, 459, 2827

Hamers A. S., Portegies Zwart S. F., 2016b, MNRAS, 462, L84

Han Z., 1998, MNRAS, 296, 1019

Harrington R. S., 1968, AJ, 73, 190

Hernandez M. S. et al., 2021, MNRAS, 501, 1677

Hernandez M. S. et al., 2022, Monthly Notices of the Royal Astronomical Society, stac604

Holberg J. B., Bergeron P., 2006, AJ, 132, 1221

Hollands M. A., Koester D., Alekseev V., Herbert E. L., Gänsicke B. T., 2017, MNRAS, 467, 4970

Hurley J. R., Pols O. R., Tout C. A., 2000, MNRAS, 315, 543

Hurley J. R., Tout C. A., Pols O. R., 2002, MNRAS, 329, 897

Ito T., Ohtsuka K., 2019, Monographs on Environment, Earth and Planets, 7, 1

Ivanova N., 2018, ApJ, 858, L24

Ivanova N. et al., 2013, A&A Rev., 21, 59

Ivanova N., Justham S., Podsiadlowski P., 2015, MNRAS, 447, 2181

Kalirai J. S., Hansen B. M. S., Kelson D. D., Reitzel D. B., Rich R. M., Richer H. B., 2008, ApJ, 676, 594

Kaufer A., Pasquini L., 1998, in Optical Astronomical Instrumentation, Vol. 3355, p. 844

Kawahara H., Masuda K., MacLeod M., Latham D. W., Bieryla A., Benomar O., 2018, AJ, 155, 144

Koester D., Gänsicke B. T., Farihi J., 2014, A&A, 566, A34

Kordopatis G. et al., 2013, AJ, 146, 134

Kowalski P. M., Saumon D., 2006, ApJ, 651, L137

Kozai Y., 1962, AJ, 67, 591

Kroupa P., Tout C. A., Gilmore G., 1993, MNRAS, 262, 545

Kruse E., Agol E., 2014, Science, 344, 275

Krushinsky V. et al., 2020, MNRAS, 493, 5208

Kunder A. et al., 2017, AJ, 153, 75

Lagos F. et al., 2020, MNRAS, 494, 915

Lallement R., Babusiaux C., Vergely J. L., Katz D., Arenou F., Valette B., Hottier C., Capitanio L., 2019, A&A, 625, A135

Li G., Naoz S., Kocsis B., Loeb A., 2015, MNRAS, 451, 1341

Lidov M. L., 1962, Planet. Space Sci., 9, 719

Lin D. N. C., Papaloizou J., 1986, ApJ, 309, 846

Loyd R. O. P., Shkolnik E. L., Schneider A. C., Barman T. S., Meadows V. S., Pagano I., Peacock S., 2018, ApJ, 867, 70

Maldonado R. F., Villaver E., Mustill A. J., Chávez M., Bertone E., 2020, arXiv e-prints, arXiv:2010.11403

Manser C. J. et al., 2019, Science, 364, 66

Maoz D., Mannucci F., 2012, pasa, 29, 447

Marois C., Lafrenière D., Doyon R., Macintosh B., Nadeau D., 2006a, ApJ, 641, 556

Marois C., Lafrenière D., Doyon R., Macintosh B., Nadeau D., 2006b, ApJ, 641, 556

Masuda K., Kawahara H., Latham D. W., Bieryla A., Kunitomo M., MacLeod M., Aoki W., 2019, ApJ, 881, L3

Maxted P. F. L. et al., 2014a, MNRAS, 437, 1681

Maxted P. F. L., Napiwotzki R., Dobbie P. D., Burleigh M. R., 2006, Nature, 442, 543

Maxted P. F. L., Serenelli A. M., Marsh T. R., Catalán S., Mahtani D. P., Dhillon V. S., 2014b, MNRAS, 444, 208

Melis C., Klein B., Doyle A. E., Weinberger A. J., Zuckerman B., Dufour P., 2020, arXiv e-prints, arXiv:2010.03695

Mizuno H., 1980, Progress of Theoretical Physics, 64, 544

Moe M., Kratter K. M., 2018, ApJ, 854, 44

Moe M., Kratter K. M., 2019, arXiv e-prints, arXiv:1912.01699

Mordasini C., 2018, Planetary Population Synthesis. In: Deeg H., Belmonte J. (eds) Handbook of Exoplanets. Springer, Cham, p. 2425

Muñoz D. J., Petrovich C., 2020, arXiv e-prints, arXiv:2010.04724

Murphy S. J., Moe M., Kurtz D. W., Bedding T. R., Shibahashi H., Boffin H. M. J., 2018, MNRAS, 474, 4322

Murray-Clay R. A., Chiang E. I., Murray N., 2009, ApJ, 693, 23

Mustill A. J., Villaver E., 2012, ApJ, 761, 121

Mustill A. J., Villaver E., Veras D., Gänsicke B. T., Bonsor A., 2018, MNRAS, 476, 3939

Naoz S., 2016, ARA&A, 54, 441

Naoz S., Fabrycky D. C., 2014, ApJ, 793, 137

Naoz S., Farr W. M., Lithwick Y., Rasio F. A., Teyssandier J., 2011, Nature, 473, 187

Nebot Gómez-Morán A. et al., 2011a, A&A, 536, A43

Nebot Gómez-Morán A. et al., 2011b, A&A, 536, A43

Nelemans G., Tauris T. M., 1998, A&A, 335, L85

Nelemans G., Tout C. A., 2005, MNRAS, 356, 753

Nelemans G., Verbunt F., Yungelson L. R., Portegies Zwart S. F., 2000, A&A, 360, 1011

Nelson L., Schwab J., Ristic M., Rappaport S., 2018, ApJ, 866, 88

Nomoto K., Kondo Y., 1991, ApJ, 367, L19

Nordhaus J., Spiegel D. S., 2013, MNRAS, 432, 500

O'Brien M. S., Bond H. E., Sion E. M., 2001, ApJ, 563, 971

O'Connor C. E., Liu B., Lai D., 2020, arXiv e-prints, arXiv:2010.04163

Owen J. E., Alvarez M. A., 2016, ApJ, 816, 34

Pala A. F. et al., 2017, MNRAS, 466, 2855

Parsons S. G. et al., 2020, Nature Astronomy, 4, 690

Parsons S. G., Rebassa-Mansergas A., Schreiber M. R., Gänsicke B. T., Zorotovic M., Ren J. J., 2016, MNRAS, 463, 2125

Parsons S. G. et al., 2015, MNRAS, 452, 1754

Passy J.-C., Mac Low M.-M., De Marco O., 2012, ApJ, 759, L30

Patat F. et al., 2007, Science, 317, 924

Pollack J. B., Hubickyj O., Bodenheimer P., Lissauer J. J., Podolak M., Greenzweig Y., 1996, Icarus, 124, 62

Press W. H., Teukolsky A. A., Vetterling W. T., Flannery B. P., 2007, Numerical recipes. The art of scientific computing, 3rd edn. Cambridge: University Press

Rao S., Meynet G., Eggenberger P., Haemmerlé L., Privitera G., Georgy C., Ekström S., Mordasini C., 2018, A&A, 618, A18

Rebassa-Mansergas A. et al., 2017, MNRAS, 472, 4193

Ren J. J. et al., 2020, ApJ, 905, 38

Robin A. C., Reylé C., Derrière S., Picaud S., 2004, A&A, 416, 157

Rocchetto M., Farihi J., Gänsicke B. T., Bergfors C., 2015, MNRAS, 449, 574

Rodrigo C., Solano E., 2020, in Contributions to the XIV.0 Scientific Meeting (virtual) of the Spanish Astronomical Society, p. 182

Rodrigo C., Solano E., Bayo A., 2012, SVO Filter Profile Service Version 1.0, IVOA Working Draft 15 October 2012

Ronco M. P., Schreiber M. R., Giuppone C. A., Veras D., Cuadra J., Guilera O. M., 2020, ApJ, 898, L23

Sabach E., Hillel S., Schreier R., Soker N., 2017, MNRAS, 472, 4361

Saffer R. A., Livio M., Yungelson L. R., 1998, ApJ, 502, 394

Schreiber M. R., Gänsicke B. T., 2003, A&A, 406, 305

Schreiber M. R., Gänsicke B. T., Toloza O., Hernandez M.-S., Lagos F., 2019, The Astrophysical Journal, 887, L4

Schreiber M. R., Zorotovic M., Wijnen T. P. G., 2016, MNRAS, 455, L16

Shappee B. J., Thompson T. A., 2013, The Astrophysical Journal, 766, 64

Shkolnik E. L., Barman T. S., 2014, AJ, 148, 64

Simon J. D. et al., 2009, ApJ, 702, 1157

Soker N., 1998, AJ, 116, 1308

Soker N., Grichener A., Sabach E., 2018, ApJ, 863, L14

Soker N., Harpaz A., 2003, MNRAS, 343, 456

Soummer R., Pueyo L., Larkin J., 2012, ApJ, 755, L28

Stelzer B., Marino A., Micela G., López-Santiago J., Liefke C., 2013, MNRAS, 431, 2063

Stephan A. P., Naoz S., Gaudi B. S., 2020, arXiv e-prints, arXiv:2010.10534

Stephan A. P., Naoz S., Zuckerman B., 2017, ApJ, 844, L16

Sternberg A. et al., 2011, Science, 333, 856

Tanaka H., Takeuchi T., Ward W. R., 2002, ApJ, 565, 1257

Tokovinin A., 2014, AJ, 147, 87

Tokovinin A., Fischer D. A., Bonati M., Giguere M. J., Moore P., Schwab C., Spronck J. F. P., Szymkowiak A., 2013, PASP, 125, 1336

Tokovinin A., Thomas S., Sterzik M., Udry S., 2006, A&A, 450, 681

Toonen S., Boekholt T. C. N., Portegies Zwart S., 2021, arXiv e-prints, arXiv:2108.04272

Toonen S., Nelemans G., 2013, A&A, 557, A87

Tremblay P.-E., Bergeron P., Gianninas A., 2011, ApJ, 730, 128

van Roestel J. et al., 2018, MNRAS, 475, 2560

Vanderburg A. et al., 2015, Nature, 526, 546–549

Vanderburg A. et al., 2020, arXiv e-prints, arXiv:2009.07282

Veras D., Wyatt M. C., Mustill A. J., Bonsor A., Eldridge J. J., 2011, MNRAS, 417, 2104

Vigan A., 2020, vlt-sphere: Automatic VLT/SPHERE data reduction and analysis

Vigan A., Moutou C., Langlois M., Allard F., Boccaletti A., Carbillet M., Mouillet D., Smith I., 2010a, in In the Spirit of Lyot 2010, p. E48

Vigan A., Moutou C., Langlois M., Allard F., Boccaletti A., Carbillet M., Mouillet D., Smith I., 2010b, MNRAS, 407, 71

Villaver E., Livio M., 2007, ApJ, 661, 1192

Villaver E., Livio M., 2009, ApJ, 705, L81

Vos J., Zorotovic M., Vučković M., Schreiber M. R., Østensen R., 2018, MNRAS, 477, L40

Ward W. R., 1997, Icarus, 126, 261

Webbink R. F., 1984, ApJ, 277, 355

Webbink R. F., 2008a, Astrophysics and Space Science Library, Vol. 352, Milone E. F., Leahy D. A., Hobill D. W., eds, Common Envelope Evolution Redux. p. 233

Webbink R. F., 2008b, Astrophysics and Space Science Library, Vol. 352, Common Envelope Evolution Redux. In: Short-Period Binary Stars: Observations, Analyses, and Results. Astrophysics and Space Science Library, vol 352. Springer, Dordrecht, p. 233

Weidemann V., 2000, A&A, 363, 647

Weinberg M. D., Shapiro S. L., Wasserman I., 1987, ApJ, 312, 367

Welsh B. Y., Wheatley J. M., Neil J. D., 2011, A&A, 527, A15

West A. A. et al., 2011, The Astronomical Journal, 141, 97

Williams K. A., Bolte M., Koester D., 2009, ApJ, 693, 355

Wilson E. C., Nordhaus J., 2019, MNRAS, 485, 4492

Wilson T. G., Farihi J., Gänsicke B. T., Swan A., 2019, MNRAS, 487, 133

Wonnacott D., Kellett B. J., Stickland D. J., 1993, MNRAS, 262, 277

Woods T. E., Ivanova N., van der Sluys M. V., Chaichenets S., 2012, ApJ, 744, 12

Xu X.-J., Li X.-D., 2010, ApJ, 716, 114

Yungelson L. R., Kuranov A. G., 2017, MNRAS, 464, 1607

Zorotovic M., Schreiber M. R., Gänsicke B. T., 2011, A&A, 536, A42

Zorotovic M., Schreiber M. R., Gänsicke B. T., Nebot Gómez-Morán A., 2010, A&A, 520, A86

Zorotovic M., Schreiber M. R., García-Berro E., Camacho J., Torres S., Rebassa-Mansergas A., Gänsicke B. T., 2014, A&A, 568, A68

Zorotovic M., Schreiber M. R., Parsons S. G., 2014, A&A, 568, L9

Zuckerman B., Becklin E. E., 1987, Nature, 330, 138

Zuckerman B., Melis C., Klein B., Koester D., Jura M., 2010, ApJ, 722, 725